CEP72 represents a putative Oncogene that negatively regulates the mitotic Function of Brca1 and induces Chromosomal Instability

Dissertation

for the award of the degree

“Doctor rerum naturalium”

of the Georg-August-Universität Göttingen

within the doctoral program “Molecular Biology of Cells”

of the Georg-August University School of Science (GAUSS)

submitted by

Sina Lüddecke

from Peine, Germany

Göttingen, September 2015

Members of Thesis Committee

Prof. Dr. Holger Bastians
Section of Cellular Oncology
Institute for Molecular Oncology
University Medical Center Göttingen

Prof. Dr. Sigrid Hoyer-Fender
Department of Developmental Biology
Johann-Friedrich-Blumenbach-Institute for Zoology und Anthropology
Georg-August University Göttingen

Prof. Dr. Peter Burfeind
Institute for Human Genetics
University Medical Center Göttingen

Members of the Examination Board

Referee: Prof. Dr. Holger Bastians
Section of Cellular Oncology
Institute for Molecular Oncology
University Medical Center Göttingen

2nd Referee: Prof. Dr. Sigrid Hoyer-Fender
Department of Developmental Biology
Johann-Friedrich-Blumenbach-Institute for Zoology und Anthropology
Georg-August University Göttingen

Further Members of Examination Board

Prof. Dr. Peter Burfeind
Institute for Human Genetics
University Medical Center Göttingen

Prof. Dr. Heidi Hahn
Institute for Human Genetics
University Medical Center Göttingen

Prof. Dr. Dieter Kube
Department of Haematology and Oncology
University Medical Center Göttingen

Prof. Dr. Matthias Dobbelstein
Institute for Molecular Oncology
University Medical Center Göttingen

Date of oral examination:

AFFIDAVIT

Hereby I declare that my doctoral thesis entitled "*CEP72* represents a putative Oncogene that negatively regulates the mitotic Function of Brca1 and induces Chromosomal Instability" has been written independently with no other sources and aids than quoted.

Göttingen, August 2015 _____

Sina Lüddecke

TABLE OF CONTENTS

LIST OF FIGURES

LIST OF TABLES

ABSTRACT

Proper progression through mitosis ensures the maintenance of whole chromosomal stability in a eukaryotic cell. Hence, failures during this tightly regulated process can lead to the perpetual mis-segregation of whole chromosomes, which is referred to as chromosomal instability (CIN). This process results in the generation of aneuploidy and an increased genetic variability contributing to tumourigenesis and tumour progression. Although CIN is a major hallmark of human cancer, the underlying mechanisms leading to perpetual chromosome mis-segregation during mitosis are largely unknown. Interestingly, the tumour suppressor Brca1 and its positive regulator Chk2 were found to be crucial for the proper regulation of spindle microtubule plus end polymerization within mitotic spindles, which is pivotal for correct microtubule-kinetochore attachments and faithful chromosome segregation. Consequently, loss of the *CHK2-BRCA1* axis leads to enhanced spindle microtubule plus end assembly and the induction of CIN. Despite the importance of these findings the underlying molecular mechanism remained elusive and the regulation of Brca1 during mitosis is still poorly understood.

In this study we identified the centrosomal protein Cep72 as a novel Brca1-interacting protein. Importantly, Cep72 was found to be frequently upregulated in human colorectal cancer suggesting that *CEP72* represents a putative oncogene. Overexpression of *CEP72* mirrors mitotic defects seen upon loss of *BRCA1* or its positive regulator *CHK2*, indicating a possible function for Cep72 in negatively regulating Brca1 during mitosis. In detail, overexpression of *CEP72* results in enhanced spindle microtubule plus end polymerization rates causing spindle assembly defects, lagging chromosomes and the induction of CIN. Intriguingly, these defects can be suppressed by concomitantly increasing the levels of the positive Brca1 regulator Chk2. *Vice versa*, reducing the Cep72 protein levels restores proper microtubule plus end polymerization and spindle assembly in cells with a partial loss of *CHK2*. Thus, my results suggest that the mitotic function of Brca1 is positively regulated by Chk2, and counteracted by Cep72. Furthermore, the balanced regulation of Brca1 by Chk2 and Cep72 seems to be crucial for proper microtubule dynamics and accurate chromosome segregation ensuring the maintenance of whole chromosomal stability.

1 INTRODUCTION

1.1 The eukaryotic cell cycle

Proliferating eukaryotic cells pass through a series of stages, which are collectively known as the cell cycle. Characterized by cell growth and cell division, the eukaryotic cell cycle comprises four phases, mitosis, gap 1 (G1) phase, DNA-synthesis phase (S-phase) and G2 phase (Figure 1.1). Together, G1-, S- and G2-phase are referred to as interphase. After a cell emerged from a cell division it grows in size during G1 and prepares for chromosome duplication. In the absence of growth signals, the cell can exit from the cell cycle and enter a quiescent state called G0. However, depending on cell type, cell size, nutrient availability or mitogenic signalling, the cell can re-enter the cycle by passing the restriction point. In the following S-phase the DNA is replicated and the centrosome, which forms the major microtubule organizing centre in the cell, duplicates. Subsequently, in the second gap phase (G2), the cell prepares for cell division by synthesizing essential proteins. During mitosis, the replicated DNA is equally segregated onto two emerging daughter cells, which re-enter G1 phase and start a new cell cycle on their own (Morgan 2007; Alberts et al. 2007).

1.2 Regulation of the cell cycle by reversible protein phosphorylation and ubiquitin-mediated protein proteolysis

The cell cycle progression is controlled by cyclin-dependent kinases (Cdks), which phosphorylate and therefore control the activity, stability and localization of proteins that are responsible for individual cell cycle processes. While Cdks are present throughout the cell cycle, their activity is tightly regulated by the formation of complexes with their regulatory subunits, the cyclins. The cell cycle dependent expression and proteasomal degradation of cyclins causes the oscillating activation of Cdks (Figure 1.1). Whereas initially in G1 all cyclin-Cdk complexes are inactive to prevent an unscheduled entry into the cell cycle, Cdk4 and Cdk6 are activated by cyclin D when cells pass the restriction point upon mitogenic signalling. Cyclin A and E control Cdk2 activation and mediate the entry into S-phase. In G2-phase the levels of cyclin B constantly increase, which, together with cyclin A and C, triggers the enzymatic activity of Cdk1 and thereby the entry into mitosis. Moreover, in metaphase, the proteasomal destruction of cyclin B and securin, a protein that controls sister chromatid cohesion, enables the metaphase to anaphase transition and thus, the termination of mitosis (Morgan 2007).

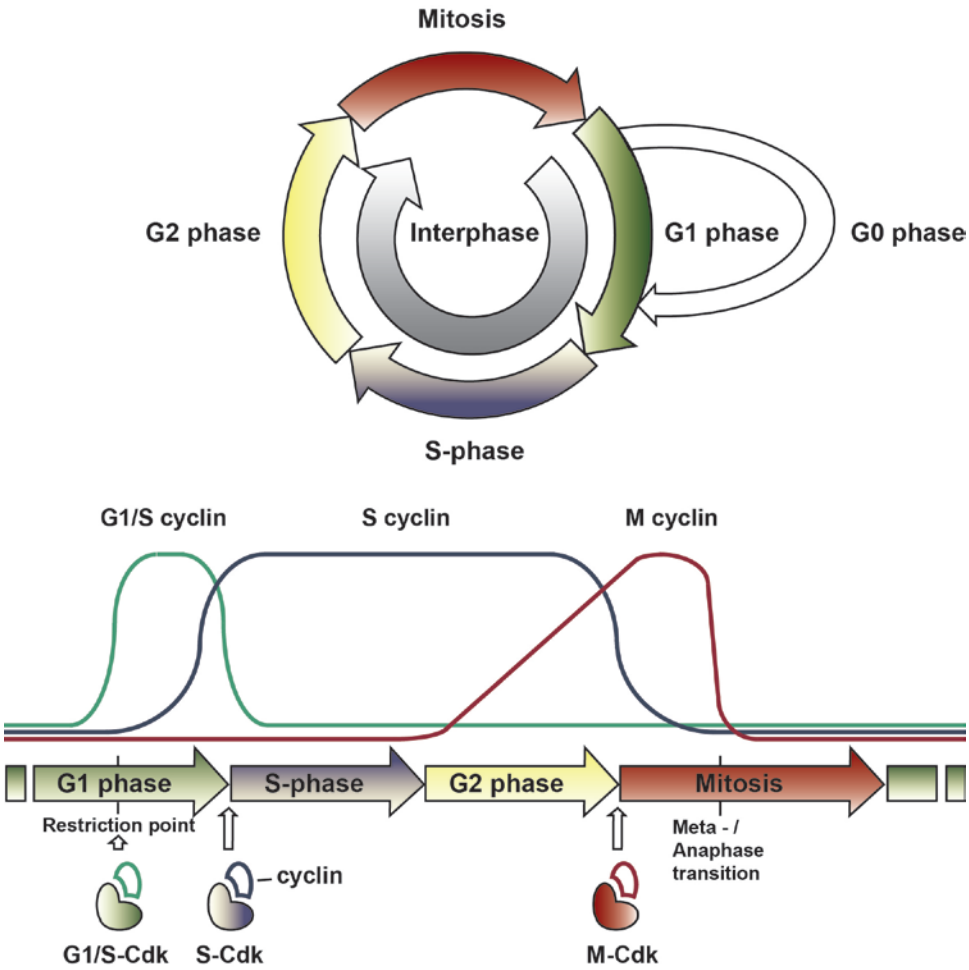

Figure 1.1 The cell cycle and its regulation. The cell cycle consists of four phases: G1 phase, S-phase and G2-phase, which are referred to as interphase and mitosis representing the stage of cell division. The cell cycle is regulated by CDKs which are activated by different cyclins oscillating in a cell cycle dependent manner. Parts of the graphic were modified from Morgan, 2007.

Although cyclins are the major regulators of Cdks, their binding alone is not sufficient to achieve a full activation. For this, an activating phosphorylation mediated by a Cdk-activating kinase (CAK) is required. Beyond, two inhibitory phosphorylations at Thr14 and Tyr15 play an important role for the regulation of Cdk activity. While they are catalysed by the kinases Wee1 and Myt1 in a localization dependent manner, their removal is carried out by phosphatases of the Cdc25 family. These antagonistically acting enzymes enable the switch-like activation of cyclin B/Cdk1 in late G2-phase, whereupon they are themselves regulated by their own substrate. Consequently, Cyclin B/Cdk1 mediated phosphorylation represses Wee1/Myt1 and promotes Cdc25 activity, hence, creating a positive feedback loop for cyclin B/Cdk1 activation and enabling the entry into mitosis. Moreover, Wee1 and Cdc25 are crucial for the cellular response upon DNA damage in S- and G2-phase. In addition to Cdk activity regulation by reversible phosphorylation, the degradation of regulatory proteins and cyclins by ubiquitin-mediated protein proteolysis is essential for irreversible cell cycle progression. In this connection, the E3-ubiquitin

ligase Skp1/Cul1/F-box (SCF) and the anaphase- promoting complex/cyclosome (APC/C) are of utmost importance (Morgan 2007; Alberts et al. 2007).

1.3 The ubiquitin pathway

The vast majority of proteins involved in all cellular processes are regulated by post-translational ubiquitination. While the best-known function of ubiquitination is to target proteins for degradation by the 26S proteasome, it also leads to activation and deactivation of proteins, modulates protein-protein-interactions and affects their cellular localization (Mukhopadhyay & Riezman 2009; Schnell & Hicke 2003; Metzger et al. 2012; Hershko & Ciechanover 1998). Ubiquitin is a 76 amino acid polypeptide of ~8.5 kDa, which is attached to substrates in a three step process. It starts with the ATP-dependent covalent binding of ubiquitin to the ubiquitin activating enzyme E1. The ubiquitin-conjugating enzyme E2 binds to both proteins and catalyses the transfer of the activated ubiquitin from E1 to its own active site. Finally, the ubiquitin transfer to substrate proteins is mediated by the E3 ubiquitin ligase, which functions as the substrate recognition module (Metzger et al. 2012; Hershko & Ciechanover 1998; Komander 2009). E3 ubiquitin ligases are subdivided into two main classes: really interesting gene (RING) finger E3s (as well as RING-related E3s) and homologous to the E6-AP carboxyl terminus (HECT) domain E3s. Whereas HECT domain E3 ubiquitin ligases transiently bind the activated ubiquitin prior to substrate ubiquitination, RING finger E3s catalyse the direct transfer of ubiquitin from the E2 activating enzyme to the substrate (Metzger et al. 2012). Monoubiquitination of proteins can either serve as modulating posttranslational modification or form the priming site for the assembly of polyubiquitin chains. Ubiquitin itself contains seven lysine residues (Lys6, 11, 27, 29, 33, 48 and 63), which provide potential acceptor sites for the addition of further ubiquitin proteins. The best studied and most abundant polyubiquitination is linked to the Lys48 site chain, which targets the substrate protein for proteasomal degradation (Komander 2009). Essential for protein degradation at metaphase to anaphase transition, the RING finger E3 ligase APC/C rather mediates Lys11- than Lys48-linkages, thus demonstrating that also Lys11-linked polyubiquitination plays an important role in proteolysis (Komander 2009; Primorac & Musacchio 2013). In contrast, the formation of Lys63-linked ubiquitin moieties and the more unusual polyubiquitination with Lys6-linkage serve as post-translational modification essential to modulate interactions and protein functions involved in DNA damage response or in signalling and trafficking processes (Komander 2009). While the human genome encodes only two E1 and 37 E2 enzymes, E3 ubiquitin ligases represent a group of over 600 different proteins indicating that the substrate specific, spatial and temporal highly regulated ubiquitination is mainly coordinated by E3 enzymes (Metzger et al. 2012; Komander 2009). Another important role in ubiquitin-dependent protein

regulation is taken by deubiquitinating enzymes (DUBs), which remove ubiquitin moieties from substrate proteins and thereby counteract the ubiquitin-assembly pathway (Reyes Turcu et al. 2009; Komander et al. 2009).

1.4 The E3-ubiquitin ligases SCF and APC/C

The E3-ubiquitin ligases SCF and APC/C are crucial for cell cycle progression. SCF is named after its subunits Skp1, Cul1 and an F-box protein. Beyond, the SCF-complex includes the RING finger motif containing protein Roc1/Rbx1, which is responsible for E2 protein binding (Lee & Diehl 2014; Vodermaier 2004; Morgan 2007). The substrate specificity is mediated by F-box proteins that bind the particular targets, whereupon the SCF mediated ubiquitination is triggered by their phosphorylation (Vodermaier 2004; Morgan 2007). Since the phosphorylation is typically catalysed by cyclin-dependent kinases, ubiquitination and proteolytic degradation of many proteins is tightly linked to specific cell cycle phases (Morgan 2007). The SCF-complex has a central function at the G1/S-transition where it is crucial for the destruction of Cdk inhibitory proteins like p21 or p27 enabling cell cycle progression and the entry into S-phase (Bornstein et al. 2003; Carrano et al. 1999; Morgan 2007). Moreover SCF is involved in G2/M-transition by promoting the proteasomal degradation of the Cdk inhibitor Wee1.

The anaphase promoting complex or cyclosome consists of 15 subunits (Apc1-11, Apc13, Apc15-16 and Cdc26) and belongs to the group of RING finger E3 ubiquitin ligases (Primorac & Musacchio 2013). In contrast to the SCF-complex, which is active throughout the cell cycle, the activity of the APC/C is restricted to mitosis and G1 phase where it is responsible for the metaphase-to-anaphase transition and the exit from mitosis (Morgan 2007; Primorac & Musacchio 2013; Vodermaier 2004). For this, two substrates are of major importance. The APC/C triggers the separase-dependent release of sister chromatid cohesion by targeting the separase inhibitor securin for proteasomal degradation. Hence, APC/C activation at metaphase, which is tightly controlled by the spindle assembly checkpoint, enables sister chromatid separation and anaphase onset. Concomitantly, the APC/C mediates the destruction of cyclin B leading to Cdk1 inactivation and the completion of mitosis. The protein ubiquitination by the APC/C is temporally controlled by binding of the activator subunits Cdc20 and Cdh1, which coordinate APC/C activation and mediate substrate binding (Morgan 2007; Primorac & Musacchio 2013; Vodermaier 2004). Upon satisfaction of the spindle assembly checkpoint at metaphase, Cdk1-dependent phosphorylation and binding of the co-activator Cdc20 lead to the activation of the anaphase-promoting complex. While in the presence of active Cdk1, Cdh1 is phosphorylated and, hence, inactivated, cyclin B degradation and Cdk1 inhibition in anaphase allows the dephosphorylation of Cdh1. Thus, Cdh1 binds to

APC/C in late mitosis and maintains its activity in G1. When the cell enters a new cell cycle the APC/C is phosphorylated and inhibited by G1/S-Cdks (Morgan 2007; Primorac & Musacchio 2013). The substrate recognition by Cdc20 and Cdh1 is mediated by motifs in the amino acid sequence of the target protein, whereas the destruction box (D-box) and KEN-box motifs are prevalent (Morgan 2007).

1.5 DNA damage response

Each eukaryotic cell is subject to endogenous or environmental DNA damaging conditions like reactive oxygen species, ultraviolet light, background radiation or environmental mutagens (Smith et al. 2010; Morgan 2007; Reinhardt & Yaffe 2009). In order to faithfully maintain the encoded information and thus, the genetic stability of a cell, there is a need for DNA damage repair. While many forms of DNA damage can be quickly corrected, defects including nucleotide damage, stalled replication forks and double strand breaks trigger a DNA damage response, which blocks the cell cycle progression until the damaged sites are repaired. Since DNA damage can occur at any time of the cell cycle, eukaryotic cells are featured with DNA damage checkpoints at G1-, S- and G2 phase (Morgan 2007; Shaltiel et al. 2015). The DNA damage response is orchestrated by the key protein kinases ataxia telangialectasia mutated (ATM) and ATM/Rad3-related (ATR), which are activated upon double strand breaks (DSBs) and by single stranded DNA (ssDNA), respectively (Smith et al. 2010; Shaltiel et al. 2015; Morgan 2007). The particular response differs with respect to the cell cycle phase at which the DNA damage occurs. Upon double strand breaks ATM is activated and recruited to damaged sites by a sensory complex consisting of Mre11, Rad50 and Nbs1 (MRN-complex). ATM phosphorylates the histone variant H2AX leading to the recruitment of mediator proteins like breast cancer 1, early onset (Brca1), mediator of DNA damage checkpoint 1 (MDC1), or p53 binding protein 1 (53BP1), which in turn amplify the ATM signal and provide a platform for the assembly of the DNA damage response machinery (Shaltiel et al. 2015; Morgan 2007). In addition, ATM activates the checkpoint kinase 2 (Chk2), which subsequently transduces the DNA damage response signal. In G1 phase, ATM and Chk2 promote the stabilization of p53 leading to the transcription and accumulation of the Cdk inhibiting protein p21 (CDKN1A). Moreover, ATM activates the p38 MAPK family, which further stabilizes the p21 encoding mRNA. The p21-dependent inhibition of Cdk4/6 and Cdk2 is complemented by ATM-, Chk2- and p38-dependent pathways, which concomitantly promote the degradation of cyclin D and the Cdk activating phosphatase Cdc25A, hence, preventing S-phase entry (Shaltiel et al. 2015; Reinhardt et al. 2007). While in G1 phase DNA double strand breaks can only be repaired by error-prone non homologous end joining (NHEJ), error-free correction by homologous recombination (HR) is enabled in the presence of active Cdk2 during S- and G2-phase (Shaltiel et al. 2015).

Single-stranded DNA generated by HR associated DNA-strand resection or stalled replication forks triggers the additional activation of ATR and the checkpoint kinase 1 (Chk1). Although the activation of the ATM-Chk2- and ATR-Chk1-pathway stabilizes p53 during S-phase, the accumulation of p21 during DNA replication is prevented by the PCNA-associated $CRL4^{Cdt2}$ ubiquitin ligase (Shaltiel et al. 2015). Thus, in contrast to G1, the intra-S-phase arrest depends on Chk1 mediated activation of the Cdk inhibitor Wee1 and Chk1/2 dependent inhibition of Cdc25A (Shaltiel et al. 2015; Reinhardt & Yaffe 2009). For the checkpoint response in G2-phase, the Wee1 induced inhibition of Cdks remains crucial and the p21-dependent Cdk inhibition is reinstated. Whereas the ATM-Chk2-pathway still controls the establishment of the cell cycle arrest, ATR-Chk1 pathway signalling is essential for the maintenance of the G2 checkpoint. Moreover, ATM/ATR dependent p38 signalling might induce the destruction of Cdc25A and B, hence, contributing to checkpoint maintenance in G2 (Shaltiel et al. 2015; Reinhardt et al. 2007).

1.6 Mitosis

Mitosis represents the key event during the eukaryotic cell cycle, in which the duplicated DNA is equally distributed onto two emerging daughter cells. Coming along with dramatic morphological changes, mitosis is subdivided into five phases: prophase, prometaphase, metaphase, anaphase and telophase (Figure 1.2). In prophase the centrosomes maturate by growing in size and increasing their microtubule nucleation potential (Lee & Rhee 2011; Menella et al. 2014; Menella et al. 2012). Additionally, the chromosomes condense and the centrosomes are separated, thus starting the assembly of a bipolar spindle, which is fundamental for proper chromosome segregation (Tanenbaum & Medema 2010; Morgan 2007). Moreover, the nuclear envelope breaks down (Burke & Ellenberg 2002). In prometaphase the spindle further develops and kinetochore protein complexes assemble at centromeric regions of the chromosomes, hence, providing docking sites for microtubules (Cheeseman et al. 2006; Cheeseman & Desai 2008; Cheeseman 2014). Dynamic microtubules search and capture the kinetochores and align the chromosomes at the equatorial plane. By excessive microtubules *de novo* nucleation and amplification huge kinetochore fibres consisting of 20-40 microtubules attach to the kinetochore protein complex (Meunier & Vernos 2012; McEwen et al. 1997). A correct amphitelic attachment mediates tension between the kinetochores of sister chromatids, which is needed for satisfying the spindle assembly checkpoint (SAC). One unattached kinetochore, which is accompanied by an unsatisfied SAC is sufficient to block the E3 ubiquitin ligase APC/C that is indispensable for anaphase onset by targeting cyclin B and securin (amongst others) for proteasomal degradation. Finally, when all chromosomes

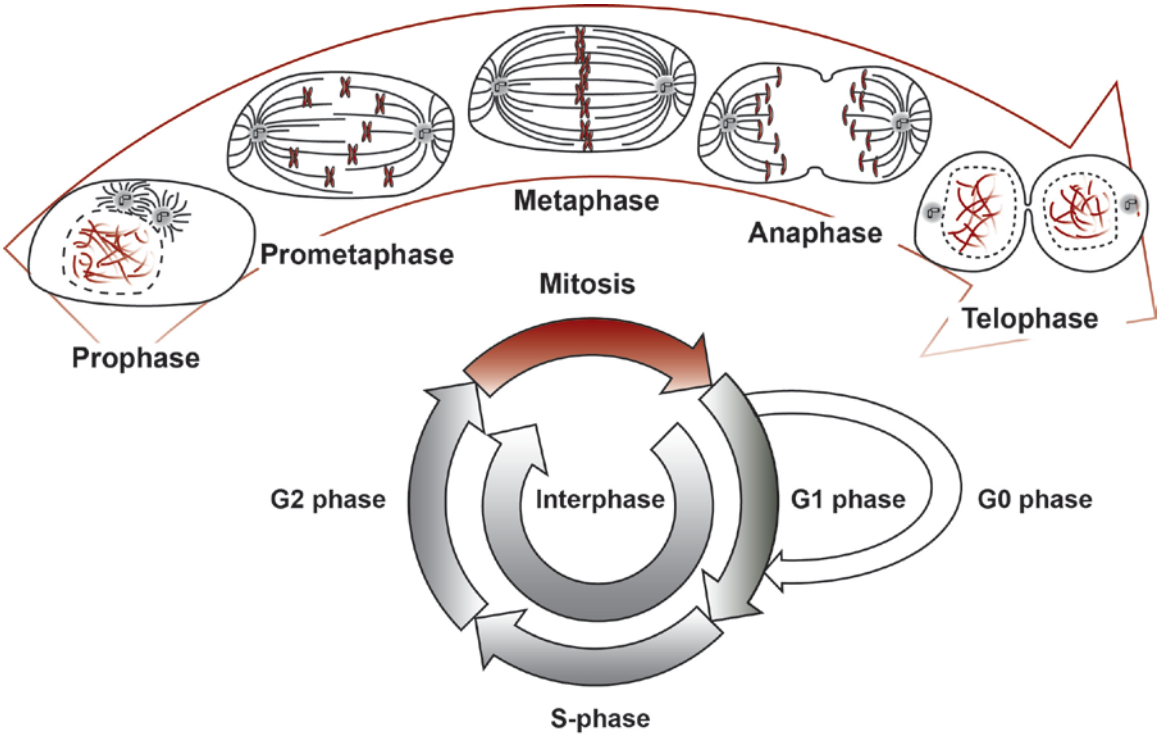

Figure 1.2 Subphases of mitosis. Mitosis is subdivided into the five phases prophase, prometaphase, metaphase, anaphase and telophase. In prophase centrosomes undergo a maturation process and start to separate. Moreover the chromosomes condense and the nuclear envelope breaks down. During Prometaphase the spindle further develops and chromosomes are aligned in equatorial plane by microtubule search and capture. When the chromosomes are perfectly aligned in metaphase, sister chromatids are separated and pulled to opposing poles in anaphase. In Telophase the spindle disassembles, the chromosomes decondense and the nuclear envelope is re-assembled. Moreover the cell divides by cytokinesis.

are properly attached, the condensin protein complexes that link sister chromatids, are abruptly cleaved (Musacchio & Salmon 2007; Morgan 2007; Primorac & Musacchio 2013; Mehta et al. 2013) and the separated sister chromatids are pulled to opposing spindle poles by plus-end depolymerization of kinetochore fibres and motor-protein mediated poleward transport. Following this process, designated as anaphase A, the centrosomes are pushed farther apart from each other, thus completing sister chromatid segregation (anaphase B). In telophase the mitotic spindle disassembles and the chromosomes de-condense. Moreover, the nuclear envelope re-assembles around chromosomes located at the spindle poles thereby forming two daughter nuclei and terminating mitosis (Morgan 2007). Over the time period from early anaphase to the end of telophase cytokinesis takes place. The cell forms a contractile ring consisting of actin-myosin-filaments, which constricts the cell membrane and finally divides the cell (Akhshi et al. 2014).

1.7 The spindle assembly checkpoint

In order to achieve an equal distribution of sister chromatids onto daughter cells, the chromosomes have to be properly attached to the spindle apparatus. For this, centromere bound kinetochore complexes mediate the connection between chromatids and spindle microtubules (Cheeseman 2014; Foley & Kapoor 2013; Lara-Gonzalez et al. 2012). In a proper amphitelic attachment, the sister kinetochores bind to microtubules emanating from opposing spindle poles. However, especially during the early phases of mitosis, inappropriate kinetochore-microtubule attachments including the attachment of only one kinetochore (monotelic), the attachment of both sister-kinetochores to one pole (synthelic) or the simultaneous attachment of one sister kinetochore to both poles can occur (Cheeseman 2014) (Figure 1.3). In order to prevent chromosome mis-segregation during anaphase, both, erroneous microtubule-kinetochore attachments have to be dissolved and mitotic progression must be delayed until all chromosomes are properly attached (Foley & Kapoor 2013). The Aurora B kinase plays an essential role in error correction (Primorac & Musacchio 2013; Cheeseman 2014; Foley & Kapoor 2013). Localized to the inner centromere Aurora B phosphorylates different outer kinetochore components like the Ndc80-, the Dam1- and the Skp1-complex leading to the elimination of inappropriate kinetochore-microtubule connections (Cheeseman 2014). Amphitelic attachments create tension causing intra- and inter-kinetochore stretching and the spatial separation of Aurora B and its substrates. Thus, phosphorylation is abolished, which allows the formation of stable microtubule-kinetochore attachments (Primorac & Musacchio 2013; Foley & Kapoor 2013; Cheeseman 2014). The transient inhibition of the

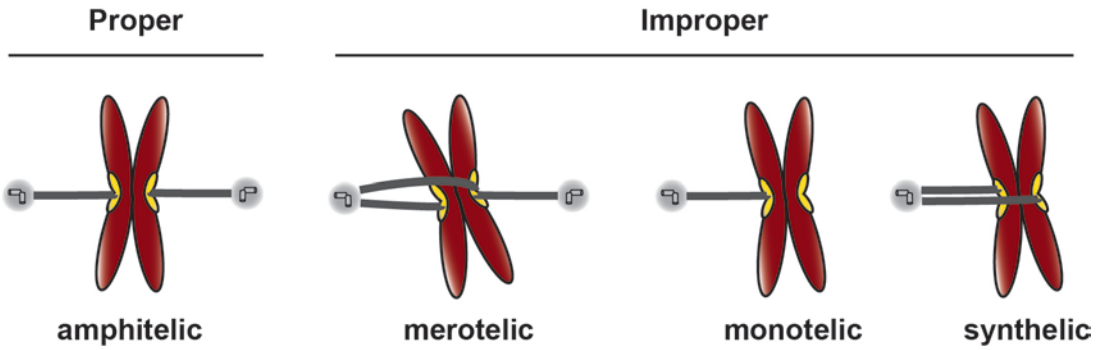

Figure 1.3 Kinetochore-microtubule attachments. Amphitelic attachments are characterized by the linkage of microtubules emanating from both spindle poles to one kinetochore each and represent the only form of attachment, which ensures proper chromosome segregation. While chromosomes with monotelic attachments are linked with only one kinetochore to one pole, the attachment of both kinetochores to microtubules emanating from the same pole are termed synthelic. One kinetochore linked to spindle microtubules emanating from opposing poles represents a merotelic attachment.

metaphase-to-anaphase transition is caused by an active spindle assembly checkpoint (SAC). Unattached kinetochores catalyse the formation of mitotic checkpoint complexes consisting of Mad2, Bub3 and BubR1, which sequester and inhibit the APC/C activating protein Cdc20 (Primorac & Musacchio 2013; Foley & Kapoor 2013). Moreover, the mitotic checkpoint complex directly binds to the APC/C and thus, prevents its activation. When all chromosomes are properly attached, the spindle assembly checkpoint is satified and the APC/C is activated leading to securin and cyclin B degradation and metaphase-to-anaphase transition (Primorac & Musacchio 2013; Foley & Kapoor 2013; Lara-Gonzalez et al. 2012).

1.8 The dynamic instability of microtubules

Microtubules represent the main structural component of the mitotic spindle and their intrinsic properties are essential for spindle assembly and function. They consist of α- and ß- tubulin heterodimers, which are linked in a head-to-tail fashion, thus forming protofilaments, which assemble laterally to build a hollow cylindrical structure of ~25 nm in diameter. Since all tubulin subunits within are oriented the same way, a microtubule exhibits a minus end exposing α-tubulin and a plus end, which is characterized by ß-tubulin. Both ends differ with respect to their dynamic properties (Figure 1.4). While at the minus-end α- and ß- tubulin heterodimers mainly dissociate, the rate of tubulin association at the plus end is much higher. Tubulin subunits are GTPases, which in the cytoplasm mainly exist in the GTP-bound form. When they are incorporated in a growing microtubule they rapidly catalyse their hydrolysis, thus mediating a conformational change and influencing their binding capacities. Newly added α- and ß- tubulin heterodimers form a “GTP-cap” at the plus tip, which leads to a continuous growing of the microtubule. However, when the GTP hydrolysis exceeds the addition of new GTP-bound tubulin, heterodimers start to dissociate from the plus tip and the polymer shrinks. Thus, microtubules abruptly switch between growing and shrinking states, a behaviour known as dynamic instability. Therefore, the transition from polymerization to depolymerization at the plus end is referred to as catastrophe, whereas the sudden change from shrinking to growing is termed rescue. Moreover, the addition of tubulin subunits at the plus tip and the concomitant dissociation of α- and ß- tubulin at the minus end leads to a process termed treadmilling, which describes the continuous migration of α- and ß- tubulin heterodimers from the plus end to the minus end (Helmke et al. 2013; Morgan 2007). The dynamic properties of microtubules are mainly modulated by microtubule associated proteins, which influence growth and shrinkage speed, as well as the frequency of catastrophe and rescue events (van der Vaart et al. 2009; Helmke et al. 2013).

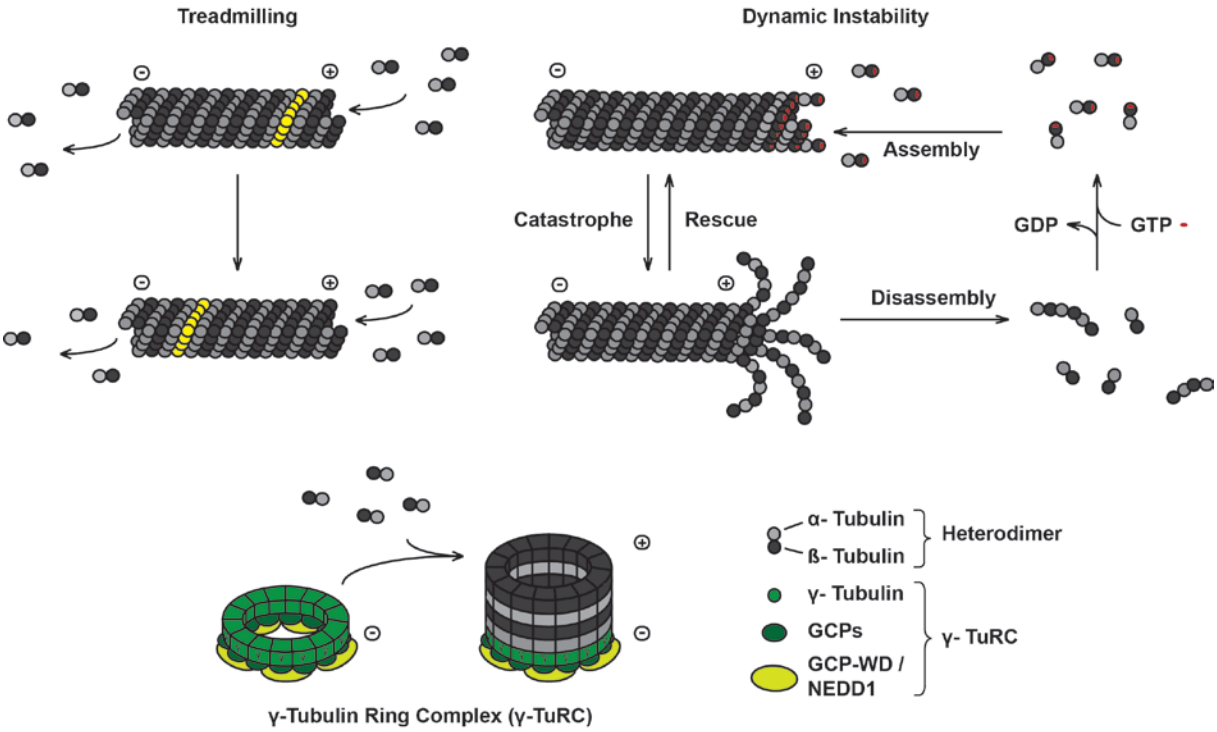

Figure 1.4 Microtubules and their dynamic instability. Microtubules are assembled by α- and ß- tubulin heterodimers, which are incorporated at the plus end. The concomitant assembly at the plus tip and disassembly at the minus end without any net changes in length is termed treadmilling. Moreover microtubules exhibit dynamic instability. The increased incorporation of α- and ß- tubulin heterodimers at the plus-end causes microtubule polymerization and net growth, whereas the disassembly at the tip results in microtubule shrinkage. The transition between growth and shrinkage is referred to as catastrophe and rescue, respectively. γ-tubulin ring complexes (γ-TuRCs), which consists of γ-tubulin and γ-tubulin complex proteins (GCPs), form the basis for microtubule nucleation. Their localization to centrosomes or the mitotic spindle is dependent on the γ-TuRC subunit GCP-WD/NEDD1. Graphic in part modified from Raynaud-Messina & Merdes, 2007.

The nucleation of microtubules is based on pre-existing nucleation centres, of which the most important one is the γ-tubulin ring complex (γ-TuRC) (Figure 1.4). It consists of γ-tubulin complex proteins (GCPs) forming a ring like structure, in which γ-tubulin provides the basis for α- and ß- tubulin heterodimer assembly. Importantly, the γ-TuRC associated protein GCP-WD/NEDD1, which potentially represents a γ-TuRC component itself, is responsible for targeting γ-TuRCs to centrosomes and spindle microtubules, thereby ensuring the assembly of the spindle during mitosis (Raynaud-Messina & Merdes 2007; Lüders & Stearns 2007; Lüders et al. 2006; Haren et al. 2006).

1.9 The assembly of the mitotic spindle

The assembly of the mitotic spindle starts with the separation of the two centrosomes, a process for which the activity of motor proteins is of major importance. While most kinesins (except kinesin-14 familiy members) exhibit a plus-end directed motility along microtubules, dyneins move to their minus-ends. Centrosome separation is mainly

mediated by the mitotic kinesin Eg5 (Tanenbaum & Medema 2010). Its tetrameric composition allows Eg5 to cross-link and slide apart antiparallel microtubules, thus pushing centrosomes to opposing sites (Kapitein et al. 2005). Additionally, the kinesin Kif15 was shown to generate similar outward forces during mitotic spindle formation, however, its role in centrosome separation is only minor (Tanenbaum et al. 2009). Beside its function in spindle positioning, also cortical dynein has been implicated in centrosome separation. Additionally, in cooperation with HSET (Mountain et al. 1999), it maintains permanent inward force for the maintenance of a functional spindle. Importantly, to ensure spindle pole integrity and tension generation for proper chromosome segregation, it is of major importance to keep the balance between outward and inward forces within an established spindle (van Heesbeen et al. 2014).

Microtubules represent the fundamental structure of the mitotic spindle apparatus. Its highly dynamic behaviour is modulated by different microtubule associated proteins (MAPs), which influence polymerization, depolymerization and stability. While, amongst others, TACC3/ch-TOG, EB1 and HURP represent stabilizing MAPs (Cheeseman et al. 2013; Booth et al. 2011; Wong & Fang 2006; Mimori-Kiyosue et al. 2005; Piehl et al. 2004), members of the kinesin families 13, 14 and 8 (e.g. MCAK, Kif2A, Kif2B, Kif18A) as well as AAA ATPase family members were shown to destabilize microtubules (Helmke et al. 2013; Ganem & Compton 2004; Manning et al. 2007; Stumpff et al. 2012; van der Vaart et al. 2009). Within the mitotic spindle three different types of microtubules can be defined. Astral microtubules reach from the poles to the cell cortex and mediate the anchorage and proper positioning of the spindle (Kiyomitsu & Cheeseman 2013; Kiyomitsu & Cheeseman 2012). In contrast, interpolar microtubules range from the poles to the centre being essential for spindle bipolarity, chromosome congression and the assembly of the central spindle (Cai et al. 2009; Magidson et al. 2011; Meunier & Vernos 2012). Moreover, k-fibres, consisting of 20-40 microtubules, link the centrosome with the kinetochore region of chromosomes and directly mediate chromosome congression and segregation (McEwen et al. 1997; Meunier & Vernos 2012; Helmke et al. 2013).

In early stages of mitosis microtubules are mainly nucleated by the centrosome (Figure 1.5). The Aurora A kinase recruits a complex containing TACC3 and ch-TOG to the centrosome and phosphorylates TACC3 at S558, thereby promoting microtubule nucleation activity and the localization of TACC3 (pS558) / ch-TOG complexes to the mitotic spindle (Barr & Gergely 2008; LeRoy et al. 2007; Thakur et al. 2013). The microtubule polymerase ch-TOG stabilizes pre-existing microtubules and mediates the incorporation of α/ß tubulin heterodimers (Brouhard et al. 2008; Widlund et al. 2011). Additionally, along microtubules, the TACC3 (pS558) / ch-TOG complexes interact with clathrin heavy chains and further stabilize microtubule fibres by intermediary cross

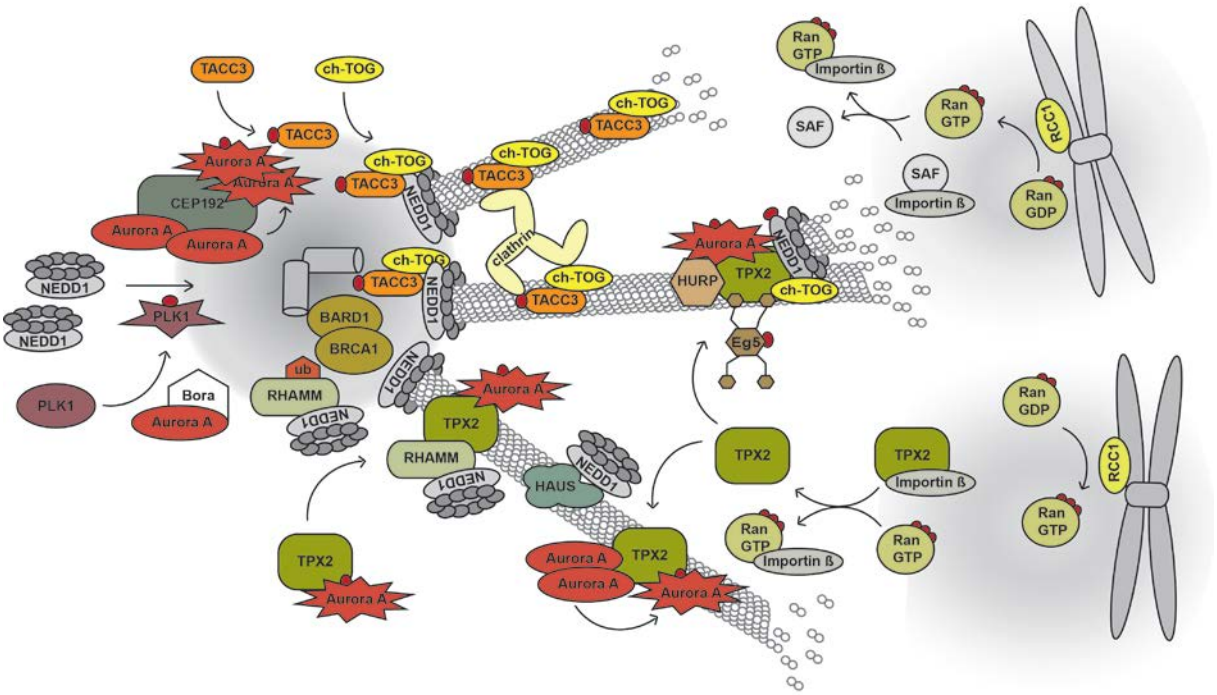

Figure 1.5 Mechanisms of mitotic spindle assembly. For centrosome dependent assembly of the mitotic spindle the Aurora A kinase and its cofactor Bora activate the Polo-like kinase 1 (Plk1). Plk1 is involved in γ-TuRC recruitment to the centrosome and coordinates mitotic progression. The recruitment of Aurora A to the centrosome is mediated by Cep192, which simultaneously triggers the auto-activation of the kinase. Aurora A recruits TACC3 to the centrosome, which, when phosphorylated, recruits and interacts with the microtubule polymerase ch-TOG. Together both proteins might contribute to microtubule nucleation at the centrosome and promote microtubule polymerization at the plus tip. Additionally, TACC3 and ch-TOG interact with clathrin, which cross-links microtubules and therefore, increases their stability. Furthermore, spindle assembly is promoted by the chromosome associated Ran GTP dependent pathway. The chromatin-associated nucleotide exchange factor RCC1 creates a Ran-GTP gradient around the chromosomes. Ran-GTP in turn triggers the release of TPX2 (and other spindle associated factors (SAFs)) from importins mediating its localization to spindle microtubules. Here TPX2 recruits Aurora A, facilitates its auto-phosphorylation at T288 and initiates the formation of a complex containing γ-TuRCs, ch-TOG, HURP and Eg5. Thus, the Aurora A mediated phosphorylation of the complex components triggers centrosome separation and microtubule de novo nucleation at the mitotic spindle. Simultaneously the TPX2/Aurora A complex is involved in RHAMM dependent recruitment of γ-TuRCs to the mitotic spindle. Moreover, the HAUS complex mediates γ-TuRC dependent microtubule amplification on the basis of pre-existing microtubules.

linking (Thakur et al. 2013; Royle 2012; Lin et al. 2010; Booth et al. 2011; Fu et al. 2010). After nuclear envelope breakdown (NEB) microtubule nucleation is also centrosome independently controlled by the chromatin mediated Ran GTP dependent pathway (Gruss et al. 2002; Gruss et al. 2001; Meunier & Vernos 2012) (Figure 1.5). Present on chromatin the Ran guanine nucleotide exchange factor RCC1 (Karsenti & Vernos 2001; Li et al. 2003) creates a Ran-GTP gradient that is formed around the chromosomes triggering the release of importin α and ß from many spindle assembly factors and therefore enabling their function in spindle assembly (Meunier and Vernos 2012). Most importantly, the Ran-GTP gradient in the vicinity of chromosomes leads

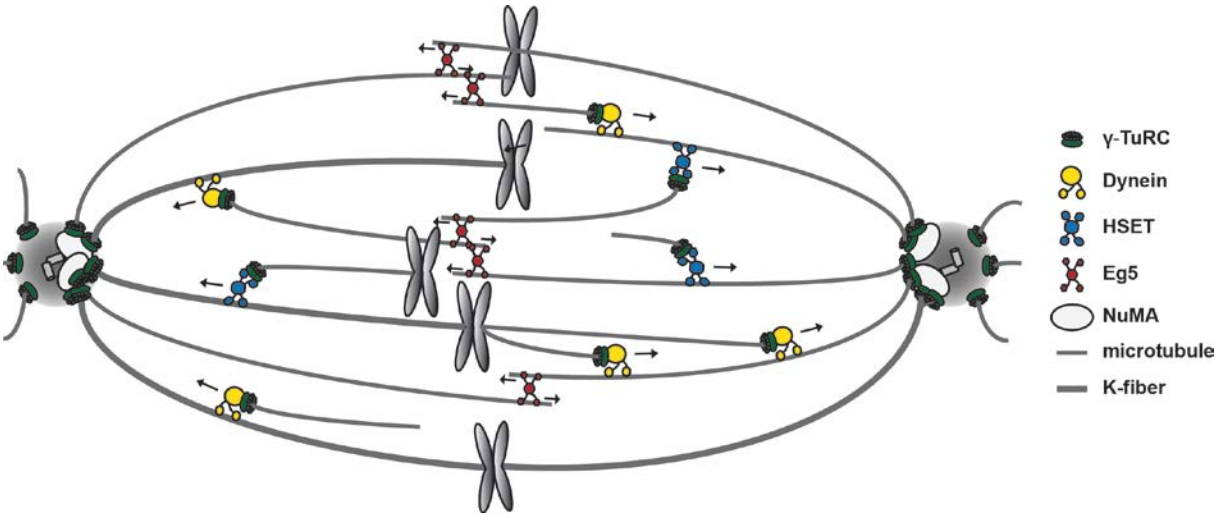

Figure 1.6 Focussing γ-TuRCs at centrosomes. Centrosome independent spindle assembly pathways cause microtubule nucleation on the basis of γ-TuRCs within the mitotic spindle. Thus, γ-TuRCs are distributed along spindle microtubules in proximal distance to the poles and have to be focussed at centrosomes. Their direct transport is mediated by the minus-end directed motor proteins dynein and HSET. Additionally, the poleward movement of γ-TuRCs is facilitated by the plus-end directed kinesin Eg5, which cross-links antiparallel microtubules and generates outward forces by antiparallel sliding. The incorporation of γ-TuRCs into the pericentriolar material is mediated by NuMA. Parts of the graphic were modified from (Lecland & Lüders 2014).

to a release of TPX2 from importin ß, which then localizes to spindle microtubules (Gruss et al. 2002; Gruss et al. 2001) where it provides a binding platform for Aurora A (Eyers & Maller 2004; Eyers & Maller 2003; Neumayer et al. 2014). This interaction promotes a conformational change of Aurora A, hence, triggering its auto-activation and simultaneously protecting Aurora A from dephosphorylation by the protein phosphatase 1 (PP1) (Neumayer et al. 2014). Bound to TPX2 the activity of Aurora A is required for the formation and activation of a complex consisting of TPX2, Eg5, HURP, ch-TOG, γ-tubulin and Aurora A itself being involved in spindle morphogenesis (Neumayer et al. 2014; Tsai et al. 2003; Wong & Fang 2006; Wong et al. 2008; Eyers & Maller 2003). Moreover, TPX2 was shown to be involved in RHAMM (HMMR) dependent recruitment of γ-TuRCs to the mitotic spindle, where the Aurora A mediated phosphorylation of NEDD1/GCP-WD40 at S405 leads to microtubule nucleation (Scrofani et al. 2015; Pinyol et al. 2013).

Another non-centrosomal pathway for microtubule amplification is dependent on pre-existing microtubules and involves the Augmin or homologous to augmin subunits (HAUS) complex, which mediates the NEDD1/GCP-WD40 and γ-TuRC based microtubule nucleation within the spindle (Lawo et al. 2009; Goshima et al. 2008; Goshima & Kimura 2010) (Figure 1.5).

Thus, both, the Augmin/HAUS and the Ran-GTP dependent microtubule nucleation pathway result in microtubules being attached to γ-TuRCs, which are distributed along microtubules in proximal distance from the spindle poles. In order to cluster the minus

ends at the centrosome γ-TuRCs are transported along microtubules by the minus-end directed motors dynein and HSET (Lecland & Lüders 2014) (Figure 1.6). Additionally, Eg5 participates in poleward movement by connecting antiparallel microtubules at the central spindle and generating an outward force by sliding (Kapitein et al. 2005; Lecland & Lüders 2014; Tanenbaum & Medema 2010). Thus γ-TuRCs accumulate at the centrosome where they are incorporated into the pericentriolar material by NuMA (Fant et al. 2004; Lecland & Lüders 2014).

1.10 The centrosome and centriolar satellites

The centrosome represents the major microtubule organizing centre (MTOC) in the cell being involved in the regulation and maintenance of cell motility, adhesion and polarity (Bettencourt-Dias & Glover, 2007; Nigg & Raff, 2009; Pihan 2013). Additionally it forms the basis for the establishment of the primary cilium (Hoyer-Fender 2010). While the MTOC enables intra cellular transport of proteins and organelles along microtubules in interphase (Stearns & Kirschner 1994), it plays a major role in mitosis where it ensures the proper segregation of chromosomes by establishing and anchoring the mitotic spindle (Bettencourt-Dias & Glover, 2007; Nam et al. 2014; Pihan, 2013).

Centrosomes consist of two orthogonally arranged centrioles, which are formed by nine sets of microtubule triplets being organized in a cartwheel structure (Figure 1.7). The centrioles form the structural scaffold promoting the organization of the pericentriolar material (PCM), which consists of over 100 proteins implicated in protein degradation, cell cycle progression and cell division (Menella et al 2014, Pihan 2014, Andersen 2003, Bettencourt-Dias 2007, Bornens 2012, Lüders and Stearns 2007, Nam et al. 2014, Pihan et al. 2013). It provides a platform for protein signalling, regulation and redistribution, and functions to anchor microtubules. In contrast to the assumption that the PCM is an amorphous mass of proteins (Bornens 2012; Bärenz et al. 2011), new high resolution fluorescence microscopy revealed a highly organized structure of two organization layers (Menella et al. 2012; Sonnen et al. 2012; Fu & Glover 2012; Lawo et al. 2012; Menella et al. 2014). The so called proximal layer is organized as molecular fibres mainly consisting of pericentrin or Cep152, which are C-terminally anchored to centrioles, while their N-terminal part localizes to the periphery (Figure 1.7). Around the centriole wall the second layer is organized in a matrix structure being interspersed with proteins like Cep192, CDK5RAP2/Cep215 and γ-tubulin (Menella et al. 2012; Sonnen et al. 2012; Fu & Glover 2012; Lawo et al. 2012; Menella et al. 2014). When centrosomes maturate in late G2 phase and early mitosis, the PCM drastically expands (Lee & Rhee, 2010; Nam et al., 2014; Menella et al., 2014) accumulating proteins, including the mitotic kinases Plk1 and Aurora A, that regulate mitotic entry, spindle assembly, sister chromatid separation

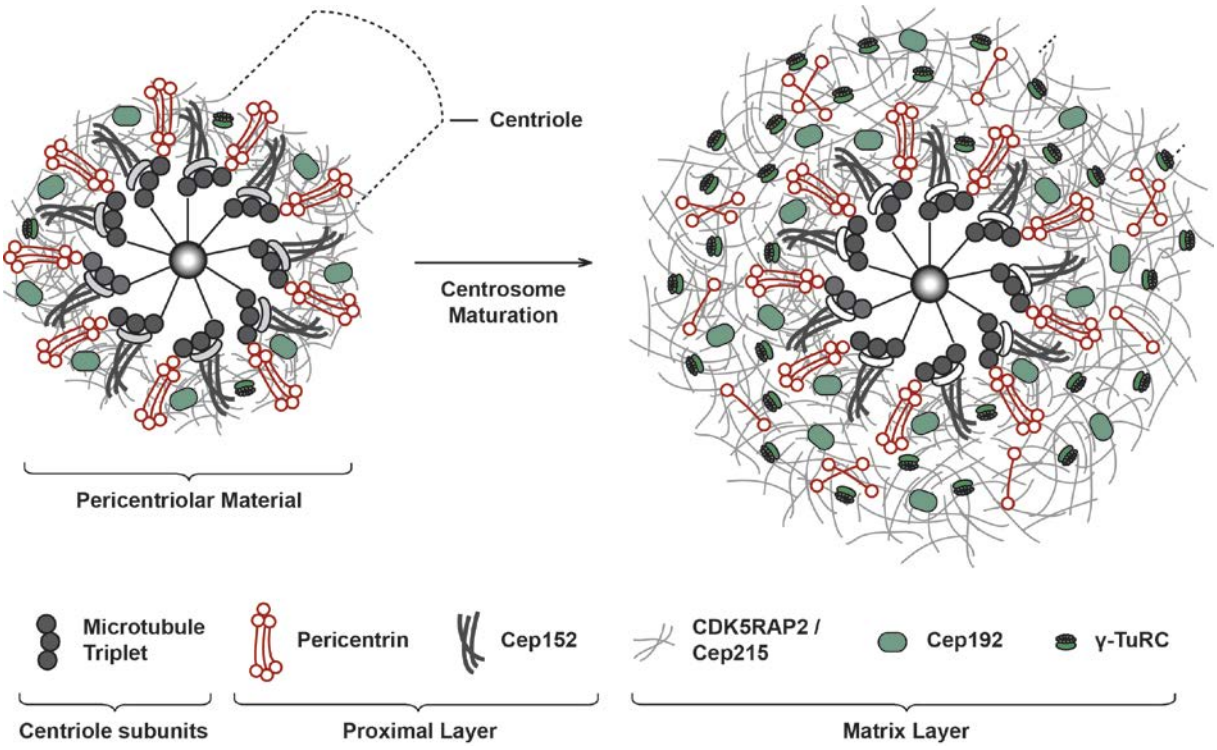

Figure 1.7 Centrosome structure. Centrosomes consist of two orthogonally arranged centrioles, which are formed by nine sets of microtubule triplets being arranged in a cartwheel structure. The pericentriolar material, which surrounds the centrioles is organized in two main layers. The proximal layer is organized as molecular fibres mainly consisting of pericentrin or Cep152. Around the centriole wall CDK5RAP2/Cep215 is arranged in a matrix structure, which is interspersed with proteins like Cep192 and γ-tubulin. When the centrosome undergoes maturation the PCM drastically expands and accumulates proteins involved in mitotic regulation. Both, the proximal and the matrix layer extend to the outer environment and γ-TuRCs are increasingly incorporated into the PCM matrix. Graphic modified from Menella et al., 2014.

(Macůrek et al. 2008; Seki et al. 2008; Nigg 2002) and coordinate the progression through mitosis (Taylor & Peters 2008; Petronczki et al. 2008; De Cárcer et al. 2011; Hochegger et al. 2013). Additionally Plk1 phosphorylates the centrosomal regulator Kizuna, which is crucial for the stabilization of the PCM and thus, ensures its structural integrity. In order to form the mitotic spindle the amount of γ-TuRCs increases more than threefold during centrosome maturation (Khodjakov & Rieder, 1999; Lüders et al. 2006). While γ-TuRCs are recruited to the centrosome by CDK5RAP2/Cep215, pericentrin/kendrin and AKAP450/CG-NAP, their anchorage is mediated by ninein and GCP-WD/NEDD1 (Haren et al. 2006; Lüders et al. 2006; Oshimori et al. 2009; Pihan 2013; Delgehyr et al. 2005; Raynaud-Messina & Merdes 2007; Takahashi et al. 2002; Zimmerman et al. 2004; Fong et al. 2008). Tethered to the PCM, γ-TuRCs provide a platform for microtubule nucleation and polymerization being essential for mitotic spindle formation and anchorage (Raynaud-Messina & Merdes 2007; Wiese & Zheng 2006; Zheng et al. 1995). Since after cell division the emerging daughter cells only possess one centrosome consisting of a mother and a daughter centriole, the centrosome has to be

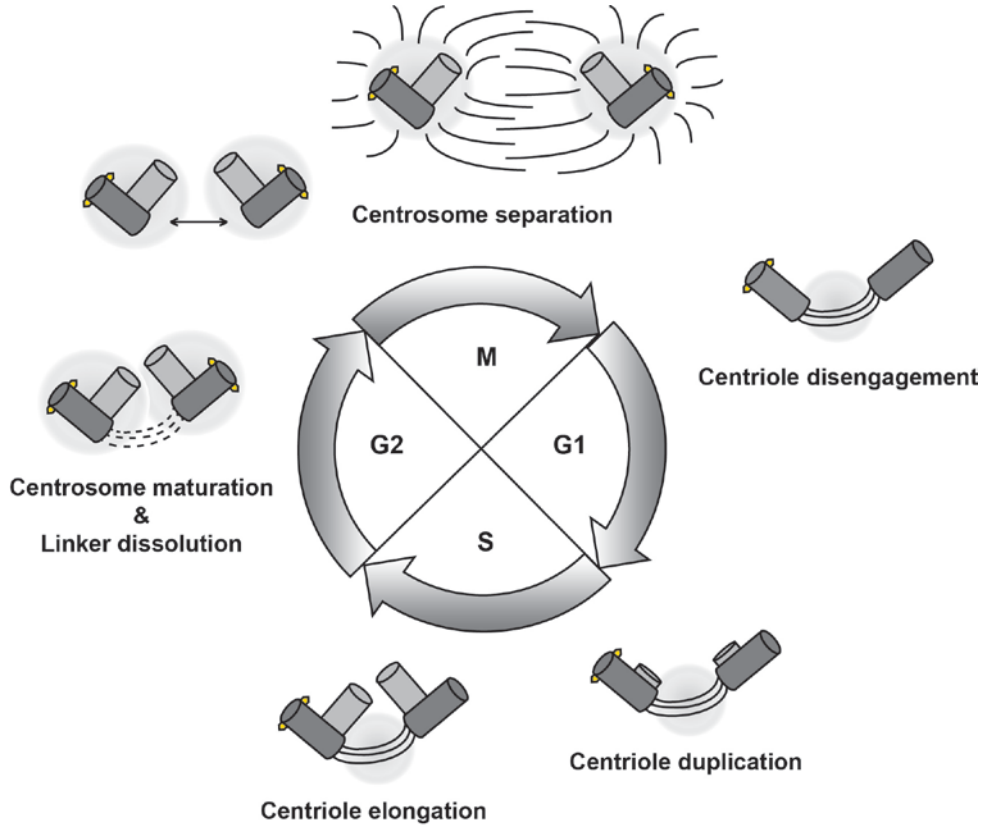

Figure 1.8 The Centriole duplication cycle. As cells exit from mitosis the daughter centriole disengages from the mother centriole (marked with yellow appendages). In early S-phase both centrioles starts to form new centrioles which elongate until G2-phase. In late G2 centrosome maturation takes place. Upon linker dissolution, centrosomes separate in order to form a bipolar spindle. Parts of the graphic were modified from Nam et al. 2014 and Mardin & Schiebel 2012.

duplicated once per cell cycle (Figure 1.8) During early G1 phase the daughter centriole disengages from the mother centriole, leading to the loss of the orthogonal arrangement (centriole disengagement). However, both centrioles remain connected by a linker. In early S phase a new daughter centriole is synthetized by each centriole (centriole duplication), which elongates until it reaches a final length in late G2 phase (centriole elongation). At the G2/M transition the two pairs of centrioles loose the flexible linker and run through the maturation process in early mitosis. Subsequently the two centrosomes separate and are finally segregated onto daughter cells where they start a new duplication cycle on their own (Nigg & Raff 2009; Nigg 2002; Holland et al. 2010; Bettencourt-Dias & Glover 2007; Mardin & Schiebel 2012; Nam et al. 2014).

Around the centrosome centriolar satellites localize in a cell cycle dependent manner. While they are present throughout interphase, they gradually disappear in mitosis and re-accumulate in telophase (Kubo & Tsukita 2003; Bärenz et al. 2011). Moving along microtubules in a dynein and possibly kinesin dependent manner, centriolar satellites provide a networking platform for several different proteins (Bärenz et al. 2011).

Since centriolar satellites contain a range of centrosomal proteins, they are proposed to fulfil a function in protein storage and delivery to the centrosome supporting key cellular processes that are dependent on a rapid change of the centrosomal protein composition such as cell division and primary cilium formation (Bärenz et al. 2011; Villumsen et al. 2013). In accordance with this, the localization of several key centrosomal proteins like centrin, pericentrin and ninein was shown to be dependent on the pericentriolar protein 1 (PCM1) forming the central molecular scaffold for centriolar satellites (Dammermann & Merdes 2002; Purohit et al. 1999). Interestingly PCM1 containing centriolar satellites have also been implicated in the transport of the Nek2 kinase involved in G2/M transition and proteins protecting the structural integrity of the centrosome against spindle mediated forces during mitosis like Kizuna, Cep72, Cep90 and SSX2IP (Bärenz et al. 2011; Bärenz et al. 2013; Kim et al. 2012). Accordingly, interfering with the transport function of pericentriolar satellites effects centrosome structure and results in improper microtubule anchorage and organization (Bärenz et al. 2011). Moreover, many proteins involved in cilia formation such as BBS4, Cep290, Cep72, Cep131, FOR20, Ccdc13 and OFD1 localize to centriolar satellites and their delocalization is linked to the induction of ciliopathies indicating that centriolar satellites are crucial for ciliogenesis (Bärenz et al. 2011; Staples et al. 2012; Staples et al. 2014). In the absence of PCM1 and, hence, centriolar satellites, proteins such as Cep290, Cep72, ODF1 and FOR20 accumulate at the centrosome, suggesting that centriolar satellites might also fulfil a function in restraining the direct centrosomal localization of such proteins, thus contributing to the regulation of the centrosome (Stowe et al. 2012; Lopes et al. 2011).

1.11 Aneuploidy and chromosomal instability

The proper progression through mitosis ensures the maintenance of a defined set of chromosomes and thereby the euploidy of a cell. However, only subtle defects in this tightly regulated process can lead to chromosome mis-segregation and aneuploidy, representing a common state of most solid tumours (Orr & Compton 2013). Actually, around the turn of the 18th to the 19th century, David Hansemann and Theodor Boveri already stated that abnormal cell division induces aneuploidy and tumourigenesis (Boveri 1914; von Hansemann 1890). Nonetheless, the connection between aneuploidy and cancer remains controversially discussed (Ricke & van Deursen 2013; Holland & Cleveland 2012; Weaver et al. 2007). Beside the unique gain or loss of one or a few chromosomes, the perpetual mis-segregation of chromosomes during mitosis, which is defined as whole chromosomal instability (W-CIN), is a common cause for aneuploidy and represents a hallmark of human cancer. In contrast to W-CIN, in which cells are unable to properly segregate whole chromosomes, the susceptibility to structural rearrangement including translocations, inversions, deletions and duplications of

chromosomal parts is referred to as structural chromosomal instability (S-CIN) (Ricke & van Deursen 2013; Thompson et al. 2010). However, the further course of this work focusses on whole chromosomal instability, so that the term CIN refers to W-CIN.

In general, the rate of chromosome mis-segregation is crucial for the cells fate. While CIN at low levels (0.2 to maximal 1 chromosome per cell cycle) enables the accumulation of tumour promoting factors and the ability for environmental adaption (Orr & Compton 2013; Thompson et al. 2010; Lengauer et al. 1997), high rates of chromosome mis-segregation cause mitotic catastrophe and subsequent apoptosis (Vakifahmetoglu et al. 2008; Manchado et al. 2012; Kops et al. 2004). Moreover, CIN was shown to be disadvantageous for cell proliferation and tumour growth, which might be due to the fact that altered chromosome numbers lead to proteotoxic stress and changes in the metabolism (Ertych et al. 2014; Sheltzer & Amon 2011; Williams et al. 2008; Weaver et al. 2007). However, CIN increases the genetic variability and adaptability of cells and tumours, hence, providing a trigger for tumour initiation and the basis for tumour formation and therapy resistance (Orr & Compton 2013; Thompson et al. 2010; Lengauer et al. 1997; Holland & Cleveland 2012).

1.12 Routes to whole chromosomal instability

Whole chromosomal instability is defined as the perpetual gain and loss of chromosomes during mitosis. Accordingly, various defects within this tightly regulated cell cycle phase can lead to continual mis-segregation. An impaired mitotic spindle assembly checkpoint represents the first lesion suspected to cause CIN (Cahill et al. 1998; Holland & Cleveland 2012; Orr & Compton 2013). To ensure proper chromosome segregation the SAC senses proper kinetochore microtubule attachments and emits a diffusible “wait anaphase” signal until all chromosomes are amphitelically attached to microtubule emanating from two opposing spindle poles (Figure 1.3). Hence, an impaired SAC results in premature anaphase onset in the presence of mal-attached kinetochores, which in turn leads to chromosome mis-segregation during cell division. Nonetheless, mutations in SAC associated genes are very rare (Barber et al. 2008) and a total loss of the spindle assembly checkpoint leads to cell death (Kops et al. 2004). Therefore, the relevance of a weakened mitotic SAC for the induction of CIN in human cancer is controversial (Orr & Compton 2013). However, it is clear that the persistence of erroneous microtubule kinetochore attachments is associated with CIN (Silkworth & Cimini 2012; Gregan et al. 2011). Especially merotelic attachments, in which a single kinetochore is concomitantly attached to spindle microtubules emanating from both poles (Figure 1.3) are critical for the maintenance of chromosomal stability. Since the kinetochores are bound to microtubules and tension between the two sister kinetochores is generated, merotely is

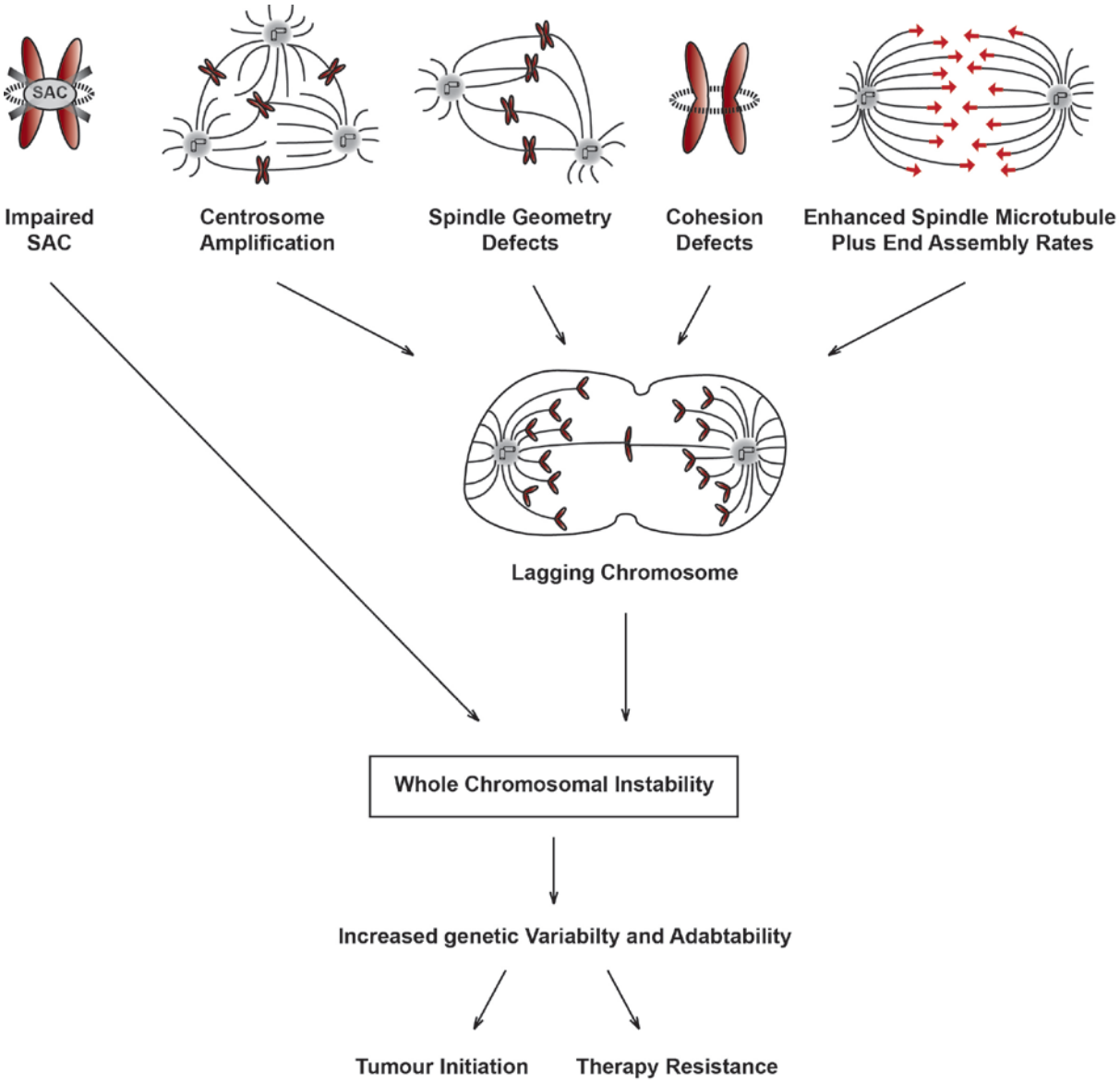

Figure 1.9 Routes to whole chromosomal instability. An impaired spindle assembly checkpoint leads to premature anaphase onset and the perpetual missegregation of whole chromosome during mitosis (whole chromosomal instability). Moreover centrosome amplification, spindle geometry defects, cohesion defects or increased spindle microtubule plus end assembly rates trigger the formation of merotelic microtubule-kinetochore attachments and lagging chromosomes representing a main cause for CIN. Chromosomal instability increases the genetic variability and adaptability of a cell, thus, providing a trigger for tumour initiation and therapy resistance.

not detected by the SAC and anaphase is initiated. As a consequence, the respective chromatid fails to be properly segregated and lags in the equatorial plane of the cell. Such 'lagging chromosomes' are subsequently distributed onto daughter cells by chance and represent a main cause for chromosomal instability (Orr & Compton 2013; Vitre & Cleveland 2012; Thompson et al. 2010; Silkworth & Cimini 2012; Gregan et al. 2011). Another route to CIN is the presence of supernumerary centrosomes, which mainly arises from defects in their biogenesis or by overduplication (Vitre & Cleveland 2012; Holland & Cleveland 2012), promoting the formation of merotelic attachments, lagging

chromosomes and the induction of CIN (Orr & Compton 2013). Albeit enhanced numbers of centrosomes are usually clustered by the kinesin-14 family member HSET to allow the formation of a bipolar spindle before anaphase onset (Brinkley 2001), a transient multipolar intermediate state is sufficient to induce kinetochore-microtubule mal-attachments (Ganem et al. 2009; Silkworth & Cimini 2012) (Figure 1.10). Similarly, altered centromere geometry caused by pericentric cohesion defects impedes the establishment of amphitelic attachments (Ng et al. 2010; Solomon et al. 2011). Additionally, the tight regulation of centrosome separation in prophase ensuring proper bi-oriented spindle geometry is crucial for the maintenance of chromosomal stability (Nam et al. 2014; Silkworth & Cimini 2012; Silkworth et al. 2012). Delayed centrosome separation results in a state where centrosomes are still located in close proximity when the nuclear envelope breaks down. By transient formation of monopolar or near-monopolar spindle intermediates, kinetochores are accessible to microtubules emanating from both spindle poles, which promotes the formation of synthelic or merotelic attachments. When centrosomes separate in the further course of mitosis, mal-attachments persist and facilitate chromosome mis-segregation in anaphase (Nam et al. 2014; Silkworth & Cimini 2012). Moreover, both, delayed and accelerated centrosomes disjunction as well as improper anchoring of astral microtubules at the cell cortex can result in spindle asymmetry in metaphase that might additionally trigger the formation of merotelic kinetochore-microtubule attachments, lagging chromosomes and improper chromosome segregation (Nam et al. 2014). Importantly, our group identified enhanced spindle microtubule plus end assembly rates during mitosis as novel route to chromosomal instability. Like lesions described before, increased spindle microtubule polymerization triggers transient spindle geometry defects, which are accompanied by the establishment of hyper-stable kinetochore-microtubule attachments and lagging chromosomes (Ertych et al. 2014). Since error-correction is not affected by enhanced spindle microtubule dynamics it is supposed that the increased formation of erroneous microtubule-kinetochore attachments overwhelms the error-correction machinery (Ertych et al. 2014; Stolz et al. 2014). Remarkably, increased spindle microtubule plus end assembly seems to be a key trigger for the induction of CIN in human colorectal cancer. Whereas chromosomally stable colorectal cancer cell lines showed proper spindle microtubule polymerization rates during mitosis, it was determined to be significantly increased in all chromosomally instable cell lines analysed. Moreover, genetic lesions like loss of the tumour suppressor genes *CHK2* and *BRCA1* as well as amplification of the oncogene *AURKA,* which are found to be present in up to 70% of colorectal cancer patients are linked to the induction of elevated spindle microtubule assembly rates. Thus, increased microtubule polymerization during mitosis represent a fundamental mechanism influencing CIN (Ertych et al. 2014; Stolz et al. 2014).

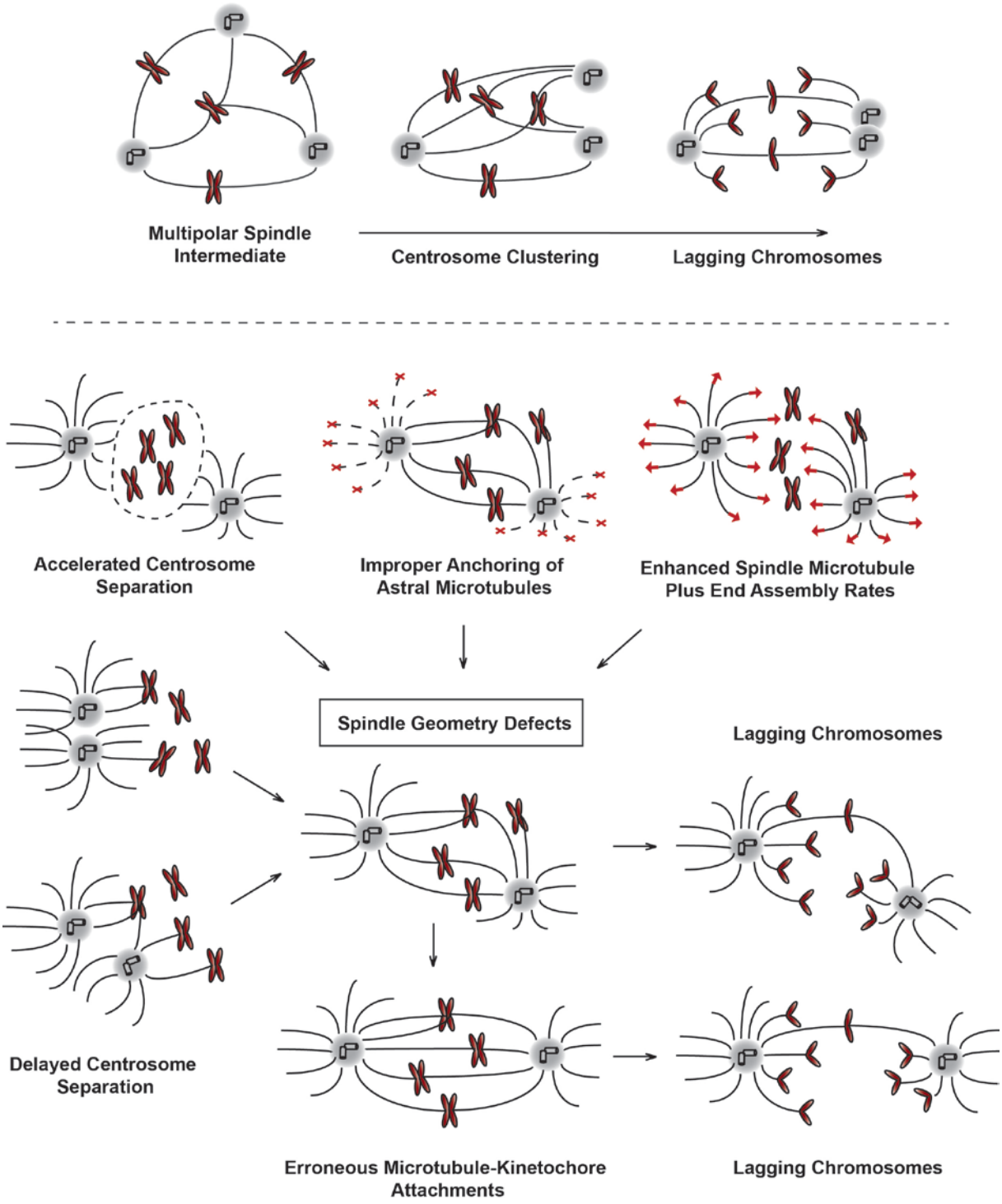

Figure 1.10 Spindle geometry defects lead to merotelic kinetochore-microtubule attachments and the formation of lagging chromosomes. a) Supernumerary centrosomes result in the formation of multipolar spindles. In order to form a bipolar spindle centrosomes are clustered, which promotes merotelic attachments and lagging chromosomes. **b)** Delayed centrosome separation and, hence, centrosomes located in close proximity when the nuclear envelope breaks down results in transient monopolar or near-monopolar spindles triggering the formation of merotelic attachments. In addition, accelerated centrosome separation as well as improper anchoring of astral microtubules and increased spindle microtubule plus end assembly rates causes (transient) spindle geometry defects promoting erroneous kinetochore-microtubule attachments and lagging chromosomes. Parts of the graphic were modified from Silkworth & Cimini 2012.

In addition to lagging chromosomes being a main reason for the mis-segregation of whole chromosomes during mitosis (W-CIN), other segregation errors like chromatin bridges and acentric chromatin can be observed during anaphase. These kinds of defects are mainly caused by DNA damage as well as replication stress and represent hallmarks of structural chromosomal instability (Burrell et al. 2013). Moreover, lagging chromosomes, which are finally not segregated onto daughter cells, are partitioned in micronuclei where they undergo severe DNA damage during interphase. Subsequently these chromosomes are partially reincorporated into daughter cells and thus, contribute to the emergence of S-CIN (Crasta et al. 2012). Apart from the well-founded assumption that W-CIN is mainly dependent on chromosome segregation errors during mitosis, a recent study proposed that pre-mitotic events like replication stress causing S-CIN are responsible for most anaphase defects (Burrell et al. 2013). Supporting this notion it was shown, that DNA-damage during mitosis partially triggers the DNA damage response by ATM dependent phosphorylation of the checkpoint kinase 2 (Chk2), which in turn results in Aurora A and Plk1 dependent hyper-stability of microtubule-kinetochore attachment, lagging chromosomes and W-CIN (Bakhoum et al. 2014). However, whether DNA damage is a cause or a consequence of W-CIN remains unclear.

1.13 The tumour suppressor gene *BRCA1*

The tumour suppressor gene breast cancer 1, early onset *(BRCA1)* was initially identified in 1994 as the first gene influencing the susceptibility to breast and ovarian cancer (Miki et al. 1994).

Brca1 is a protein of 220 kDa exhibiting at least three different functional domains. The N-terminus features a RING domain, which allows the formation of a heterodimer with its obligatory binding partner Brca1 associated RING domain protein 1 (BARD1). This binding is crucial for interdependent protein stabilization and together Brca1 and BARD1 complement an E3-ubiquitin ligase being responsible for the ubiquitination of numerous substrates (e.g. H2A, H2B, H3, H4, CtIP, NPM1, RPB8 and TFIIE) (Hashizume et al., 2001; Wu et al. 2008; Savage & Harkin, 2014). Importantly the Brca1/BARD1 complex mainly mediates the uncommon K6-linked ubiquitination, which rather represents a protein modification than a signal for degradation (Morris & Solomon, 2004; Nishikawa et al., 2004; Wu-Baer et al. 2003). In addition to signals for the nuclear import and export (NLS and NES), Brca1 exhibits two BRCA1 C-Terminal (BRCT) domains representing phospho-protein specific binding motifs (Henderson 2012; Yu 2003). Thus, Brca1 forms a scaffold for the formation of various protein complexes being involved in numerous cellular processes throughout the cell cycle (Savage & Harkin 2014).

Brca1 plays an important role in the cellular stress response upon DNA damage, where it is regulated by phosphorylation mediated by different serine/threonine kinases (e.g. ATM, ATR, CDK1, CDK2, Chk2) (Savage & Harkin 2014; Ouchi 2006; Scully et al. 2004). It is involved in the regulation of transcription and mRNA splicing in order to efficiently produce proteins being involved in DNA damage repair and cell cycle checkpoint arrest (Savage & Harkin 2014). By targeting RNA polymerase II for degradation, Brca1 simultaneously inhibits the mRNA stabilizing 3' polyadenylation and thus, blocks the protein translation after DNA damage (Kleiman et al. 2005). Additionally it is assumed that Brca1 participates in non-homologous end joining (NHEJ), however, its direct role remains unknown (Wei et al., 2008; Zhong, Boyer et al., 2002; Zhong, Chen et al., 2002). In contrast, the function of Brca1 in homologous recombination (HR) is mainly characterized and defined by four independent Brca1 protein complexes: BRCA1-A including RAP80, MERIT40, BRCC36/45 and Abraxas, BRCA-B (Brca1, TopBP1 and BACH1), BRCA1-C consisting of Brca1, MRN (Mre11, Rad50, Nbs1) and CtIP and the BRCC complex (Brca1, Brca2, PALB and Rad51). DNA damage initially causes the formation of single stranded DNA, which is recognized and bound by the replication protein A (RPA) in order to prevent the formation of secondary structures (Savage & Harkin 2014). Based on Chk2-mediated phosphorylation of Brca1 at Ser988 (Scully et al. 2004; J. Zhang et al. 2004), the BRCA1-C complex promotes HR compared to the error prone NHEJ. Moreover, BRCA1-C initiates and, in combination with BRCA1-B, Exo1 and DNA2, extends the resection of double strand break ends. Additionally BRCA1-B and -C activate the intra-S-phase checkpoint, whereas BRCA1-A prevents over-resection and stimulates the G2/M checkpoint. Subsequently, the BRCC complex mediates the exchange of RPA by Rad51, thereby initiating sister chromatid invasion and the formation of Holliday junctions. Based on the complementary DNA strand of the sister chromatid the DNA is replicated, whereupon the Holliday junction is resolved and the DNA ends are re-ligated (Savage & Harkin 2014; Liu et al. 2014; Escribano-Díaz et al. 2013; Sy et al. 2009; Cruz-Garcia et al. 2014).

Aside from its function in DNA damage repair, Brca1 plays an important role at the centrosome, where it is localized throughout the cell cycle (Starita & Parvin 2006). Here the Brca1/BARD1 complex together with Obg-like ATPase 1 (Ola1) interacts with and ubiquitinates γ-tubulin as well as an unknown adaptor protein during interphase, leading to a disassembly of γ-TuRCs from the centrosome and a low microtubule nucleation potential (Matsuzawa et al., 2014; Sankaran & Parvin, 2006; Sankaran et al., 2005; Sankaran et al., 2006; Starita et al., 2004). During mitosis Brca1 is phosphorylated by the Aurora A kinase at S308, which inhibits its E3-ubiquitin ligase activity (Ouchi et al. 2004). Thus, the Brca1/BARD1 mediated ubiquitination of γ-TuRC subunits is abolished resulting in a high microtubule nucleation potential during mitosis (Sankaran et al.,

2007). Additionally, the ubiquitination activity of the Brca1/BARD1 heterodimer was shown to inhibit centrosome amplification and hyperactivation in breast cancer cell lines (Schlegel et al., 2003). However, this could not be observed in other cell types (Starita et al. 2004; Starita & Parvin 2006).

While most studies only focus on its interphase function, Brca1 might play a major role during mitosis, where Brca1 is mostly localized at centrosomes (Hsu & White 1998). Here, the Chk2 mediated phosphorylation of Brca1 at S988 ensures the proper assembly of the mitotic spindle (Stolz et al. 2010). However, a loss of Brca1 or Chk2 leads to an accumulation of active Aurora A kinase at mitotic centrosomes, which in turn causes increased spindle microtubule plus end polymerization and spindle orientation defects resulting in chromosome mis-segregation and chromosomal instability (Stolz et al. 2010; Ertych et al. 2014). Nevertheless, the exact mechanism and how the pathway is regulated during mitosis remain elusive. Beside this centrosomal function, Brca1 was also shown to be involved in centrosome independent Ran-GTP mediated spindle formation during mitosis. Here it is assumed that the Brca1/BARD1 heterodimer ubiquitinates the microtubule associated protein RHAMM (HMMR) and modulates its function to form a bipolar mitotic spindle (Joukov et al. 2006; Maxwell et al. 2003).

BRCA1 is a major tumour suppressor gene, which is mainly associated with breast and ovarian cancer where Brca1 mutations or a loss of the gene itself are most prominent. These lesions have been shown to be associated to cancer predisposition and formation, whereupon the exact reason and also the tissue specificity remains less understood (Savage & Harkin 2014). Since Brca1 exhibits various functions, it is unclear how Brca1 exerts its tumour suppressive function. Additionally, it is controversially discussed, which domain of Brca1 is crucial for maintaining its tumour suppressive role. While some observations suggest that the ubiquitin-E3-ligase activity is needed to prevent tumour formation (Zhu et al. 2011), others claim that this function is dispensable and that the BRCT domains providing phospho-peptide binding motifs play the major role in tumour suppression (Shakya et al. 2011). In turn another study shows that the binding to Bard1 might be most important for the tumour suppressing activity of Brca1 (Drost et al. 2011).

1.14 The centrosomal protein Cep72

Cep72 (centrosomal protein of 72 kDa) is a protein, which was initially identified in a mass-spectrometry based proteomic analysis of human centrosomes (Andersen et al. 2003). It comprises 647 amino acids and harbours with two leucine-rich repeats (N-terminal region) and a coiled coil domain (C-terminal region) two structural motifs, whose function remains unclear. To date Cep72 is a poorly studied protein, which was shown to exhibit at least two main functions.

Cep72 localizes to centrosomes throughout the cell cycle. It was shown to be involved in the maintenance of the structural integrity by targeting the centrosomal regulator Kizuna to the centrosome, where it fulfils its function in stabilizing the pericentriolar material. Especially during mitosis, when the forces emerging from microtubules being attached to chromosomes are particularly high, this function prevents centrosome disintegration and the formation of multipolar spindles (Oshimori et al. 2009; Oshimori et al. 2006). Additional observations indicate that Cep72 is involved in the recruitment of γ-tubulin ring complexes to the centrosomes where it also maintains their microtubule potential by simultaneous recruitment of the centrosomal scaffolding protein CG-NAP/AKAP450 conferring microtubule nucleation activity (Oshimori et al. 2009; Takahashi et al. 2002).

Moreover, Cep72 was shown to interact with the scaffolding component of centrosomal satellites PCM1. Consequently, Cep72 also localizes to centrosomal satellites where it is involved in proper cilium formation of resting cells. Cep72 is crucial for the localization of the ciliopathy associated protein Cep290 and together both proteins mediate the relocalization of the Bardet-Biedl syndrome (BBS)ome component BBS4 from centriolar satellites to the centrosome in order to form the BBSome complex. Additionally Cep72 was shown to maintain a normal distribution of centrosomal satellites, however, an overexpression results in their disassembly and the formation of cytoplasmic aggregates. The depletion of PCM1 and thus, the destruction of centrosomal satellites leads to an accumulation of Cep72 to centrosomes, indicating that centrosomal satellites might sequester Cep72 and prevent its pericentriolar localization (Stowe et al. 2012). Our group has identified Cep72 as a protein interacting with Brca1 during mitosis, which represents the basis for this work.

1.15 Scope of the study

BRCA1 is a major tumour suppressor gene, which is mainly associated with breast and ovarian cancer (Miki, Y. et al. 1994). Since Brca1 represents a multifunctional protein being involved in a variety of cellular processes throughout the cell cycle, the way Brca1 exerts its tumour suppressive function remains a topic of debate. During mitosis, Brca1 is required to ensure proper spindle microtubule polymerization and chromosome segregation, thereby maintaining the whole chromosomal stability of the cell (Ertych et al. 2014). However, how Brca1 is regulated during mitosis remains largely elusive. Importantly, our group identified the centrosomal protein Cep72 as a novel interaction partner of Brca1. Thus, the aim of this study was to investigate whether Cep72 participates in the function of Brca1 to regulate chromosome segregation during mitosis and to elucidate whether Cep72 might contribute to oncogenic induction of aneuploidy in human cancer.

2 MATERIAL AND METHODS

2.1 Materials

2.1.1 Equipment

The equipment, which was used for this study is listed in Table 2.1.

Table 2.1 Equipment

Equipment	Model	Purchased from
Cell culture materials		Sarstedt, Nümbrecht, Germany Ibidi, Martinsried, Germany
Centrifuge, cooling	Multicentrifuge X3R	Thermo Fisher Scientific, Karsruhe, Germany
Electroporation system	GenePulser Xcell™	BioRad, Hercules; CA, USA
Flow cytometer	BD FACSCanto™ II	Becton Dickinson San Jose, CA, USA
Gel documentation	Gel iX Imager	Intas, Göttingen, Germany
Heating block	Thermomixer Comfort R & TDB-120 Dry Block Thermostat	Eppendorf, Hamburg, Germany Biosan, Riga, Latvia
Horizontal gel electrophoresis	Sub-Cell GT cell	BioRad Laboratories, München, Germany
Incubator	HERAcell 240 CO_2 incubator	Thermo Fisher Scientific, Karlsruhe, Germany
Laboratory scale	Sartorius Research R200D	Sartorius , Göttingen, Germany
Magnetic stirrer	IKAMAG® RCT	IKA Labortechnik, Staufen, Germany
Medical X-ray film	Fuji Super RX	FUJIFILM corporation, Düsseldorf, Germany
Microscope camera adaptor	A3474-07	HAMAMATSU Photonics, Hamamatsu, Japan

Equipment	Model	Purchased from
Microscope cameras	sCMOS camera & Leica DFC360 FX & Hamamatsu 1394 ORCA-II ER & Hamamatsu C4742-95	GE Healthcare Chalfont St. Giles, Great Britain Leica, Wetzlar, Germany Hamamatsu Photonics, Herrsching am Ammersee, Germany
Multilable reader	VICTOR™ X3	PerkinElmer, Rodgau, Germany
Semidry blotting system	PerfectBlue™	Peqlab, Erlangen, Germany
PVDF membrane	ImmobilionR-P (PVDF)	Merck Millipore, Darmstadt,Germany
Nitrocellulose membrane	Protran BA 85	GE Healthcare, Chalfont St. Giles, Great Britain
Pipettes	Pipetman® P2, P10, P20, P200, P1000	Gilson International, Limburg-Offheim, Germany
Pipettor	PIPETBOY acu	Integra Biosciences, Fernwald, Germany
Power supply	Power Supply EV231	Peqlab, Erlangen, Germany
Sterile workbench	HERAsafe®	Thermo Fisher Scientific, Karsruhe, Germany
Spectrophotometer	NanoDrop 2000	Thermo Fisher Scientific, Karsruhe, Germany
Tabletop centrifuge	Biofuge pico	Thermo Fisher Scientific, Karsruhe, Germany
Tabletop centrifuge, cooling	Biofuge fresco	Thermo Fisher Scientific, Karsruhe, Germany
Tank blotting system		Own manufacturing
Vertical electrophoresis system		Own manufacturing
Vortex mixer	VORTEX-GENIE® 2	Scientific Industries Inc., Bohemia, NY, USA
X-Ray film processor	Optimax	Protec, Oberstenfeld, Germany

The data collected in this study was analysed by using the software listed in Table 2.2.

2.1.2 Software

Table 2.2 Software

Software	Company
BD FACSDiva™	Becton Dickinson, San Jose, CA, USA
Leica LAS-AF software	Leica, Wetzlar, Germany
NanoDrop 2000/2000c software	Thermo Fisher Scientific, Karsruhe, Germany
softWoRx Explorer1.3.0	Applied Precision, a GE Healthcare Company, Chalfont St. Giles, Great Britain
SoftWorx 6.0	Applied Precision, a GE Healthcare Company, Chalfont St. Giles, Great Britain
Hokawo Launcher 2.1	Hamamatsu Photonics, Herrsching am Ammersee, Germany

2.1.3 Chemicals

All standard chemicals used in this study were purchased from Amersham Biosciences (Buckinghamshire, England), AppliChem (Darmstadt, Germany), BD Biosciences (Heidelberg, Germany), Biomol (Hamburg, Germany), BioRad (Hercules, CA, USA), Carl Roth (Karlsruhe, Germany), Enzo Life Sciences inc. (New York, USA), Fermentas (St. Leon-Rot, Germany), GE Healthcare (Uppsala, Sweden), Invitrogen (Carlsbad, CA, USA), Merck (Darmstadt, Germany), New England Biolabs (Beverly, MA, USA), PAA Laboratories (Pashing, Australia), Polyplus-transfection SA (Illkirchen, France), Promega (Madison, WI, USA) Roche Diagnostics GmbH (Mannheim, Germany), Sigma Aldrich (St. Louis, MO, USA), Thermo Fisher Scientific (Waltham, MA, USA), Th. Geyer (Renningen, Germany), VWR International (West Chester, PA, USA), in a quality for analysis or molecular biological applications.

2.1.3.1 Inhibitors

All inhibitors used in this study including their working concentrations are listed in Table 2.3. Potential aberrations are specified separately in the respective experiment.

Table 2.3 Inhibitors

Inhibitor	Final concentration	Effect	Company
Dimethylenastron	2 µM	Inhibition of the Eg5/KSP-kinesin	PAA Laboratories, Pasching, Australia Enzo Life Sciences inc., New York, USA
G418 (Neomycin)	300 µg/ml	Inhibition of the polypeptide synthesis	PAA Laboratories, Pasching, Australia
MG132	20 µM	Inhibition of the proteasome	Enzo Life Sciences Inc., New York, USA
MLN8054	0.5 µM	Inhibition of the Aurora A kinase	Millennium Pharmaceuticals Inc., Cambridge, MA, USA
Nocodazole	300 nM	Interferes with microtubule dynamics, depolymerizes microtubules	Sigma-Aldrich, St. Louis, MO, USA
Puromycin	1 µg/ml	Inhibition of the mRNA translation	Sigma-Aldrich, St. Louis, MO, USA
Taxol®	0.2 – 150 nM	Interferes with microtubule dynamics, stabilizes microtubules by binding of ß-tubulin	Sigma-Aldrich, St. Louis, MO, USA
Thymidine	2 mM	Inhibition of nucleotide-synthesis, blocks DNA synthesis	Sigma-Aldrich, St. Louis MO, USA

2.1.3.2 Antibodies

Primary Antibodies

All primary antibodies used in this study including the host species, the antibody type as well as the used dilution, are listed in Table 2.4.

Table 2.4 Primary antibodies

Antigen	Host	Antibody type	Dilution	Purchased from
ANA (anti-nuclear antibody) Crest	human	polyclonal	IF 1:800	Europa Bioproducts, Wicken, Ely, UK
Aurora A (35C1)	mouse	monoclonal	WB 1:1000	Santa Cruz Biotechnology, Inc., Dallas, TX, USA
ß-Actin (AC-15)	mouse	monoclonal	WB 1:10000	Sigma Aldrich, St. Louis, MO, USA
Bard1 (H-300)	rabbit	polyclonal	WB 1:1000	Santa Cruz Biotechnology, Inc., Dallas, TX, USA
Brca1 (D-9)	mouse	monoclonal	WB 1:350 IP 0.75 µg/mg protein	Santa Cruz Biotechnology, Inc., Dallas, TX, USA
Brca1 (C-20)	rabbit	polyclonal	WB 1:350	Santa Cruz Biotechnology, Inc., Dallas, TX, USA
Cep72 (A301-297A)	rabbit	polyclonal	WB 1:1000 IP 4 µg/mg protein	Bethyl Laboratories, Inc., Montgomery, TX, USA
Cep192 (A302-324A)	rabbit	polyclonal	WB 1:1000	Bethyl Laboratories, Inc., Montgomery, TX, USA
Chk2 (DSC-270)	mouse	monoclonal	WB 1:800	Santa Cruz Biotechnology, Inc., Dallas, TX, USA
CKAP5 (H4) (ch-TOG)	mouse	monoclonal	WB 1:1000	Santa Cruz Biotechnology, Inc., Dallas, TX, USA
MPM-2	mouse	monoclonal	FC 1:1600	Millipore, Billerica, MA, USA
α-Tubulin (B5-1-2)	mouse	monoclonal	IF 1:650	Santa Cruz Biotechnology, Inc., Dallas, TX, USA

Antigen	Host	Antibody type	Dilution	Purchased from
γ-Tubulin (T6557)	mouse	monoclonal	WB 1:2000	Sigma Aldrich, St. Louis, MO, USA
γ-Tubulin (T3559)	rabbit	polyclonal	IF 1:550	Sigma Aldrich, St. Louis, MO, USA
Tpx2 (18D5)	mouse	monoclonal	WB 1:1000	Santa Cruz Biotechnology, Inc., Dallas, TX, USA
P-Aurora A (Thr288)/ Aur B (Thr232)/ Aur C (Thr198) (D13A11)	rabbit	polyclonal	WB 1:1000	Cell Signaling, Beverly, MA, USA
P-Tacc3 (S558)	rabbit	polyclonal	WB 1:1000	Cell Signaling, Beverly, MA, USA

Secondary antibodies

The secondary antibodies used for the detection of all primary antibodies (Table 2.4) are listed in Table 2.5. The table shows all secondary antibodies used in this study including the host species, the antibody type, the conjugated molecule as well as the used dilution.

Table 2.5 Secondary antibodies

Antigen	Host antibody type	Conjugated with	Dilution	Purchased from
Anti-human	goat polyclonal	AlexaFluor594	IF 1:1000	Invitrogen, Carlsbad, CA, USA
Anti-mouse	goat polyclonal	Horseradish peroxidase (HRP)	WB 1:10000	Jackson ImmunoResearch Laboratories Inc., Baltimore Pike, PA, USA
Anti-mouse	goat polyclonal	AlexaFluor488	IF 1:1000 FC 1:2000	Invitrogen, Carlsbad, CA, USA

Antigen	Host antibody type	Conjugated with	Dilution	Purchased from
Anti-mouse	goat polyclonal	AlexaFluor594	IF 1:1000	Invitrogen, Carlsbad, CA, USA
Anti-rabbit	goat polyclonal	Horseradish peroxidase (HRP)	WB 1:10000	Jackson ImmunoResearch Laboratories Inc., Baltimore Pike, PA, USA
Anti-rabbit	goat polyclonal	AlexaFluor488	IF 1:1000	Invitrogen, Carlsbad, CA, USA
Anti-rabbit	goat polyclonal	AlexaFluor594	IF 1:1000	Invitrogen, Carlsbad, CA, USA

2.1.3.3 Chromosome enumeration probes

The chromosome enumeration probes (CEP), which were used in this study for the detection of specific chromosomes via CEP-FISH including the locus and the chromosome region are listed in Table 2.6.

Table 2.6 Chromosome enumeration probes

Chromosome	Locus	Chromosome Region	Purchased from
7	D7Z1	7q11.1-q11.1	Cytocell aquarius, Cambridge, UK
15	D15Z4	157q11.1-q11.1	Cytocell aquarius, Cambridge, UK

2.1.3.4 Oligonucleotides

The oligonucleotides used in this study were synthetized by Sigma Aldrich (Taufkirchen, Germany). They were diluted to a concentration of 100 µM in H_2O dest. and stored at -20°C.

DNA oligonucleotides

The primer used for this study including their sequence and application are listed in Table 2.7.

Table 2.7 DNA oligonucleotides

Primer	Primer sequence	Application
Brca_I26A_for	5′-CTTAGAGTGTCCCGCC TGTCTGGAGTTG-3′	forward primer for the mutagenesis of the Brca1 RING-domain, exchange of isoleucine 26 to alanine
Brca_I26A_rev	5′-CAACTCCAGACAGGC GGGACACTCTAAG-3′	reverse primer for the mutagenesis of the Brca1 RING-domain, exchange of isoleucine 26 to alanine
Cep72_HindIII_pEGFP_for	5′-TATAAGCTTCGATGGC GCGGGCTGG-3′	amplification of human *CEP72*, adds a HindIII restriction site to N-terminus
Cep72_KpnI_rev	5′-TATCCATGGTCAGCAG GCCTGGCAG-3′	amplification of human *CEP72* including stop codon, adds a KpnI restriction site to C-terminus
Cep72_sh_forward	5′-GATCCCCGCAGATCGC TGGACTTCAATTCAAGAGA TTGAAGTCCAGCGATCTGCTT TTTGGAAA-3'	cloning of pRetroSuper-Cep72-shRNA (Table 2.11) for stable expression of shRNA against human *CEP72*
Cep72_sh_reverse	5′-AGCTTTTCCAAAAAGC AGATCGCTGGACTTCAATCTC TTGAATTGAAGTCCAGCGATC TGCGGG-3'	cloning of pRetroSuper-Cep72-shRNA (Table 2.11) for stable expression of shRNA against human *CEP72*

shRNA

The shRNAs used for this study including their sequence and the corresponding reference are listed in Table 2.8.

Table 2.8 shRNAs

shRNA against	shRNA sequence	Reference
BRCA1	5′- GGAACCUGUCUCCACAAAG -3′ 5′- GAAAGUACGAGAUUUAGUC –3′	Stolz et al., 2010
CEP72	5′- GCAGATCGCTGGACTTCAA -3′	Oshimori *et al.* 2009

shRNA against	shRNA sequence	Reference
SCRAMBLED	5'- CAUAAGCUGAGAUACUUCA -3'	Brummelkanp *et al.* 2002

siRNA

The siRNAs used for this study including their sequence and the corresponding reference are listed in Table 2.9.

Table 2.9 siRNAs

siRNA against	shRNA sequence	Reference
AURKA	5'-GGCAACCAGTGTACCTCAT-3'	Macůrek et al., 2008
BARD1	5'-CATTCTGAGAGAGCCTGT-3'	Ryser et al., 2009
BRCA1	5'-GGAACCUGUCUCCACAAAG(DT)(DT)-3'	Lou et al. 2003
CEP72	5'-TTGCAGATCGCTGGACTTCAA-3'	Oshimori et al. 2009
CEP192	5'-AGCAGCUAUUGUUUAUGUUGAAAA-3'	Gomez-Ferreria et al., 2007
CHK2	5'-CCUUCAGGAUGGAUUUGCCAAUC-3'	Invitrogen
CH-TOG/CKAP5	5'-GAGCCCAGAGTGGTCCAAA-3'	van der Vaart et al., 2011
KIF2A	5'-GGAAUGGCAUCCUGUGAAA-3'	Jang et al., 2008
TACC3	5'-GTGGATTACCTGGAGCAGT-3'	Schneider et al., 2007
TPX2	5´-GAAUGGAACUGGAGGGCUU-3'	Gruss et al. 2002
LUCIFERASE	5´-CUUACGCUGAGUACUUCGAUU-3'	Elbashir et al., 2001

2.1.3.5 Plasmids

Used plasmids

The plasmids used for this study are listed in Table 2.10. Additionally the table shows their application as well as the corresponding tag and resistance gene. A reference is given for plasmids provided by others. For plasmids, which were constructed in this study, the corresponding cloning strategy is listed in Table 2.11.

Table 2.10 Used Plasmids

Plasmid	Tag	Resistance	Encoding for	Reference
pcDNA3	none	neomycin (G418) ampicillin	Human expression plasmid with CMV (cytomegalovirus)-promotor	Invitrogen, Germany
pcDNA3.1-attB-FA-Myc-His	FA, Myc, His	neomycin (G418) ampicillin	Human expression plasmid with CMV promotor and attB sites for site-specific integration of genes in the human genome *via* phage integrase	provided by Prof. Dr. Olaf Stemmann, Bayreuth, Germany
pcDNA3.1-attB-FA-Myc-His-CEP72	none	neomycin (G418) ampicillin	Human expression plasmid with CMV promotor and attB sites for site-specific integration of *CEP72* in the human genome *via* phage integrase	this study see
pcDNA3-Brca1-sh-resistant-HA	HA	neomycin G418 ampicillin	Expression plasmid for the overexpression of human *BRCA1*, full length, which cannot be targeted by sh/siRNA (96) anymore.	AG Bastians
pcDNA3-*BRCA1*-sh-resistant-cassette	HA	neomycin (G418) ampicillin	Temporary vector for the cloning of a *BRCA1*-shRNA-resistant cassette	this study see Table 2.11
pcDNA3-HA-3xFLAG-Brca1-I26A	HA 3xFLAG	neomycin (G418) ampicillin	Expression plasmid for the overexpression of human HA-3xFLAG-tagged Brca1-I26A mutant in mammalian cells. The I26A mutant of Brca1 is deficient for the E3-ubiquitin-ligase activity.	provided by Dr. Kristoffer Valerie, Richmond, VA, USA

Plasmid	Tag	Resistance	Encoding for	Reference
pcDNA3-HA-Brca1-I26A siRNA resistant	HA	neomycin (G418) ampicillin	Expression plasmid for the overexpression of HA-tagged sh/si-resistant I26A-mutant of human *BRCA1*.	this study see Table 2.11
pCEF-Chk2-wt	none	puromycin ampicillin	Human expression plasmid with EF1 promotor for the overexpression of human *CHK2* in mammalian cells	Stolz et al., 2010
pCMV-INT-phiC31	none	neomycin (G418) ampicillin	Mammalian expression plasmid with CMV promotor for the overexpression of phage integrase (phiC31). phiC31 enables the efficient site-specific integration of genes harbouring attB sites in the genome of human cells.	provided by Prof. Dr. Olaf Stemmann, Bayreuth, Germany
pCMV-flag-PLK4	FLAG	kanamycin	Mammalian expression plasmid with CMV promotor for the overexpression of *PLK4* in human cells	provided by Prof. Dr. Ingrid Hoffmann, Heidelberg, Germany
pCR2.1®-TOPO®		kanamycin ampicillin	Vector with covalently bound topoisomerase I for fast cloning and recombinants including 3´-T overhangs for direct ligation of *Taq*-amplified PCR products	Life Technologies / Thermo Fisher Scientific, Darmstadt, Germany
pCR2.1-*CEP72*		kanamycin ampicillin	Temporary vector for the subcloning of *CEP72* cDNA	this study see Table 2.11

Plasmid	Tag	Resistance	Encoding for	Reference
pEGFP-*EB3*	GFP	neomycin (G418) kanamycin	Mammalian expression vector with CMV promoter and *GFP* gene for the overexpression of *EB3* in human cells. The expression of GFP-tagged Eb3 enables the tracking of MT plus-ends in live cell microscopy	provided by Prof. Dr. Linda Wordemann, Seattle, USA
pRetroSuper	none	puromycin ampicillin	Mammalian expression vector with H1 promoter for the expression of shRNA constructs.	kindly provided by Martin Eilers, Würzburg, Germany
pRetroSuper-scrambled-shRNA	none	puromycin ampicillin	Mammalian expression vector with H1 promoter for the expression of shRNA (scrambled) without any target sequence in the human genome	Stolz et al., 2010
pRetroSuper-Cep72-shRNA	none	puromycin ampicillin	Mammalian expression vector with H1 promoter for the stable expression of shRNA against human *CEP72*	this study see Table 2.11

Cloning of used plasmids

In Table 2.11 the plasmids generated in this study are listed. The table also shows the donor and target plasmids as well as the applied restriction enzymes.

Table 2.11 Cloning of used plasmids

Plasmid	Generation
pRetroSuper-Cep72-shRNA	The double stranded *CEP72* shRNA oligo (Cep72_sh_forward + Cep72_sh_reverse (Table 2.7)) was cloned into the BglII / HindIII restriction sides of pRetroSuper

Plasmid	Generation
pCR2.1-*CEP72*	*CEP72* was amplified from the DNA of the MGC premier cDNA clone for *CEP72* (BC000132, Biocat, Heidelberg, Germany) using the primers Cep72_HindIII_pEGFP_for and Cep72_KpnI_rev (Table 2.7). Subsequently the PCR product was cloned into pCR2.1 *via* TA cloning sites.
pcDNA3.1-attB-FA-Myc-His-CEP72	The fragment of *CEP72* (STOP codon inclusive) was released from pCR2.1-*CEP72* by HindIII / XbaI digest and cloned into the HindIII / XbaI restriction site of pcDNA3.1-attB-FA-Myc-His
pcDNA3- *BRCA1*-sh-resistant-cassette	The sh-resistant (nt 96ff) fragment of *BRCA1* was released from pcDNA-Brca1-sh-resistant-HA by HindIII / EcoRI and subcloned into the HindIII / EcoRI restriction site of pcDNA3
pcDNA3-HA-Brca1-I26A siRNA resistant	An *in vitro* mutagenesis was performed on pcDNA3- *BRCA1*-sh-resistant-cassette with oligos Brca_I26A_for and Brca_I26A_rev (Table 2.7). The I26A mutated and sh-resistant fragment of *BRCA1* was then released by HindIII / EcoRI and cloned into HindIII / EcoRI restriction site of pcDNA-Brca1_sh-resistant-HA.

2.1.3.6 Human cell lines

Human cell lines

The human cell lines used for this study are listed in Table 2.12 . Additionally the table provides information about their origin and the used culture medium, which was purchased from Sigma-Aldich (Taufkirchen, Germany) and PAA (Cölbe, Germany).

Table 2.12 Human cell lines

Cell line	Origin	Medium	Selection	Reference
HCT116	colon	Roswell Park Memorial Institute 1640 (RPMI-1640)	none	Brattain et al. 1981
HCT116-*CHK2*$^{-/-}$	colon	Roswell Park Memorial Institute 1640 (RPMI-1640)	neomycin (G418)	Jallepalli et al. 2003
HCT116-*BRCA1*-sh (clone O32)	colon	Roswell Park Memorial Institute 1640 (RPMI-1640)	puromycin	Stolz et al., 2010

Stable cell lines

All cell lines, which were generated in this study are listed in Table 2.13. The table also provides information about the parental cell line, the used plasmid and the respective selection of the cell lines.

Table 2.13 Constructed stable cell lines

Cell line	Parental cell line	Plasmid	Selection
HCT116-scr-shRNA	HCT116	pRetroSuper-scrambled-shRNA	puromycin
HCT116-*CEP72*-shRNA	HCT116	pRetroSuper-*CEP72*-shRNA	puromycin
HCT116-ctr	HCT116	pcDNA3.1-attB-FA-Myc-His	neomycin (G418)
HCT116-*CEP72*	HCT116	pcDNA3.1-attB-FA-Myc-His-*CEP72*	neomycin (G418)

2.1.3.7 Microorganisms

Escherichia coli strain

DH5α F^- Φ80*lacZ*ΔM15 Δ(lacZYA-argF)U169 deoR recA1 endA1 hsdR17(r_k^-, m_k^+) phoAsupE44 thi-1 gyrA96 relA1λ^-.

2.2 Methods

2.2.1 Cell culture

All cell lines were cultivated in RPMI1640 medium supplemented with 10% (v/v) fetal calf serum, 100 µg/ml streptomycin and 100 U/ml penicillin (Sigma Aldrich) using a humidified incubator with 5% CO_2 at 37°C. The selection medium additionally contained 300 µg/ml G418 and 1 µg/ml puromycin, respectively. For experimental setups medium without any antibiotics was used.

Cells in permanent culture were passaged three times a week to enable sufficient nutrient supply and enough space for proliferation. For long term storage were cryopreserved. Therefor cells were harvested and resuspended in RPMI1640 containing 20% (v/v) FCS and 10% (v/v) DMSO. The cell suspension was slowly cooled down to -80°C using a cryo 1°C freezing container and stored at -196°C.

2.2.2 Cell cycle synchronization of human cells

Cells were synchronized in the cell cycle at the G1/S transition *via* double thymidine block. For this, the cells were treated with 2 µM thymidine in RPMI1640 for 16h. To release the cells from the block, they were washed with PBS over a time period of 30 min (approximately 6 times) and subsequently supplied with fresh medium. After 8 h the cells were again treated with 2 µM thymidine in RPMI1640 for 16h. The cells were released from the block by repeated washing steps with PBS. Provided with fresh medium the cells re-enter the cell cycle and progress through S phase, G2 phase, mitosis and G1 phase. To further arrest the cells in mitosis they were treated with 20 µM of the proteasome inhibitor MG132 for another 3 h, 6.5 h after being released. In this manner the degradation of cyclin B is inhibited and the cells are blocked in metaphase.

For mitotic synchronization cells were treated with 150 nM Taxol®, 300 nM nocodazole or 2 µM dimethylenastron (DME) for 16 h.

2.2.3 Transfection of human cells

2.2.3.1 Electroporation

2.5 million cells were harvested and resuspended in 400 µl RPMI1640 without any supplements. The cell suspension was mixed with 1 – 20 µg of plasmid and transferred into an electroporation cuvette with 4 mm in diameter (BioRad, Hercules, CA, USA). Using the electroporation system GenePulser Xcell™ (BioRad, Hercules, CA, USA) the electroporation was performed with 300 V, 500 µF and ∞ resistance. The cells were seeded into prewarmed fresh medium and the medium was changed after 4 h. The analysis of the cells was done 48 h after transfection.

2.2.3.2 PEI Transfection

Cells were seeded at 70% density in 6-well plates. The cells were washed with PBS and supplemented with 1 ml of fresh medium without any FCS and antibiotics. 0.0025% (v/v) PEI, pH7.0 in 100 µl PBS was mixed with 0.5 – 5 µg of plasmid in 100 µl PBS by pipetting up and down for 10 s. The mixture was incubated at RT for 20 min and added dropwise to the prepared cells. The medium was changed after 4 h and the cells were analysed 48 h after transfection.

2.2.3.3 siRNA transfection

Cells were seeded at 70% density in 6-well plates. The cells were washed with PBS and supplemented with 1 ml of fresh medium without any FCS and antibiotics. For the siRNA transfection exclusively RNAse-free reaction tubes and pipet tips were used. A final volume of 200 µl RPMI1640 medium was supplemented with 40 – 60 pmol siRNA and 4 – 6 µl of Interferin™ (Polyplus-transfection SA, Illkirchen, France). Subsequently the

mixture was vortexed for 10 s and incubated at RT for 10 min. The solution was added dropwise to the prepared cells and after 6 h the medium was changed. The cells were analysed 48 h after transfection.

2.2.3.4 Metafectene® transfection

To generate cell lines with a stable expression of certain plasmids, the cells were transfected using Metafectene® according to the manufacturer's protocol (Biontex Laboratories GmbH, Martinsried, Germany).

2.2.4 Generation of stable cell lines

For the generation of stable cell lines, cells were transfected using Metafectene® (2.2.3). To select stable cells, they were seeded into selection medium (1 µg/ml Puromycin, 300 µg/ml G418) 24 h after transfection. A resistance gene encoded on the respective plasmid enables a selection for cells which were successfully transfected. In order to ensure the generation of clones based on a single cell, different dilutions (1:50, 1:100, 1:200, 1:500, 1:1000, 1:1500 and 1:2000) were seeded. After 7 days small colonies from single cells appear. This single cell clones were transferred to 24-well plates and further cultivated.

2.2.5 Karyotype analyses *via* metaphase chromosome counting

For the analysis of the karyotype, single cell clones were cultivated for 30 generations and seeded in 6-well plates. To arrest cells in mitosis, they were treated with 300 nM nocodazole for 5 h. Afterwards the cells were harvested and centrifuged at 2000 rpm for 5 min. The cells were resuspended in 700 µl 40% RPMI / 60% H_2O dest. and incubated at RT for 30 min. The incubation process in the hypotonic solution leads to a swelling of the cells, which were subsequently prefixed by addition of 300 µl ice cold Carnoy's fixative (25% (v/v) methanol, 75% (v/v) glacial acetic acid (Mehlhop and Gardner 1982). The cell suspension was centrifuged at 2000 rpm for 5 min. After removal of the supernatant, 1 ml ice cold Carnoy's fixative was gently added to the cells. This step was repeated once. Then the cells were either stored at -20°C until further usage or directly processed. The cell suspension was again centrifuged at 2000 rpm for 5 min and the cell pellet was resuspended in 100 µl - 500 µl glacial acetic acid. Afterwards 3 drops of the cell suspension were dropped onto wet and precooled object slides from a vertical height of about 30 cm. The object slides were incubated in a wet chamber at 42°C for 5 minutes. After the object slides had been thoroughly dried at RT, the chromosomes were stained by incubation in a 10% (v/v) Giemsa staining solution (Merck, Darmstadt, Germany) for 20 min and rinsed subsequently with H_2O dest. The stained object slides were dried and the chromosome spreads were embedded in Euparal (Carl Roth, Karlsruhe, Germany). The chromosome counting was performed using a Zeiss Axioscope FS microscope (Zeiss,

Oberkochen, Germany) equipped with a Hamamatsu C4742-95 camera and the Hokawo Launcher 2.1 software (Hamamatsu Photonics, Herrsching am Ammersee, Germany).

2.2.6 Karyotype analyses *via* CEP-FISH analysis

For CEP-FISH analysis chromosome enumeration probes (CEP), which chromosome specifically hybridize to highly repetitive human satellite DNA sequences, were applied. In this study probes specifically recognizing chromosome 7 and 15 (Aquarius®Kit, Cytocell, Cambridge, Great Britain) were used.

Cells were swollen in hypotonic medium and fixed using Carnoy's fixative as described in 2.2.5. The cell suspension was centrifuged at 2000 rpm for 5 min and the cell pellet was resuspended in 100 µl - 500 µl glacial acetic acid. Then 1 drop of the cell suspension was dropped onto a wet, precooled cover slip (10 x 10 mm) and dried at RT. Afterwards the cover slip was incubated in 2x SSC solution (0.3 M sodium chloride, 30 mM trisodium citrate, pH 7) for 2 min at room temperature followed by dehydration in an ethanol series (70 %, 85 % and 100 %, each for 2 min at RT) and drying. For two-probe hybridization 0.6 µl of each CEP-FISH probe and 0.8 µl hybridization solution were mixed and pipetted onto a pre-warmed object slide. Subsequently the cover slip containing the cells was placed up site down onto the drop. To avoid evaporation the cover slip was sealed with nail polish. For denaturation the object slide was placed on a 75°C heating block for 2 min. Afterwards it was transferred to a humid lightproof chamber and incubated for 2 h in an incubator at 37°C. The cover slip was removed from the object slide, transferred into a 24-well containing pre-warmed 0.25x SSC and incubated for 6 min in a 75°C water bath. Subsequently the slide was washed with 2x SSC + 0.05% Tween20 and stained with Hoechst 33342 (1:15000 in 2x SSC + 0.05% Tween20) for 5 min each. After three further washing steps with 2x SSC + 0.05% Tween20, the coverslip was dried, embedded in Vectashield® (Vector Laboratories, Burlingame, California, USA) and finally sealed with nail polish. Counting signals was done using immunofluorescence microscopy as described in 2.2.8.

2.2.7 Flow Cytometry

Fluorescence activated cell sorting (FACS) analysis was performed using a BD FACS Canto II (Becton Dickinson, San Jose, CA, USA). The analysis was performed using the BD FACS Diva™ (Becton Dickinson, San Jose, CA, USA) software.

Cells were harvested, transferred to a 1.5 ml reaction tube, centrifuged at 2000 rpm for 5 min and resuspended in 200 µl PBS. The cells were fixed with 1 ml ice cold 70% ethanol, which was added dropwise while the suspension was continuously vortexed. Subsequently the cells were stored at 4°C overnight.

PI-staining

For the detection of the DNA content the DNA intercalating dye propidium iodide (PI) was used. Fixed cells were centrifuged at 2000 rpm for 5 min, the cell pellet was washed with 1 ml PBS, resuspended in 100 µl RNAse A (1µg/ml in PBS) and incubated at RT for 15 min. 50 µg/ml PI in PBS was added and the cells were analysed.

MPM2 staining

To detect mitotic cells anti-MPM2 antibody was used. This antibody specifically recognizes mitotic phospho-epitopes at kinetochores, chromosome arms, the midbody and spindle poles (Tapia *et al.* 2006). Fixed cells were centrifuged at 2000 rpm for 5 min, washed with 1 ml washing buffer (0.05% Triton- X-100 in PBS) and incubated in 80 – 100 µl of an anti-MPM2 antibody solution (1:1600 in 2% (v/v) FCS, 0.2% Triton-X-100 in PBS) at 4°C for 2h. Afterwards the cells were washed twice with 1 ml washing buffer and incubated in 80 – 100 µl of a fluorochrome-coupled secondary antibody solution (1:2000 AlexaFluor488 in 2% (v/v) FCS, 0.2% Triton-X-100 in PBS) at 4°C for 2h. The cells were washed twice with washing buffer and once with PBS. After the cells had been incubated with 100 µl RNAse A solution (1µg/ml in PBS) for 15 min, 200 – 600 µl PI (50 µg/ml in PBS) was added and the samples were analysed.

2.2.8 Immunofluorescence microscopy

Cells were seeded onto 10x10 mm cover slips, which were placed in a 24-well plate. The next day the cells were fixed with 2% paraformaldehyde (PFA) in 1x PHEM (60 mM PIPES pH7.0, 27 mM HEPES, 10 mM EGTA and 4 mM $MgSO_4$) at RT for 5 min. For permeabilization and extraction the cells were subsequently treated with ice cold 100% methanol at -20°C for further 5 min. The cover slips were washed three times with PBST (0,75% (v/v) Tween-20 in PBS). To avoid unspecific antibody binding the cells were incubated with 5% (v/v) FCS in PBST for 30 min. After washing with PBST, they were incubated with the primary antibody (3% (v/v) FCS in PBST) (primary antibodies see Table 2.4) either at RT for 2h or at 4°C overnight. The cells were washed three times with PBST and incubated with the secondary antibody (3% (v/v) FCS in PBST) (secondary antibodies see Table 2.5) again either at RT for 2h or at 4°C overnight. Then the cells were stained with Hoechst33342 (1.33 µg/ml in PBST) for 5 min. After three further washing steps with PBST and two washing steps with PBS, the cover slips were dried and the cells were embedded in Vectashield® (Vector Laboratories, Burlingame, California, USA). Finally the cover slips were sealed with nail polish.

Microscopy was done on a Leica DM6000B microscope (Leica, Wetzlar, Germany) and a DeltaVision–ELITE microscope (Applied Precision / GE Healthcare, Chalfont St- Giles, Great Britain) equipped with a CoolSnap-HQ2 (Photometrics, Tucson, Arizona, USA) or PCO Edge sCMOS (PCO, Kelheim, Germany) camera. Images were taken by means of an Olympus 60x 1.40 NA or Olympus 100x 1.40 NA objective with a Z-optical spacing of 0.2 µm. Subsequently the images were deconvolved and analysed using the SoftWorx 5.0/6.0 and softWoRx Explorer 1.3.0 software (Applied Precision / GE Healthcare, Chalfont St- Giles, Great Britain).

2.2.9 Live cell microscopy

Measurement of microtubule plus-end assembly rates

The microtubule plus-end assembly rates were measured by tracking the plus-end binding protein EB3 conjugated to GFP in living cells. (Stepanova et al. 2003; Ertych et al. 2014). Cells were transfected *via* electroporation with 9 µg of pEGFP-EB3 (Table 2.10) and seeded onto glass-bottom dishes µ-dish (Ibidi, Martinsried, Germany). 24h after the transfection the cells were treated with 2 µM of the Eg5/Kif11 inhibitor dimethylenastron (DME) for 2 h. This synchronization step was useful to ensure the measurement of mitotic spindles in the same mitotic state, but did not affect the microtubule plus-end assembly rate *per se* (Ertych et al. 2014). For the image acquisition a Deltavision ELITE microscope equipped with a CoolSnap-HQ2 (Photometrics, Tucson, Arizona, USA) or a PCO Edge sCMOS camera (PCO, Kehlheim, Germany) was used. By means of an Olympus 100x 1.40 NA objective four sections with a Z-optical spacing of 0.4 µm were taken every 2 sec. The images were deconvolved and analyzed using the SoftWorx 5.0/6.0 and softWoRx Explorer 1.3.0 software (Applied Precision/ GE Healthcare, Chalfont St- Giles, Great Britain). Average microtubule plus-end assembly rates were calculated on the basis of 20 microtubules per cell.

2.2.10 Determination of lagging chromosomes

For the determination of lagging chromosomes, cells were synchronized in G1/S-phase *via* double thymidine block and released into fresh medium. To achieve an accumulation of cells in anaphase, cells were fixed 9.5 h after being released. Subsequently the cells were analysed using immunofluorescence microscopy by quantification of CREST positive chromosomes lagging in the middle of the equatorial plane. Only chromosomes clearly separated from the two pole-oriented chromosome groups were counted as lagging.

2.2.11 Determination of abnormal spindles

Cells were synchronized in G1/S-phase *via* double thymidine block and released into fresh medium. To synchronize the cells in metaphase they were treated with 20 µM MG132 for 3 h, 6.5 h after release from the block. Cells were fixed in total 56 h after

transfection and stained for spindles (α-tubulin), kinetochores (CREST) and DNA (Hoechst33342). Subsequently the spindle morphology was evaluated.

2.2.12 Determination of pole-to-pole distance and the average microtubule length

Cells were synchronized in metaphase as described in 2.2.2. using MG132 treatment, fixed and stained for spindles (α-tubulin), centrosomes (γ-tubulin) and DNA (Hoechst33342). Using an Olympus 100x 1.4 NA objective images of sections with a Z-optical spacing of 0.2 µm were acquired. The distance between the two centrosomes as well as the average microtubule length from pole to pole was determined (Figure 2.1 using the SoftWoRx 6.0 and the softWorX Explorer 1.3.0 software (Applied Precision/ GE Healthcare, Chalfont St- Giles, Great Britain).

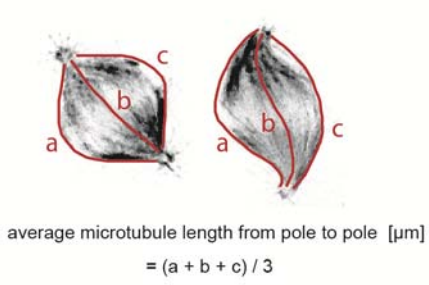

Figure 2.1 Schematic depiction for the determination of the average microtubule length from pole to pole.

2.2.13 Determination of centrosome numbers

Cells were fixed and stained for spindles (α-tubulin), centrosomes (γ-tubulin) and DNA (Hoechst33342). Subsequently the centrosome number in interphase cells was determined *via* immunofluorescence microscopy and the percentage of cells harboring more than 2 centrosomes was determined.

2.2.14 Analysis of monopolar spindle assembly

As a readout for abnormal microtubule plus end assembly (Stolz et al. 2015) the monopolar spindle morphology was determined. For this, cells were treated with 2 µM DME (PAA Laboratories, Pashing, Australia) for 4h. Afterwards the cells were fixed with PFA/Methanol and stained for spindles (α-tubulin), kinetochores (Crest) and DNA (Hoechst33342) (see 2.2.8 and Table 2.4). The analysis was done by immunofluorescence microscopy (2.2.8).

2.2.15 Cultivation of *E. coli* cells

Escherichia coli (*E. coli*) cells were cultivated in LB-Medium (1% (w/v) peptone 140, 0.5% (w/v) yeast extract, 0.5% (w/v) NaCl) in an incubator shaker with 140 rpm at

37°C or on plates containing 1.5% (w/v) agar. For the selection of transformed bacteria the respective antibiotics were added with a final concentration of 100 mgl/l for ampicillin and 50 mg/l for kanamycin.

2.2.16 Generation of chemically-competent *E. coli* cells

For the generation of chemically-competent *E. coli* cells 2 x 10 ml LB-medium (1% (w/v) peptone 140, 0.5% (w/v) yeast extract, 0.5% (w/v) NaCl) were inoculated with *E. coli* DH5α and grown overnight at 37°C. The next day 2 x 250 ml of SOB medium (2% (w/v) tryptone, 0.5% (w/v) yeast extract, 10 mM $MgSO_4$, 10 mM NaCl, 10mM $MgCl_2$) were prewarmed to 25°C and inoculated with 10 ml of the overnight culture. Then the bacteria were grown at 25°C to an OD_{600} = 0.6, filled into 50 ml tubes and cooled on ice for 10 min. The bacteria were centrifuged at 3000 rpm and 4°C for 15 min, the cell pellet of each tube was resuspended in 20 ml icecold TB buffer (55 mM $MnCl_2$, 250 mM KCl, 10 mM PIPES / KOH pH7.0, 15 mM $CaCl_2$) and incubated on ice for 10 min. After centrifugation for further 15 min, the pellets of all tubes were pooled and resuspended in a total volume of 40 ml icecold TB buffer. The *E. coli* suspension was incubated on ice for 10 min. Quickly, aliquots with 100 µl were prepared in pre-cooled reaction tubes, which were immediately frozen in liquid nitrogen and stored at -80°C.

2.2.17 Transformation of *E. coli* cells

Chemically competent *E. coli* cells were thawed on ice and 20 µl of ligation reaction or 1 µl of pure plasmid was added and gently mixed. The mixture was incubated on ice for 20 min and the cells were heat shocked for 1 min at 42°C. Subsequently the cell suspension was incubated on ice for further 2 min. Then 1 ml pre-warmed LB medium (1% (w/v) peptone 140, 0.5% (w/v) yeast extract, 0.5% (w/v) NaCl) was added and the mixture was incubated for 45 – 60 min at 37°C and 350 rpm in a Thermomixer Comfort R (Eppendorf, Hamburg, Germany). The *E. coli* suspension was transferred to 5 ml or 200 ml LB medium supplemented with the appropriate selection marker or plated on the respective LB agar plates and incubated at 37°C overnight. The next day the plasmids were prepared from the *E. coli* cells as described in 2.2.18.

2.2.18 Plasmid preparation from *E. coli* cells

Mini-preparation

4 ml *E. coli* cells from an overnight culture were pelleted in a 2 ml reaction tube by centrifugation at 14800 rpm for 30 sec. The pellet was resuspended in 200 µl resuspension buffer (50 mM Tris / HCL pH8.0, 10 mM EDTA pH8.0, 100 µg / ml RNaseA). Subsequently 200 µl of lysis buffer (200 mM NaOH, 1% (w/v) SDS) were added and the suspension was gently inverted 5 times. After incubation for 3 min at RT, 200 µl of neutralization buffer (3M potassium acetate pH 5.5) were added. The mixture was

immediately inverted 5 – 10 times and centrifuged at 14800 rpm for 10 min. Afterwards the supernatant was transferred to a new 1.5 ml reaction tube and 400 µl isopropanol was added. The precipitated DNA was pelleted by centrifugation at 14800 rpm for 20 min and washed with 800 µl 70% (v/v) ethanol. After another centrifugation step at 14800 for 5 min, the supernatant was removed. The pellet was dried at RT and subsequently resuspended in 30 µl H_2O dest.

Midi-preparation

For midi-preparation of plasmid DNA the NucleoBond® Xtra Midi Kit (Machery-Nagel, Düren, Germany) was used according to the manufacturer's protocol.

2.2.19 Polymerase chain reaction (PCR)

The standard PCR protocols for the Phusion® High Fidelity Polymerase (New England Biolabs, Beverly, Massachusetts, USA) and the GoTaq® polymerase (Promega, Madison, Wisconsin, USA) are listed in Table 2.14 and Table 2.15, respectively.

Table 2.14 PCR protocol Phusion High Fidelity DNA Polymerase

Component	Concentration
5x HF Phusion® Buffer	1x
dNTPs	je 200 µM
primer forward	0,1 µM
primer reverse	0,1 µM
Phusion® High fidelity DNA Polymerase	2 U
template	1 ng
dH_2O	ad. 50 µL

Table 2.15 PCR protocol Go®Taq DNA Polymerase

Component	Concentration
5x Green GoTaq® Reaction Buffer	1x
dNTPs	je 100 µM
primer forward	0,5 µM
primer reverse	0,5 µM
$MgCl_2$	20 mM
GoTaq® DNA Polymerase	0,25 U
colony	

For the PCR reactions the two following programs were used (Table 2.16 and Table 2.17). X is defined as the optimal annealing temperature for the respective pair of primers.

Table 2.16 PCR programm Phusion® High Fidelity DNA Polymerase

Step	Temperature	Time	Cycles
initial denaturation	98 °C	2 min	1x
denaturation	98 °C	10 s	
annealing	X °C	30 s	30x
elongation	72 °C	15 – 30 s / kb	
final Elongation	72 °C	10 min	1x
cooling	16 °C	∞	1x

Table 2.17 PCR programm Go®Taq Polymerase

Step	Temperature	Time	Cycles
initial denaturation	95 °C	2 min	1x
denaturation	94 °C	15 s	
annealing	X °C	20 s	25x
elongation	72 °C	1 min / kb	
final Elongation	72 °C	10 min	1x
cooling	16 °C	∞	1x

2.2.20 Restriction digest of DNA

Purified DNA was mixed with the specific enzyme and the required supplements according to the manufacturer's protocol (Thermo Fisher Scientific, Waltham, Massachusetts, USA).

2.2.21 Cloning

Digested plasmids were dephosphorylated by FastAP Thermosensitive Alkaline Phosphatase (Thermo Fisher Scientific, Waltham, Massachusetts, USA) according to the manufacturer's protocol. The ligation of DNA fragments was done *via* T4-DNA ligase (Promega, Madison, Wisconsin, USA) and a vector:insert ratio of 1:3 was chosen. The calculation for the required amount of DNA is shown below.

$$amount_{insert}\,[ng] = \frac{amount_{vektor}[ng] \times length_{insert}[kb]}{length_{vektor}[kb]} \times 3$$

The ligation reaction was incubated at 16°C overnight. Subsequently the ligation was stopped by incubation at 65°C for 10 min. A typical ligation protocol is shown in Table 2.18.

Table 2.18 Composition of a typical ligation reaction

Component	Concentration
10x ligation buffer	1x
vector	50 – 500 ng
insert	Y
T4-DNA ligase	0,5 - 1 µl
dH_2O	ad. 50 µl

2.2.22 Generation of whole cell lysates

Cells were harvested and lysed in Boehringer lysis buffer containing 50 mM Tris-HCl, pH7.4, 150 mM NaCl, 5 mM EDTA, 5 mM EGTA, 1% (v/v) Igepal (NP-40), 0.1% (w/v) sodium dodecylsulfate (SDS), 0.1% sodium desoxycholate, 20 mM Na_2VO_4, 25 mM ß-glycerophosphate, 50 mM NaF, 5 mM Na_2MoO_4, 0.5 nM microcystin-LR and complete protease inhibitor cocktail EDTA-free (Roche, Switzerland) (1:25). The lysis was performed on ice for 20 min and cell debris were separated by centrifugation at 148000 rpm for 20 min.

2.2.23 Protein determination

To determine the exact amount of protein within the cell lysate, the Bio-Rad DC™ Assay was applied according to the manufacturer's protocol. BSA was used as a standard. The photometric measurement at a wavelength of 705 nm was performed using the Victor™X3 (PerkinElmer, Rodgau, Germany).

2.2.24 Immunoprecipitation (IP) of proteins

Cells were harvested and lysed in IP lysis buffer (50 mM Tris-HCl pH7.4, 150 mM NaCl, 0.25% Igepal (NP-40), 0.1 mM EDTA, 10% (v/v) glycerol, 20 mM Na_2VO_4, 25 mM ß-glycerophosphate, 50 mM NaF, 5 mM Na_2MoO_4, 0.5 nM microcystin-LR, complete protease inhibitor cocktail EDTA-free (Roche, Switzerland) (1:25)). For the immunoprecipitation 2 mg whole cell lysate with a concentration of 7 mg/ml was incubated with 1.5 µg of the respective antibody (see Table 2.4) in a rotator at 4°C for 1.5 h. The protein-antibody mixture was supplemented with 15 µl a 50% solution of protein G sepharose beads and incubated in a rotator at 4°C for additional 1.5 h. By gentle inversion and centrifugation at 2000 rpm for 1 min the beads were washed three

times with 800 µl of lysis buffer. Then 20 µl SDS sample buffer (15% (w/v) SDS, 15% ß-mercaptoethanol, 50% (v/v) glycerol, 0.25% (w/v) bromophenol blue) was added to the beads and they were incubated at 95°C for 5 min.

2.2.25 Sodium dodecylsulfate polyacrylamide gel electrophoresis

2.2.25.1 (SDS-PAGE)

For the separation of proteins according to their molecular weight a discontinuous SDS-PAGE was performed (Laemmli, 1970). The gel composed of a 5% stacking gel (300 mM Tris-HCl pH 6.8, 0.1% (w/v) SDS, 5% (v/v) Rotiphorese® Gel 30) and a 7.5% resolving gel (600 mM Tris-HCl pH8.8, 0.1% (w/v) SDS, 7.5% (v/v) Rotiphorese® Gel 30). For sample preparation 50 µg of protein lysate was mixed with 5x SDS sample buffer (15% (w/v) SDS, 15% ß-mercaptoethanol, 50% (v/v) glycerol, 0.25% (w/v) bromophenol blue), incubated for 5 min at 95°C and loaded onto the gel. For the determination of the molecular weight 5 µl of a prestained protein standard (PageRulerTM Prestained Protein Ladder (Fermentas, St. Leon-Rot, Germany) was used. By means of running buffer (25 mM Tris-HCl pH 6.8, 192 mM glycine 0.15% (w/v) SDS) the proteins were separated in a SDS-PAGE device at 28 mA for 1h and subsequently at 38 mA for approximately 4h.

2.2.26 Western blotting

After the proteins had been separated by SDS-PAGE, the protein transfer and immobilization on a polyvinyliden fluoride (PVDF) (Immobilion-P, Millipore, USA) or nitrocellulose (Protran™, Whatman®, Germany) membrane was performed using a tank blot system. The PVDF membrane was activated by incubation in 100% methanol for 3 sec and the blot was built up. The SDS-PAGE gel was put on the membrane between three layers of Whatman paper, respectively and placed in the tank blot system filled with transfer buffer (0.0025% (w/v) SDS, 24.8 mM Tris-HCl pH 8.0, 170 mM glycine, 20% (v/v) methanol). The transfer was performed at 450 mA for 2h 45 min. To visualize the immobilized proteins the membrane was stained with Ponceau S solution (0.1% (w/v) Ponceau S in 5% (v/v) glacial acedic acid)

To avoid unspecific antibody binding the membrane was incubated with 5% milk in TBS-T (0.05% (v/v) Tween-20 in TBS (50 mM Tris-HCl pH 7.2, 160 mM NaCl) for 30 min. Subsequently the membrane was washed and incubated with the respective primary antibody (in 5% (w/v) BSA in TBS) at 4°C overnight. The next day the membranes were washed for 30 min with TBS-T and subsequently incubated with the appropriate HRP-conjugated secondary antibody (in 5% milk in TBS) at RT for 2 h. The membranse were washed three times with TBS-T and TBS and the immunodetection was done by enhanced chemo luminescence. For this, the membrane was incubated in 0.1 M Tris-HCl, pH 8.5 containing 0.6% (w/v) luminol, 0.3% (w/v) coumaric acid and 0.02 (v/v) H_2O_2

and the membrane was exposed to Fuji Medical X-Ray Films which were processed using the OPTIMAX X-Ray Film Processor.

3 RESULTS

3.1 Identification of Cep72 as a novel Brca1 interacting protein

Previous results from our group showed, that the E3-ubiquitin ligase Brca1 plays an essential role in mitotic progression, where the Chk2-mediated phosphorylation of Brca1, ensures proper spindle formation and accurate chromosome segregation. Consequently Brca1's function during mitosis is crucial for the maintenance of chromosomal stability (Stolz et al. 2010). Therefore, it is of major importance to identify proteins that participate in the mitotic Chk2-Brca1 pathway.

To identify novel proteins interacting with Brca1 during mitosis, Brca1 was immunoprecipitated from whole-cell lysates by Dr. Norman Ertych (AG Bastians, Göttingen, Germany). In collaboration with Dr. Oliver Valerius (Göttingen, Germany), Brca1 interacting proteins were identified by LC-MS/MS analysis. Importantly, 13 unique peptides for the centrosomal protein Cep72 were discovered. Thus Cep72 was clearly identified as a new interaction partner of Brca1 during mitosis (Lüddecke et al. 2015).

For validation of the results obtained by LC-MS/MS, immunoprecipitations of Brca1 from mitotic HCT116 cell lysates were performed and the (co)-immunoprecipitated proteins were analysed by western blot. In order to investigate the specificity of the interaction, cells transfected with *CEP72* siRNA were compared with control transfected cells (Figure 3.1 a). In addition to an enrichment of Brca1 protein, the Brca1 associated protein BARD1, serving as a control, was co-immunoprecipitated, showing that the immunoprecipitation was successful. Additionally a co-purification of Cep72 was clearly detected. After repression of *CEP72* a reduction in the amount of co-precipitated Cep72 protein was confirmed, so that the interaction between Cep72 and Brca1 can be considered as specific.

Moreover, the interaction between Cep72 and Brca1 in interphase was examined. For this, Brca1 immunoprecipitations were performed using cell lysates of asynchronously growing cells. Interestingly, the western blot analysis revealed an interaction between Cep72 and Brca1 in interphase cells, which was even higher than the interaction detected in mitotic cells (Figure 3.1 b).

In order to further investigate, whether the Brca1-Cep72 interaction is influenced by the mitotic, Chk2-mediated phosphorylation of Brca1, anti-Brca1 immunoprecipitations were

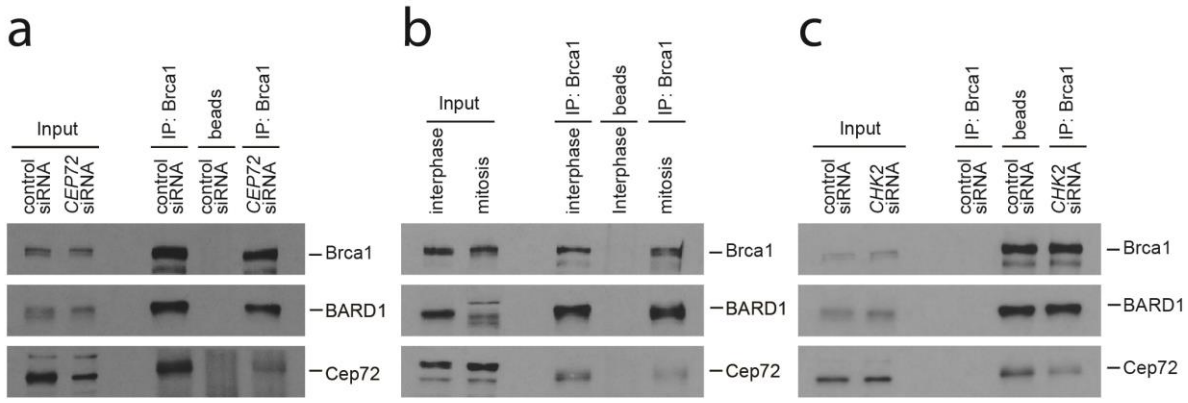

Figure 3.1 Identification of Cep72 as a novel Brca1 interacting protein. (a) For the analysis of the protein interaction between Cep72 and Brca1 anti-Brca1 immunoprecipitations of mitotic HCT116 cell lysates were performed and analysed by western blot. **(b)** To analyse the protein interaction between Cep72 and Brca1 in mitosis and interphase, anti-Brca1 immunoprecipitations of mitotic and interphase HCT116 cell lysates were performed and analysed by western blot. **(c)** In order to investigate the interaction between Brca1 and Cep72 in dependency of Chk2, anti-Brca1 immunoprecipitations were performed using mitotic lysates of HCT116 cells transfected with control or *CHK2* siRNA. The immunoprecipitation was analysed by western blot.

performed with mitotic lysates of cells, which were transfected with control or *CHK2* siRNA. The subsequent western blot analysis revealed that a repression of *CHK2* reduced the interaction between Brca1 and Cep72, whereas the interaction between Brca1 and its associated protein BARD1 remained unchanged (Figure 3.1 c).

These results showed that Brca1 and Cep72 interact both, during mitosis and even more pronounced during interphase. Additionally the mitotic interaction between Brca1 and Cep72 is positively influenced by Chk2.

Furthermore the protein levels of Brca1 and Cep72 were analysed during the cell cycle. For this, HCT116 cells were synchronized *via* double thymidine block at G1/S transition. 0, 3, 4, 6, 7, 8, 9, 10 and 11 h after thymidine removal, the protein levels of Brca1 and Cep72 were analysed by western blot (Figure 3.2 a) and linked to the respective cell cycle phases, which were determined by FACS analysis (Figure 3.2 b). It revealed that the protein levels of both, Brca1 and Cep72 gradually increased during S- and G2-phase. Brca1 levels reached a maximum after 8 h when cells started to enter mitosis. An increase in the mitotic index was further accompanied by the appearance of a double band, indicating the mitotic phosphorylation of Brca1 (Liu et al. 2002; Scully et al. 1997). Moreover the western blot showed maximal Cep72 protein levels at time points 8 and 9, which then gradually decreased again. The constant increase of Cep72 protein levels from S-phase to mitosis suggest, that Cep72 might have an important function during mitosis.

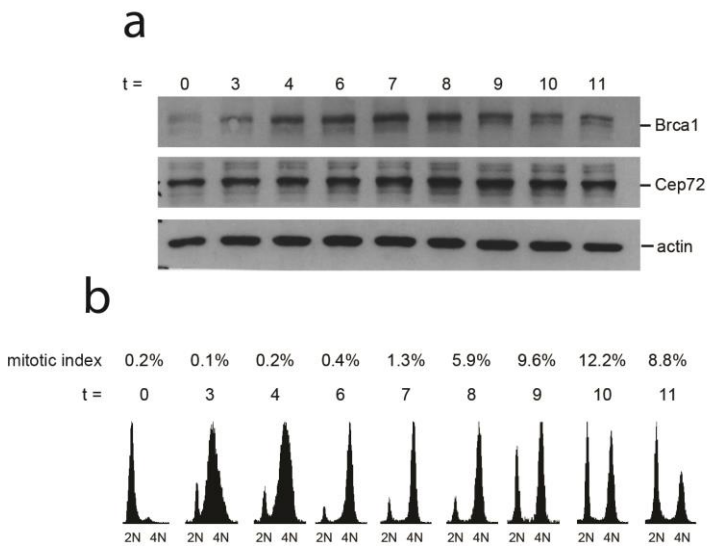

Figure 3.2 Brca1 and Cep72 protein levels peak during mitosis. (a) For the analysis of Brca1 and Cep72 protein levels during the cell cycle, cells were synchronised in G1/S phase by double thymidine block. After thymidine removal, Brca1 and Cep72 protein levels were analysed by western blot at indicated time points. **(b)** For the determination of the cell cycle phase FACS analysis using PI and MPM2 staining was performed at indicated time points.

3.2 Overexpression of *CEP72*

3.2.1 *CEP72* is frequently overexpressed in human colorectal cancer

Since Cep72 is interacting with the prominent tumour suppressor Brca1 throughout the cell cycle, the question arises, whether *CEP72* expression is altered in human cancer. Thus, an mRNA expression analysis using microarray hybridization was performed in collaboration with PD Dr. Jochen Gaedcke from the University Medical Centre Göttingen, Germany. For this, biopsies of pretherapeutic rectal tumours, which were localized in the lower and middle rectum and biopsies of the corresponding distant mucosa (at least 4 cm) were collected from >181 patients. Excluding biopsies containing less than 50% of tumour cells, RNA was isolated (RNA integrity number >5) and the mRNA expression of 181 tumour samples was analysed *via* microarray hybridization. The data, which were further analysed by Dr. Jerzy Dyczkowski (University Medical Centre Göttingen, Germany), revealed a highly significant, 3.2 fold increase in the log2(expression) of *CEP72* (Figure 3.3 a).

Furthermore the *CEP72* expression was analysed by means of immunohistochemistry in collaboration with Prof. Dr. Wilko Weichert from the University Medical Centre Heidelberg. For this, Cep72 protein levels were visualized in normal colorectal mucosa and in colorectal adenocarcinoma tissues of 357 patients, respectively, whereupon the staining

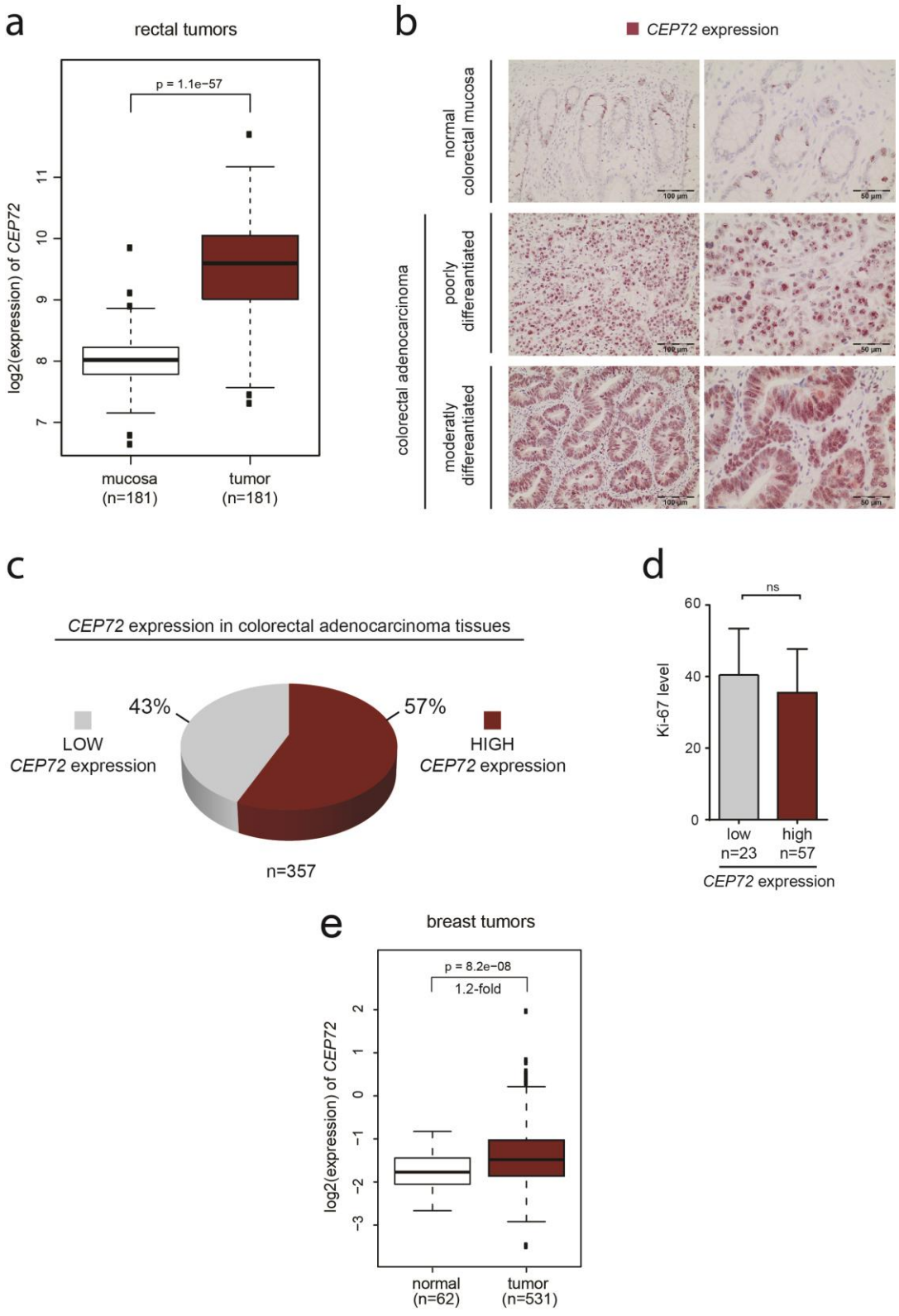

Figure 3.3 *CEP72* is frequently overexpressed in human colorectal cancer. (a) For the determination of the *CEP72* expression in rectal cancer, biopsies of pretherapeutic rectal tumours and the corresponding distant mucosa were collected from 181 patients. Subsequently the mRNA expression of *CEP72* was evaluated using microarray hybridization**. (b)** The *CEP72* expression was visualized in normal mucosa and colorectal adenocarcinoma *via* immunohistochemistry staining. While a red staining marks a *CEP72* expression *per se*, the expression level can be determined by means of the staining intensity. **(c)** Based on a classification by semi-quantitative

immunoreactivity scoring (IRS) ranging from 0-12, all analysed tumour samples were divided into tumours with a low (IRS=0) and a high (IRS>0) *CEP72* expression, respectively. **(d)** In order to determine the proliferation status of the analysed colorectal adenocarcinoma samples, the Ki-67 levels, serving as a proliferation marker, were determined. The bar plot shows the mean Ki-67 levels (± s.d.; *t*-tes) of *n*=23-57 tumour samples analysed. **(e)** In order to analyse the mRNA expression of *CEP72* in tissue samples from breast tumors and normal tissues, microarray data were downloaded from TCGA website (https://tcga-data.nci.nih.gov/tcga/dataAccessMatrix.htm), the *CEP72* expression was extracted from whole microarrays, log2 transformed and compared by paired two samples *t*-test (n=63 and 531). These data were kindly provided by PD Dr. Jochen Geadcke (a), Dr. Jerzy Dyczkowski (University Medical Centre Göttingen) (a+e), Dr. Albrecht Stenzinger and Prof. Dr. Wilko Weichert (University Medical Centre Heidelberg) (b-d).

intensity reflects the *CEP72* expression (Figure 3.3 b). Whereas in normal colorectal mucosa Cep72 was only detectable in proliferating cells at the crypt basis, poorly differentiated colorectal carcinoma showed a strong homogenous, predominantly nucleolar expression of *CEP72*. Moreover, a strong diffuse nuclear *CEP72* expression could be detected in moderately differentiated colorectal carcinomas. Subsequently the staining intensity and the percentage of immunoreactive cells were evaluated. Additionally, the tumour samples were classified by semi-quantitative immunoreactivity scoring (IRS) (Weichert et al. 2008) on the basis of the obtained data. This analysis revealed an IRS ranging from 0 – 12, whereupon the *CEP72* expression in normal colorectal mucosa was assessed as 0. All tumour samples were divided into tumours with low *CEP72* expression resembling normal colorectal mucosa (IRS=0) and tumours with high levels of Cep72 (IRS >0), respectively. This classification revealed high *CEP72* expression in 57% of all tumour samples analysed (Figure 3.3 c). In order to exclude that the enhanced protein levels of Cep72 are solely dependent on a higher amount of proliferating cells in the tumour tissue, a co-staining for the proliferation marker Ki-67 was performed. While tumours with low *CEP72* expression showed a Ki-67 level of 40.4, the Ki-67 intensity in tumour samples with high levels of Cep72 (35.4) was even lower (Figure 3.3 d). Thus, an influence of the proliferation rate on *CEP72* expression could be excluded.

Finally the *CEP72* expression was additionally analysed in breast cancer tissues, where *BRCA1* mutations are frequently present. Dr. Jerzy Dyczkowski (University Medical Centre Göttingen) extracted normalized Agilent microarray data for breast tumour and matching control samples from The Cancer Genome Atlas (TCGA) website (https://tcga-data.nci.nih.gov/tcga/dataAccessMatrix.htm) and compared the log2 expression for *CEP72* in control and breast tumour samples. While control samples revealed a log2 *CEP72* expression of -1.78, the log2 expression was only 1.2 fold increased in breast tumour samples (-1.41).

In summary, the data show that *CEP72* is frequently overexpressed in human colorectal cancer but not in breast cancer.

3.2.2 Overexpression of *CEP72* causes enhanced spindle microtubule plus-end assembly in mitosis

Since *CEP72* was shown to be frequently upregulated in human colorectal cancer tissues, this phenotype might be relevant for tumour biology. Thus, it is important to elucidate the cellular consequences of *CEP72* overexpression. Colorectal cancer cells are characterized by chromosomal instability, which in turn has been associated with tumourigenesis, poor patient prognosis and the development of therapy resistance (Bakhoum & Compton 2012). One cause for chromosomal instability is the occurrence of increased spindle microtubule plus-end assembly rates during mitosis and importantly, this phenotype could be directly linked to cells showing reduced expression of *CHK2* and *BRCA1* (Ertych et al. 2014). Thus, Chk2 and Brca1 were shown to play an important role in the regulation of spindle microtubule polymerization during mitosis. However, their exact function in this process remains elusive.

For the validation of the results obtained by Ertych et al., the spindle microtubule plus-end assembly of HCT116 cells with a transient repression of either *CHK2* or *BRCA1* was determined. To further elucidate the function of Brca1 in spindle assembly, its associated protein BARD1 (Hashizume et al. 2001) was included in the analysis. Together both proteins form a heterodimer, which is crucial for the exertion of E3 ubiquitin ligase activity. The measurement of the spindle microtubule polymerization was done by means of the end binding protein 3 (EB3), which exclusively binds to growing microtubule plus tips (Stepanova et al. 2003). By overexpression of an EB3-GFP fusion protein, growing microtubule ends can be tracked using live cell microscopy. Subsequently the distance, which the labelled protein covered within a defined time span, was determined (µm/min) (Figure 3.4).

The spindle microtubule assembly rates were measured in cells, which were synchronized in mitosis by inhibition of the kinesin Eg5/Kif11 using dimethylenastron (DME) (Müller et al. 2007). By treatment with 2 µM DME the centrosome separation is inhibited, which results in the formation of monoastral spindles exhibiting fully functional microtubules (Kapoor et al. 2000). The analysis of control transfected cells revealed mean microtubule polymerization rates of 18.1 µm/min, which was increased by 15.5%, 9.4% and 15.5% upon *BRCA1*, *BARD1* and *CHK2* knock down, respectively (Figure 3.5 a).

One way to reduce microtubule polymerization is the low dose application of the microtubule stabilizing drug Taxol® (Ertych et al. 2014). Belonging to the group of taxanes, it directly binds to microtubule subunits and stabilizes microtubules by inhibiting their dynamic properties (Jordan & Wilson 2004). In order to determine, whether the

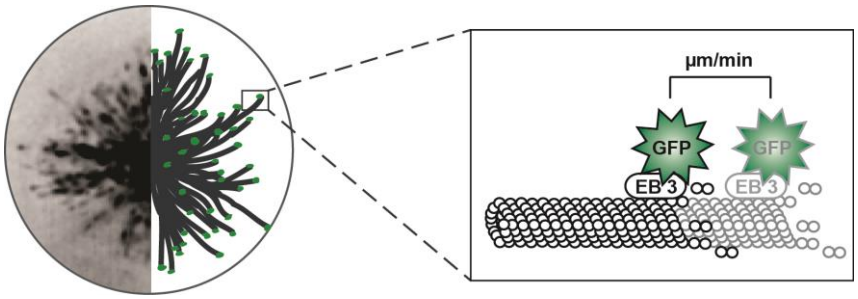

Figure 3.4 Schematic depiction of EB3 measurement for the determination of spindle microtubule plus-end assembly rates. For the measurement of spindle microtubule plus-end assembly it was taken advantage of the end binding protein 3 (EB3), which exclusively binds to growing microtubule plus tips. The overexpression of an EB3-GFP fusion protein allows the detection of polymerizing microtubules by live cell analysis. Images were acquired with a Z-optical spacing of 0.4 µm over a time period of 40 sec and every 2 sec one picture was taken. After the pictures had been deconvolved, the distance, which the EB3-protein covered within 2 sec was measured and converted into the unit µm/min. Subsequently, average microtubule plus-end assembly rates were measured on the basis of 20 microtubules per cell. The EB3 measurements were performed on monoastral mitotic spindles, which were induced by inhibition of the Eg5/Kif11 mediated centrosome separation. For this the cells were treated with 2 µM of the Eg5/Kif11 inhibitor dimethylenastron for 2 h prior to live cell analysis. The Eg5/Kif11 inhibition does not interfere with spindle microtubule assembly *per se*, but allows by monopolar spindle formation an easy measurement of microtubule polymerization rates of mitotic cells being located in the same mitotic phase.

increased microtubule plus-end assembly induced by repression of *BRCA1*, *BARD1* and *CHK2* can be reversed, cells were treated with 0.2 nM Taxol® for 24 h prior to EB3 measurements. The protein expression was verified by western blot analysis and an influence of 0.2 nM Taxol® on protein levels was excluded (Figure 3.5 b). Additionally, no difference was detectable in the microtubule polymerization between control transfected cells treated with either DMSO or Taxol®. However, the increased spindle microtubule assembly rates upon *BRCA1*, *BARD1* and *CHK2* knock down could be reduced by 0.2 nM Taxol® from 20.9 µm/min, 19.8 µm/min and 20.9 µm/min to 17.9 µm/min, 17.7 µm/min and 18.0 µm/min, respectively.

These results validate that the repression of *BRCA1* and *CHK2* leads to increased spindle microtubule plus-end assembly during mitosis (Ertych et al. 2014). Additionally it was shown that also the repression of *BARD1* results in the same phenotype. Since Brca1 and BARD1 together exhibit an E3 ubiquitin ligase activity this leads to the hypothesis that the E3 ubiquitin ligase function of Brca1 might be crucial for the regulation of spindle microtubule polymerization during mitosis. To further investigate this issue, either the Brca1 mutant I26A or Brca1 wild type (WT) (shRNA resistant) was re-expressed in HCT116 stably repressing *BRCA1* (HCT116-*BRCA1*-shRNA cells). The exchange of isoleucine to alanine on position 26 inhibits the E3 ubiquitin ligase activity, but does not affect the formation of the Brca1-BARD1 heterodimer (Brzovic et al. 2003). Cells transfected with an empty vector were used as a control.

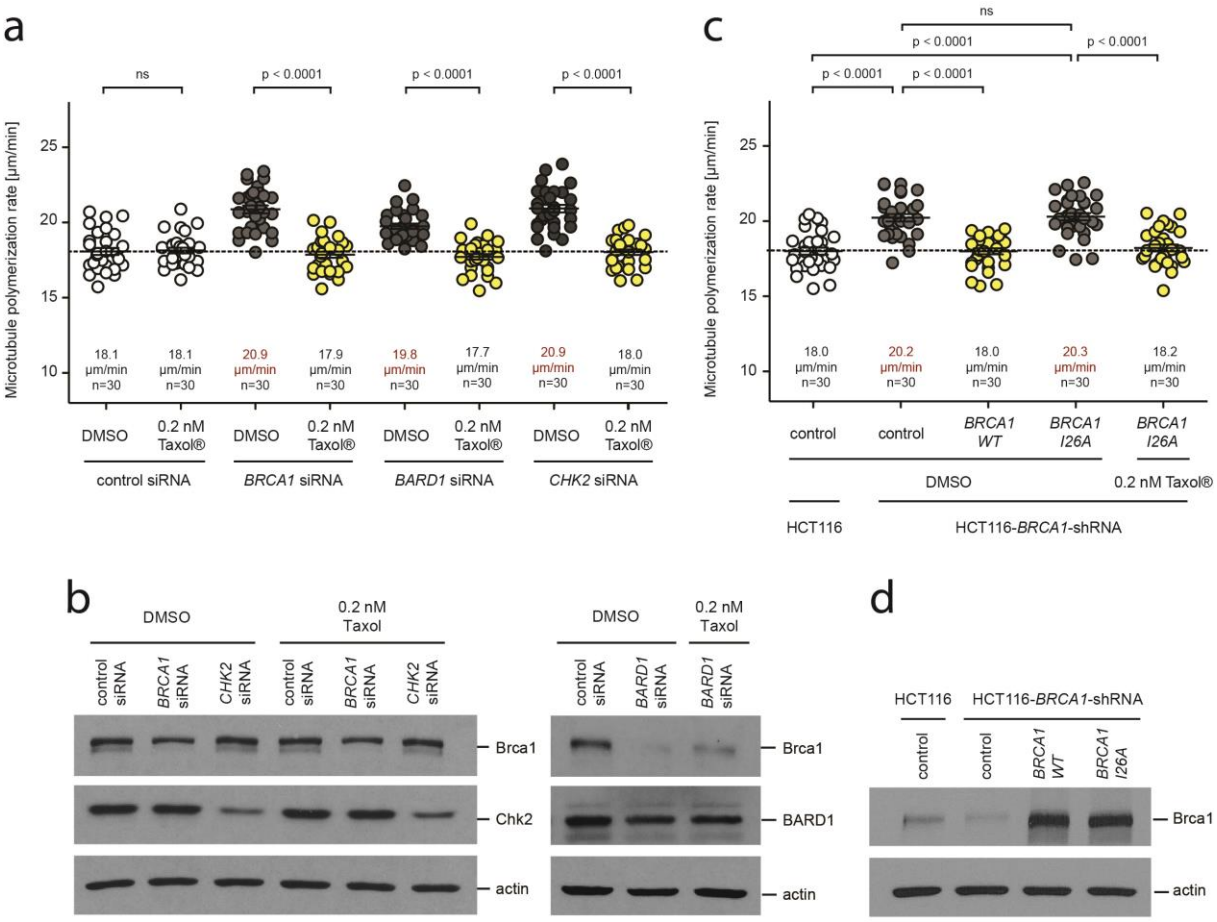

Figure 3.5 The knock down of *BRCA1, BARD1* and *CHK2* leads to enhanced spindle microtubule plus-end assembly rates during mitosis. (a) For the measurement of mitotic spindle microtubule plus-end assembly rates after transient knock down of *BRCA1, BARD1* and *CHK2*, cells were transfected with 40 pmol siRNA. Furthermore, the cells were treated with either DMSO or 0.2 nM Taxol® for 24 h prior to live cell analysis. The cells were synchronized in mitosis by treatment with 2 µM DME for 2h and the EB3 measurement was performed on monoastral spindles. The results were visualized by scatter dot plots showing the average plus-end assembly rates based on measurement of 20 microtubules per cell (mean ± s.e.m., t-test, n=30 cells from three independent experiments). **(b)** The protein repression for *BRCA1, BARD1* and *CHK2* was verified by western blot analysis. ß-actin was used as a loading control. The western blots shown are representative examples. **(c)** Determination of spindle microtubule plus-end assembly rates in stable HCT116-*BRCA1*-shRNA cells with a re-expression of either *BRCA1-WT* or the *BRCA1-I26A* mutant, which is defective for the E3 ubiquitin ligase activity. The cells were transfected with empty vector or with plasmids for CMV promoter driven expression of *BRCA1-WT* or *BRCA1-I26A*, 48h prior to live cell analysis. Additionally the cells had been treated with either DMSO or 0.2 nM Taxol® for 24 h before the cells were analysed. EB3 measurement was performed on monoastral spindles and the results were visualized by scatter dot plots showing the average plus-end assembly rates based on measurement of 20 microtubules per cell (mean ± s.e.m., t-test, n=30 cells from three independent experiments). **(d)** The protein overexpression for *BRCA1* was verified by western blot analysis. ß-actin was used as a loading control and the western blots shown are representative examples**.**

By western blot analysis the protein expression was verified (Figure 3.5 d). While cells with a stable knock down of *BRCA1* showed an increased mean spindle microtubule polymerization rate of 20.2 µm/min, the re-expression of *BRCA1-WT* restored normal spindle microtubule assembly rates of 18.0 µm/min, which was also measured in control

transfected HCT116 cells. In contrast, reconstitution of Brca1 levels by Brca1-I26A revealed a mean microtubule polymerization rate of 20.3 µm/min, resembling the value measured in control transfected HCT116-*BRCA1*-shRNA cells. This suggests that the E3 ubiquitin ligase activity of Brca1 is needed for proper spindle microtubule plus-end assembly during mitosis.

The previous results showed that Cep72 is interacting with Brca1 during mitosis, which might indicate a similar function. Additionally a role for Cep72 in spindle microtubule nucleation was already described (Oshimori et al. 2009). Thus, it is interesting to examine, whether *CEP72* overexpression influences the plus-end polymerization of spindle microtubules during mitosis. For this *CEP72* was transiently overexpressed in the human colon cancer cell line HCT116. To investigate different expression levels, cells were transfected with 1 µg, 3 µg and 5 µg of plasmid for CMV promoter driven expression of *CEP72* (pcDNA3-*CEP72*). Cells transfected with an empty vector were used as a control. The protein levels were checked by western blot, whereupon rising protein levels by transfection of 1 µg – 5 µg plasmid could be observed (Figure 3.6 a). For the determination of spindle microtubule plus-end assembly rates, the microtubule binding protein EB3 fused to GFP was co-expressed in *CEP72* overexpressing cells. The analysis by live cell microscopy revealed an increase in spindle microtubule polymerization rates from 17.1 µm/min measured in control cells to 18.2 µm/min, 20.1 µm/min and 19.4 µm/min in cells transfected with 1 µg, 3µg and 5µg pcDNA3-*CEP72* plasmid, respectively (Figure 3.6 b). To further investigate whether the increase in spindle microtubule polymerization is specific for the overexpression of *CEP72*, the overexpression levels were simultaneously repressed by *CEP72* siRNA knock down to protein levels comparable to control transfected cells (Figure 3.6 a). A subsequent EB3-measurement of cells with a simultaneous *CEP72* repression revealed spindle microtubule plus-end polymerization rates of 17.3 µm/min (1µg), 16.5 µm/min (3µg) and 16.7 µm/min (5µg), which equal microtubule assembly rates detected in control cells (Figure 3.6 b). This shows that a *CEP72* overexpression specifically leads to increased spindle microtubule plus-end assembly during mitosis.

In order to determine, whether normal spindle microtubule plus-end assembly rates in cells overexpressing *CEP72* can be restored by application of low dose Taxol®, they were treated with either DMSO or 0.2 nM Taxol® for 24 h prior to EB3-measurement. The protein expression was verified by western blot analysis (Figure 3.7 a, left panel). Furthermore the treatment with low dose Taxol® did not affect the microtubule polymerization rate of control cells (17.7 µm/min (DMSO) versus 17.8 µm/min (0.2 nM Taxol®). The overexpression of *CEP72* increased the spindle microtubule polymerization

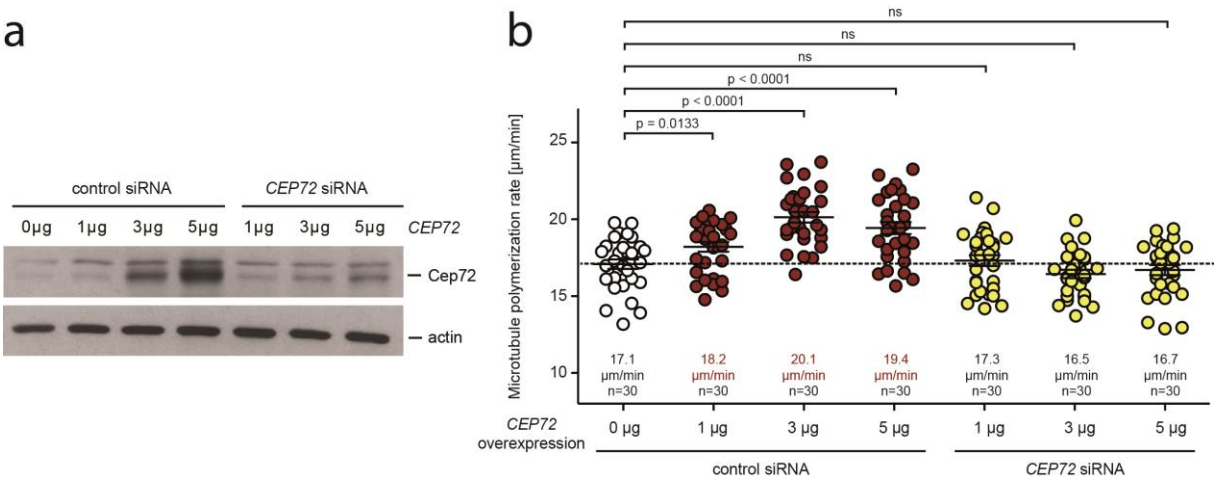

Figure 3.6 The transient overexpression of *CEP72* leads to increased spindle microtubule plus-end assembly rates during mitosis. (a) A transient overexpression of *CEP72* was achieved by transfection of either 1 µg, 3 µg or 5 µg plasmid. In order to restore normal Cep72 levels, the protein expression was simultaneously repressed by transfection of 40 pmol *CEP72* siRNA. The protein levels were verified by western blot analysis using ß-actin as a loading control. A representative example is shown. **(b)** For the investigation of mitotic spindle microtubule plus-end assembly rates upon *CEP72* overexpression, cells were synchronized in mitosis by treatment with 2 µM DME for 2h. To restore normal Cep72 protein levels, the overexpression was reduced by simultaneous *CEP72* repression. The EB3 measurements were performed on monoastral spindles. The scatter dot plots show average plus-end assembly rates based on measurement of 20 microtubules per cell (mean ± s.e.m., t-test, n=30 cells from three independent experiments).

to 20.0 µm/min (1 µg), 20.1 µm/min (3 µg) and 19.9 µm/min (5 µg), which could be reduced by treatment with 0.2 nM Taxol® to 17.6 µm/min, 17.5 µm/min and 17.3 µm/min, respectively (Figure 3.7 a, right panel).

Microtubule assembly is dependent on the microtubule polymerase ch-TOG, which catalyses the addition of tubulin dimers to the microtubule plus-end (Brouhard & Rice 2014; Ertych et al. 2014). Thus, it is likely that microtubule polymerization can also be lowered by the reduction of ch-TOG protein levels. In order to elucidate, whether enhanced spindle microtubule plus-end assembly rates induced by *CEP72* overexpression can also be restored by inhibiting the microtubule polymerase, *CH-TOG/CKAP5* was downregulated in cells simultaneously overexpressing *CEP72*. Using western blot analysis the knock down efficiency was controlled, whereupon a 86-96% reduction of the ch-TOG protein levels could be determined (Figure 3.7 b, left panel). The EB3 measurement of *CEP72* overexpressing cells revealed an increase in spindle microtubule assembly rates to 18.2 µm/min (1 µg), 19.9 µm/min (3 µg) and 19.5 µm/min (5 µg). By simultaneous downregulation of *CH-TOG/CKAP5* the microtubule polymerization was reduced to 16.5 µm/min (1 µg), 16.5 µm/min (3µg) and 16.3 µm/min (5 µg), resembling spindle microtubule assembly rates measured in control transfected cells (17.0 µm/min) (Figure 3.7 b, right panel).

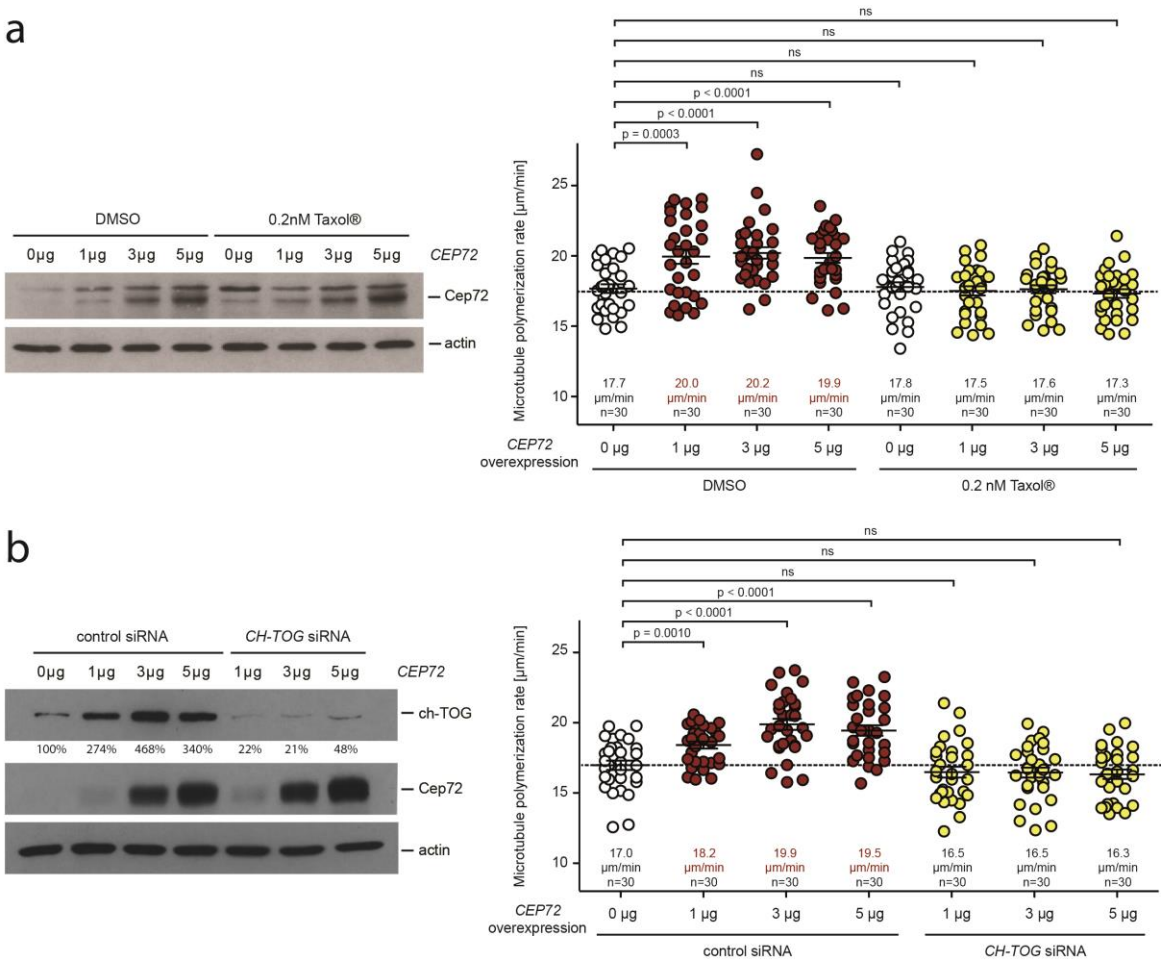

Figure 3.7 The increased spindle microtubule plus-end assembly rates caused by *CEP72* overexpression can be restored by either treatment with low dose Taxol® or by repression of *CH-TOG*. (a) To determine the influence of low dose Taxol® on spindle microtubule plus-end assembly rates after *CEP72* overexpression at indicated concentrations, cells were treated with either DMSO or 0.2 nM Taxol® for 24h prior to live cell analysis. The EB3 measurements were performed on mitotic monoastral spindles and the results are shown in form of scatter dot plots showing the average plus-end assembly rates based on measurement of 20 microtubules per cell (mean ± s.e.m., t-test, n=30 cells from three independent experiments). The protein expression was verified by western blot analysis using ß-actin as a loading control. A representative western blot is given. **(b)** In order to investigate the influence of the microtubule polymerase ch-TOG on spindle microtubule plus-end assembly rates after *CEP72* overexpression at indicated concentrations, cells were simultaneously transfected with 40 pmol of either control or *CH-TOG/CKAP5* siRNA 48h prior to live cell analysis. The EB3 measurement was performed on mitotic monoastral spindles and the results are presented in form of scatter dot plots showing the average plus-end assembly rates based on measurement of 20 microtubules per cell (mean ± s.e.m., t-test, n=30 cells from three independent experiments). The protein expression was verfied by western blot analysis using ß-actin as a loading control. A representative example is shown.

Thus, enhanced spindle microtubule plus-end assembly induced by *CEP72* overexpression can be suppressed by interfering with microtubule polymerization using low dose of Taxol® and by downregulation of the microtubule polymerase *CH-TOG/CKAP5*.

To further investigate the overexpression of *CEP72* in a stable cell system, HCT116 cells were transfected with either an empty vector or a *CEP72* expression plasmid being

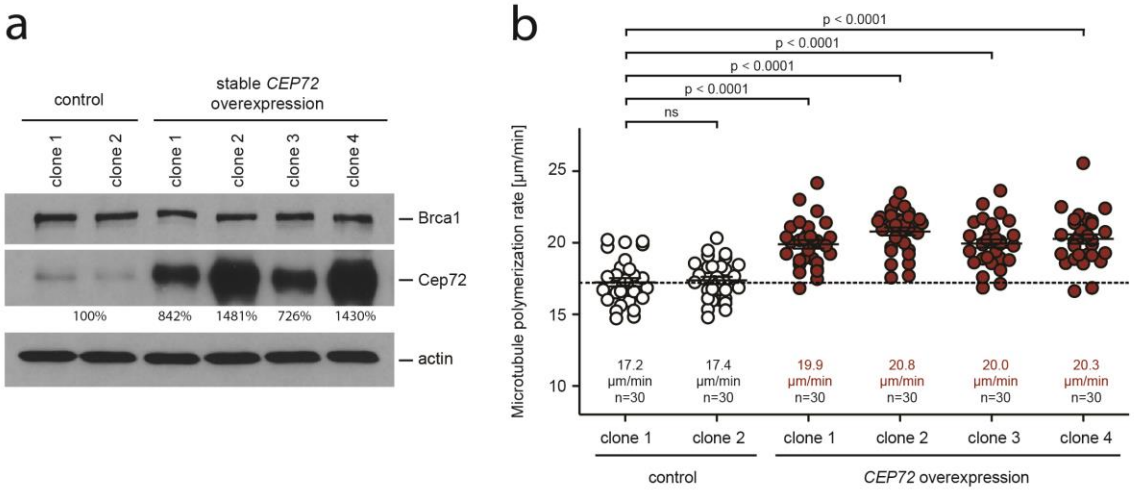

Figure 3.8 The stable overexpression of *CEP72* leads to enhanced spindle microtubule plus-end assembly rates during mitosis. (a) HCT116 cells were transfected with a control and a *CEP72* overexpression plasmid, respectively. Single cell clones were generated via G418 selection and the protein expression was verified by western blot analysis using ß-actin as a loading control. A representative example is shown. **(b)** For the investigation of mitotic spindle microtubule plus-end assembly rates upon *CEP72* overexpression, four independent single cell clones as well as two control clones were analysed. The EB3 measurements were performed on monoastral spindles and the results are represented as scatter dot plots showing the average plus-end assembly rates based on measurement of 20 microtubules per cell (mean ± s.e.m., t-test, n=30 cells from three independent experiments).

equipped with attB sites. By simultaneous expression of the phage integrase phiC31, the vectors were integrated into the human genome in a site-specific manner (Groth et al. 2000). Subsequently single cell clones stably overexpressing *CEP72* were generated *via* G418 selection and identified by western blot (Figure 3.8 a). Compared to control cells, the Cep72 protein levels of stable cell clones overexpressing *CEP72* were enhanced by 7.4 – 14.3-fold. Additionally the microtubule plus-end assembly was determined in monoastral spindles. While control clones showed a microtubule polymerization of 17.2 µm/min and 17.4 µm/min, the microtubule assembly rates in stable *CEP72* overexpression clones was enhanced by 15.0%, 20.2%, 15,6% and 17.3% (Figure 3.8 b).

Moreover, the effect of Taxol® on enhanced spindle microtubule plus-end assembly in cells stably overexpressing *CEP72* was examined. To this end, based on the stable control clone 1 and the *CEP72* overexpression clone 2, single cell subclones were generated and cultivated in the presence of either DMSO or 0.2 nM Taxol® (Figure 3.9 a). Western blot analysis after 30 generations revealed that the cultivation in the presence of 0.2 nM Taxol® did not affect the Cep72 protein levels (Figure 3.9 b). By measuring spindle microtubule polymerization rates, no difference was detectable between control subclones cultivated in either DMSO (18.7 µm/min and 19.1 µm/min) or 0.2 nM Taxol® (both 18.4 µm/min). However, the spindle microtubule plus-end assembly of *CEP72*

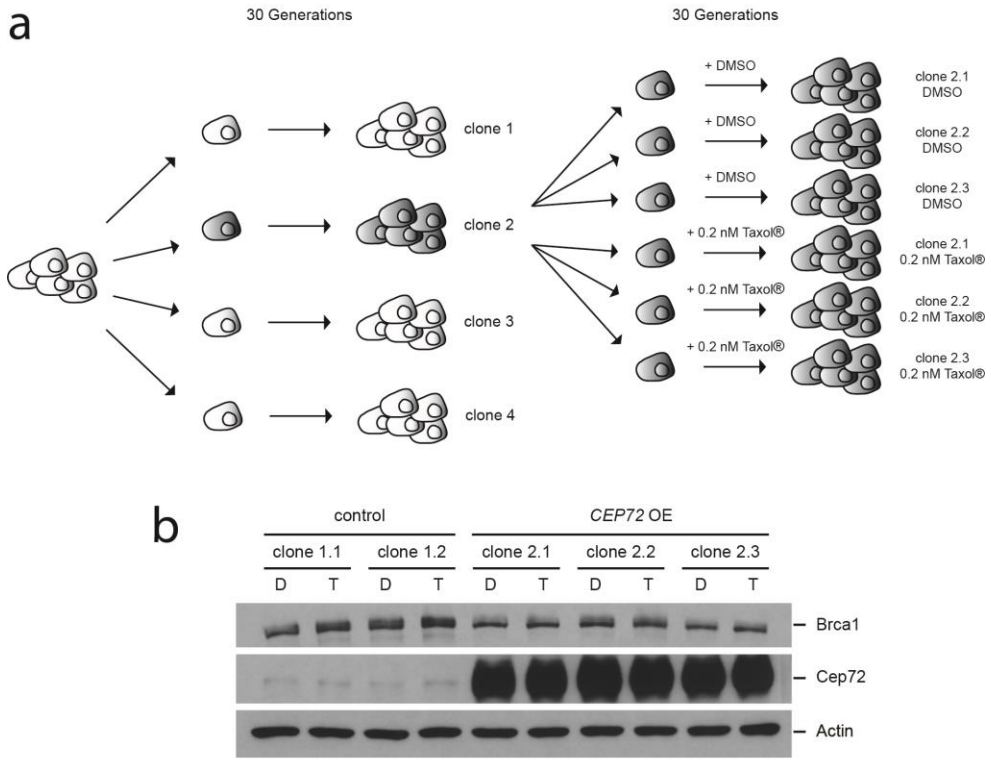

Figure 3.9 Generation of cells stably overexpressing *CEP72* in the presence and absence of 0.2 nM Taxol®. (a) Schematic overview of the generation of cell clones with a stable overexpression of *CEP72* grown for 30 generations in the presence of either DMSO or 0.2 nM Taxol®. **(b)** Based on the cell clone 2 stably overexpressing *CEP72* as well as on control clone 1 independent single cell clones were generated in the presence of DMSO (D) or 0.2 nM Taxol® (T) (shown in (a)). The protein levels of Brca1 and Cep72 were verified by western blot analysis (representative example is given). ß-actin was used as a loading control.

overexpressing subclones generated in the presence of 0.2 nM Taxol® resembled with 18.8 µm/min, 18.7 µm/min and 18.8 µm/min the microtubule polymerization rates measured in control cells, whereupon subclones cultivated in the presence of DMSO still exhibited increased spindle microtubule plus-end assembly rates of 21.6 µm/min and 22.6 µm/min.

As already shown in Figure 3.5 the knock down of *BRCA1* leads to enhanced spindle microtubule plus-end assembly rates during mitosis. In order to draw a direct comparison between *BRCA1* knock down and the overexpression of *CEP72*, also subclones of HCT116-*BRCA1*-shRNA cells were generated in the presence of DMSO and 0.2 nM Taxol®, respectively. Determination of microtubule plus end assembly rates after 30 generations revealed similar microtubule polymerization rates as observed for *CEP72* overexpression. Whereas cell subclones with a stable knock down of *BRCA1* cultivated in the presence of DMSO showed increased spindle microtubule assembly rates of 21.5 µm/min, 21.2 µm/min and 22.0 µm/min, the spindle microtubule polymerization of subclones cultivated in 0.2 nM Taxol® could be reduced to 19.3 µm/min, 19.0 µm/min and 19.2 µm/min,

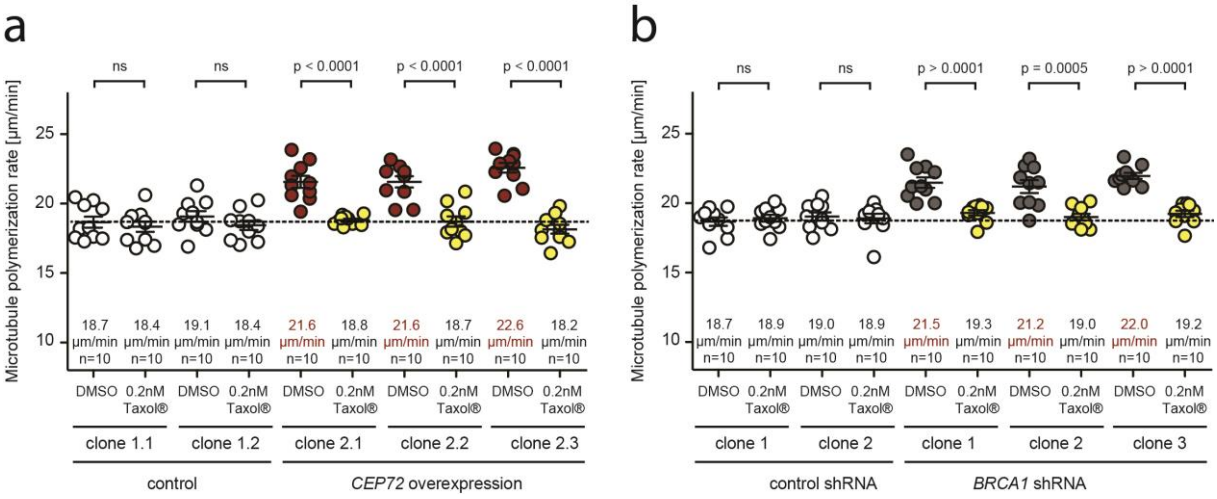

Figure 3.10 *CEP72* overexpression mirrors *BRCA1* repression in respect to increased spindle microtubule plus-end assembly. (a) Measurements of mitotic spindle microtubule plus-end assembly rates in stable cell clones with an overexpression of *CEP72* generated in the presence or absence of 0.2 nM Taxol® (depicted in Figure 3.9 a). The cells were synchronized in mitosis by treatment with 2 µM DME for 2h and the EB3 measurement was performed on monoastral spindles. The scatter dot plots show average plus-end assembly rates based on the measurement of 20 microtubules per cell (mean ± s.e.m., t-test, n=10 cells). **(b)** Measurements of mitotic spindle microtubule plus-end assembly rates in stable cell clones with a knock down of *BRCA1* generated in the presence or absence of 0.2 nM Taxol®. The cells were treated as described in (a) and the results were represented as scatter dot plots showing average plus-end assembly rates based on the measurement of 20 microtubules per cell (mean ± s.e.m., t-test, n=10 cells).

respectively. Control transfected subclones showed spindle microtubule polymerization rates from 18.7 µm/min – 19.0 µm/min, whereupon no difference could be detected between cell clones cultivated in the presence of either DMSO or 0.2 nM Taxol®.

In order to elucidate whether overexpression of *CEP72* or *BRCA1* repression influences the microtubule polymerization beyond mitosis, microtubule plus end assembly rates were determined in interphase cells. EB3 measurement of cells with a transient overexpression of *CEP72* or *BRCA1* knock down revealed average spindle microtubule plus end assembly rates of 18.3 µm/min and 18.4 µm/min resembling the rates measured in control transfected cells (18.3 µm/min) (Figure 3.11).

Thus, a stable *CEP72* overexpression causes enhanced spindle microtubule plus-end assembly rates during mitosis, which can be restored to control levels by treatment with low dose Taxol®. A direct comparison between cells with an overexpression of *CEP72* and cells with a knock down of *BRCA1* revealed that both conditions cause a very similar deregulation of microtubule assembly in mitosis, but not in interphase.

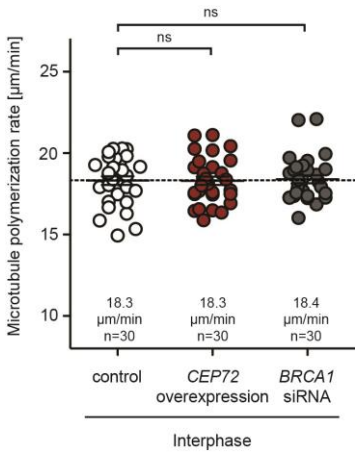

Figure 3.11 *CEP72* overexpression and *BRCA1* repression does not interfere with microtubule plus end polymerization in interphase. Measurement of microtubule plus end assembly rates upon transient overexpression of *CEP72* or *BRCA1* repression in interphase cells. The scatter dot plots show average plus-end assembly rates based on the measurement of 20 microtubules per cell (mean ± s.e.m., t-test, n=10 cells).

3.2.3 Overexpression of *CEP72* causes abnormal mitotic spindle assembly

The dynamics of microtubules essentially participates in the formation and maintenance of the mitotic spindle (Vicente & Wordeman 2015). To clarify the effects of enhanced microtubule plus-end assembly during mitosis caused by *CEP72* overexpression, the morphology of mitotic spindles was investigated. Cells with a transient overexpression of *CEP72* were synchronized in metaphase by double thymidine block and subsequent treatment with the proteasome inhibitor MG132. When cells enter mitosis in the presence of MG132 a normal spindle formation is warranted while the metaphase to anaphase transition is inhibited. Thus, cells were arrested in metaphase and analysed by immunofluorescence microscopy. Cells with a transient overexpression of *CEP72* exhibited an aberrant spindle morphology (Figure 3.12 a). While control cells showed normal, ball-like spindles, cells with a *CEP72* overexpression exhibited curved and distorted spindle microtubules, which appeared to be longer. The quantification revealed 4.5% curved spindles in control cells, which was increased by *CEP72* overexpression to 14.5% (1µg), 15.0% (3 µg) and 14% (5µg) (Figure 3.12 b).

In addition, cells with a transient *BRCA1* repression were compared to cells in which *CEP72* was transiently overexpressed. To further elucidate, whether the spindle morphology aberrations are caused by increased spindle microtubule plus-end assembly, the cells were simultaneously treated with either DMSO or 0.2 nM Taxol®. The analysis revealed that also cells with a transient knock down of *BRCA1* exhibited curved spindles in 21.3%, which was comparable to 20% of curved spindles in cells overexpressing *CEP72* (Figure 3.12 c). Additionally the portion of curved spindles was reduced to 9% in

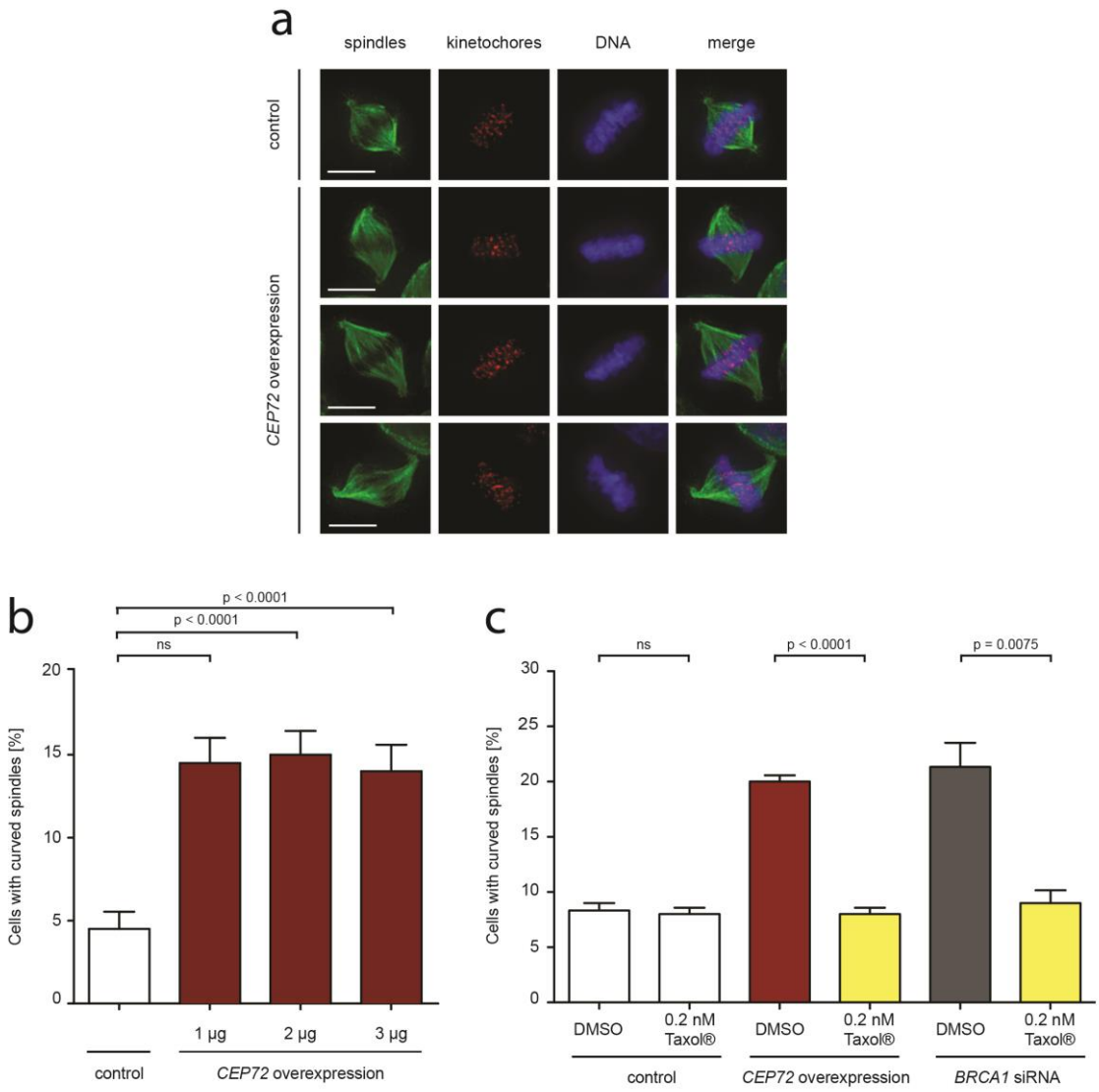

Figure 3.12 The overexpression of *CEP72* leads to spindle morphology alterations during mitosis, which is dependent on increased spindle microtubule plus-end assembly. (a) Representative images showing the mitotic spindle morphology of HCT116 cells stably transfected with either an empty vector or a plasmid for CMV promoter driven expression of *CEP72*. The cells were synchronized in G1/S phase *via* double thymidine block, released into medium for 6.5 h and arrested in mitosis by treatment with 20 µM MG132 for further 3 h. By immunofluorescence staining the spindles (α-tubulin, green), kinetochores (Crest, red) and the DNA (Hoechst33342, blue) were visualized. Scale bar: 10 µm. **(b)** Quantification of curved spindles in HCT116 cells after transient *CEP72* overexpression at indicated concentrations. Cells were treated as described in (a). Subsequently the spindle morphology was detected and quantified by immunofluorescence analysis (mean ± s.d.; t-test, n=300 bipolar spindles of three independent experiments). **(c)** Quantification of curved spindles in HCT116 cells with a transient overexpression of *CEP72* or *BRCA1* knock down. The cells were treated either with DMSO or 0.2 nM Taxol® for 24h prior to immunofluorescence analysis (mean ± s.d.; t-test, n=300 bipolar spindles of three independent experiments).

cells with a repression of *BRCA1* and to 8% in *CEP72* overexpressing cells by treatment with low dose Taxol®. In control transfected cells no difference could be detected between cells treated with DMSO (8.3%) and 0.2 nM Taxol® (8%).

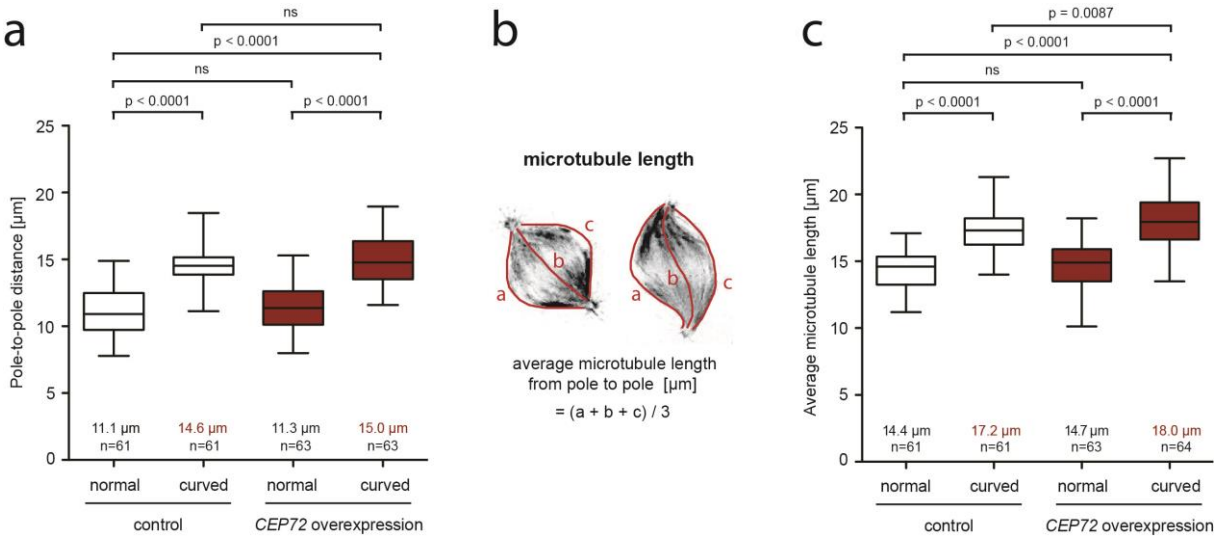

Figure 3.13 Cells showing spindle morphology alterations after *CEP72* overexpression exhibit an enhanced inter centrosomal distance and an increase in the average microtubule length. (a) In order to determine the pole-to-pole distance of normal and curved spindles in cells transiently overexpressing *CEP72*, cells were synchronized in G1/S phase *via* double thymidine block, released into medium for 6.5 h and arrested in mitosis by treatment with 20 µM MG132 for further 3 h. Subsequently, the distance between the centrosomes was measured on the basis of immunofluorescence images (spindles, anti-α-tubulin: green; centromeres, γ-tubulin: red; chromosomes, Hoechst 33342: blue; scale bar, 10 µm). The box and whisker plot shows the range, mean and quartile of the measurements (*t*-test, n=61-64 cells from three independent experiments). **(b)** Schematic depiction for the determination of the average microtubule length from pole to pole. **(c)** For the measurement of the average microtubule length from pole to pole of normal and curved spindles in cells with a transient *CEP72* overexpression, cells were arrested in mitosis as described in (a). Subsequently the average microtubule length form pole to pole was determined on the basis of immunofluorescence images as depicted in (b). The box and whisker plot shows the range, mean and quartile of the measurements (*t*-test, n=61-64 cells from three independent experiments).

Since the aberrant spindles appear to be longer when compared to control ones, the distance between the centrosomes was determined in proper spindles of control and *CEP72* overexpressing cells and compared to the pole-to-pole distance of spindles with a curved morphology. The measurement revealed an inter-centrosomal distance of 11.1 µm for normal spindles of control transfected cells (Figure 3.13 a). Compared to this, no difference in the pole-to-pole distance of proper spindles in cells overexpressing *CEP72* (11.3 µm) was detectable. However, curved spindles in control and *CEP72* overexpressing cells showed a significantly increased pole-to-pole distance of 14.6 µm and 15.0 µm, respectively.

Furthermore, the length of microtubules from pole to pole was measured following the curved morphology. For this the microtubule length was determined at both outer sides as well as in the middle of the spindle as depicted in Figure 3.13 b. Subsequently, the average microtubule length from pole to pole was calculated. Whereas normal spindles showed an average microtubule length of 14.4 µm in control and 14.7 µm in *CEP72*

overexpressing cells, the microtubule length from pole to pole of curved spindles was enhanced to 17.2 µm and 18.0 µm, respectively (Figure 3.13 c)

These data indicate that a *CEP72* overexpression or repression of *BRCA1* lead to aberrations of the mitotic spindle morphology, which is characterized by a curved and distorted phenotype, an enhanced inter-centrosomal distance and elongated microtubules. Additionally these abnormal spindles are dependent on increased spindle microtubule plus-end assembly rates.

3.2.4 Overexpression of *CEP72* causes the generation of lagging chromosomes

Alterations in the mitotic spindle formation, which are accompanied by spindle geometry defects can lead to erroneous attachments between spindle microtubules and kinetochores (Silkworth & Cimini 2012; Nam et al. 2014). One important example are merotelic attachments, which are characterized by the simultaneous attachment of spindle microtubules emanating from the two opposing poles to one kinetochore. This kind of malattachment cannot be detected by the spindle assembly checkpoint and cells enter anaphase in the presence of chromosomes being simultaneously attached to both poles. As a consequence, chromosomes cannot be separated correctly leading to chromosomes, which lag in the equatorial plane of the cell. These "lagging chromosomes" are a main cause for subsequent chromosome mis-segregation in cancer cells (Gregan et al. 2011).

To examine whether alterations in spindle assembly caused by *CEP72* overexpression lead to unresolved merotelic attachments, lagging chromosomes were quantified. Cells were synchronized in G1/S phase by double thymidine block and released into fresh medium for 9.5 h. Subsequently the cells were analysed by immunofluorescence microscopy. In this way lagging chromosomes were observed in cells overexpressing *CEP72* (Figure 3.14 a). To further investigate whether the occurrence of lagging chromosomes is dependent on increased spindle microtubule plus-end assembly, control and *CEP72* overexpressing cells were simultaneously treated with DMSO and 0.2 nM Taxol®, respectively. The quantification revealed a 2.9 fold (1µg) – 4 fold (3µg) increase in the percentage of lagging chromosomes after *CEP72* overexpression when compared to control transfected cells (Figure 3.14 c). However, the treatment with low dose Taxol® reduced the enhanced amounts of lagging chromosomes in *CEP72* overexpressing cells from 4.3% (1µg), 6.1% (3µg) and 5.0% (5µg) to 2.0% (1µg), 2.0% (3µg) and 1.3% (5µg), respectively. In contrast, Taxol® treatment did not affect the percentage of

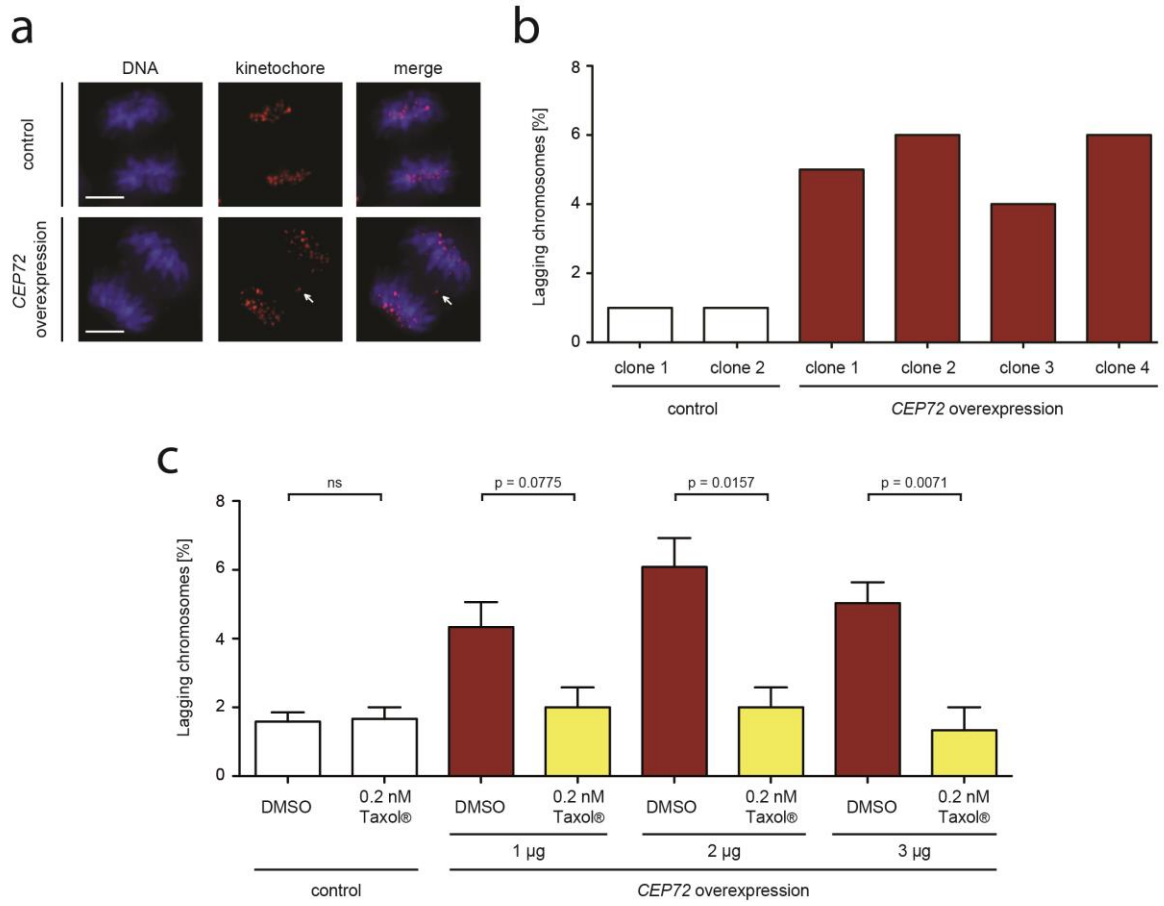

Figure 3.14 The overexpression of *CEP72* leads to chromosome mis-segregation, which can be reversed by restoration of normal spindle microtubule plus-end assembly rates. (a) Representative example of immunofluorescence images showing proper anaphase morphology in control transfected cells and lagging chromosomes (indicated by white arrow) in cells with an overexpression of *CEP72*. The cells were synchronized in G1/S phase *via* double thymidine block and released into medium for 9.5 h. By immunofluorescence staining kinetochores (Crest, red) and the DNA (Hoechst33342, blue) were visualized. Scale bar: 10 µm. **(b)** For the quantification of lagging chromosomes in cells with a stable overexpression of *CEP72*, four independent single cell clones were analysed and compared to control transfected cells. The cells were treated as described in (a) and, subsequently, lagging chromosomes were quantified by immunofluorescence analysis (n=200 cells). **(c)** To investigate the influence of low dose Taxol® on the generation of lagging chromosomes, *CEP72* was transiently overexpressed at indicated concentrations and the cells were cultivated in either DMSO or 0.2 nM Taxol® for 26 h prior to immunofluorescence analysis. The cells were treated as decribed in (a) and lagging chromosomes were quantified by immunofluorescence analysis (mean ± s.d.; t-test, n=600 cells of three independent experiments).

lagging chromosomes in control transfected cells (1.5% DMSO versus 1.7% 0.2 nM Taxol®).

Moreover, lagging chromosomes were quantified in the single cell clones stably overexpressing *CEP72* and a 4.0 – 6.0 fold enhancement in the percentage of lagging chromosomes was found when compared to the control cell clone (Figure 3.14 b). To compare the induction of lagging chromosomes after *CEP72* overexpression and *BRCA1* repression, the percentage of lagging chromosomes was additionally determined in single

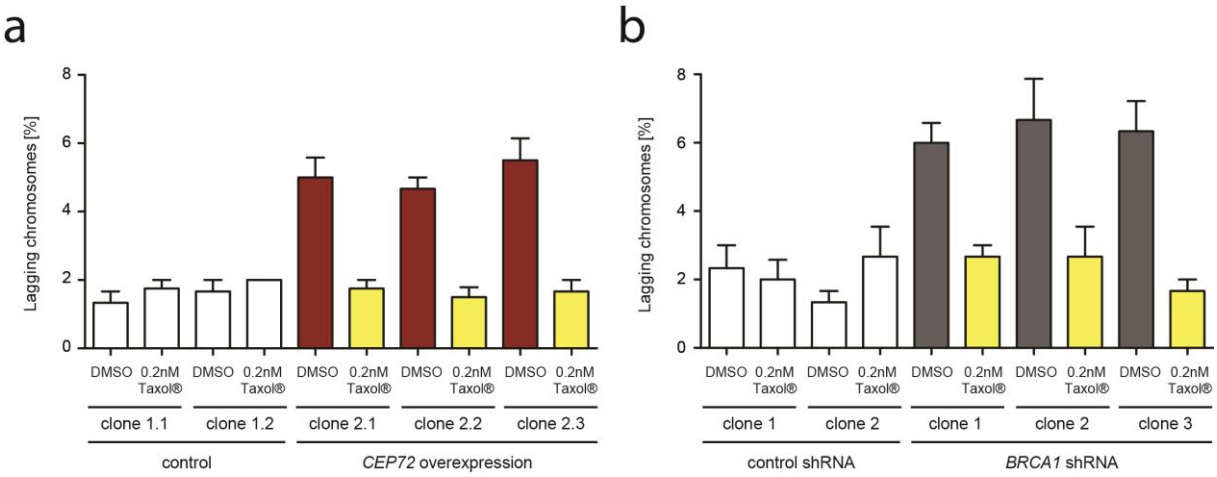

Figure 3.15 *CEP72* overexpression mirrors *BRCA1* repression with respect to the generation of lagging chromosomes. (a) Quantification of lagging chromosomes in stable cell clones with overexpression of *CEP72* grown in the presence or absence of 0.2 nM Taxol® (as depicted in Figure 3.9 a. The cells were synchronized in G1/S phase *via* double thymidine block, released into medium for 9.5 h and analysed by immunofluorescence microscopy. The graph shows mean values ± s.e.m (n=3 independent experiments with 300 cells evaluated in total). **(b)** Quantification of lagging chromosomes in stable cell clones with a *BRCA1* knock down grown in the presence or absence of 0.2 nM Taxol®. The cells were synchronized in G1/S phase *via* double thymidine block, released into medium for 9.5 h and analysed by immunofluorescence microscopy. The graph shows mean values ± s.e.m (n=3 independent experiments with 300 cells evaluated in total).

cell subclones generated in the presence of either DMSO or 0.2 nM Taxol®, which were already described in 3.2.2. In the presence of DMSO, subclones with *CEP72* overexpression exhibited a 3.1 - 3.7 fold increase in the percentage of lagging chromosomes when compared to control clones (Figure 3.15 a). Comparably, the number of cells with lagging chromosomes was enhanced to 3.3 – 3.7 fold in subclones with a stable *BRCA1* knock down (Figure 3.15 b). In both cases the long term treatment with 0.2 nM Taxol® suppressed the generation of lagging chromosomes. While in cells with an overexpression of *CEP72* the amount of lagging chromosomes was reduced from 5%, 4.7% and 5.5% to 1.8%, 1.5% and 1.7% (Figure 3.15 a), the Taxol® treatment of subclones with a *BRCA1* repression led to a reduction from 6.0%, 6.7% and 6.3% to 2.7%, 2.7% and 1.7% (Figure 3.15 b). In contrast, no difference in the percentage of lagging chromosomes was detected in subclones that were grown either in DMSO or 0.2 nM Taxol® (Figure 3.15 a: 1.3% and 1.7% versus 1.8% and 2%; Figure 3.15 b: 2.3% and 1.3% versus 2.0% and 2.7%).

These results show, that the overexpression of *CEP72* leads to chromosome mal-attachments, which results in the generation of lagging chromosomes that are caused by increased spindle microtubule plus-end assembly rates during mitosis. Moreover the data show that a stable *BRCA1* repression mirrors the phenotype observed in *CEP72* overexpressing cells.

3.2.5 Overexpression of *CEP72* causes chromosomal instability

The results obtained so far show that *CEP72* overexpression triggers the formation of lagging chromosomes. Since chromosomes, which lag in the equatorial plane are finally distributed onto daughter cells by chance, the appearance of lagging chromosomes can lead to chromosome mis-segregation and the induction of chromosomal instability (Lengauer et al. 1997; Gregan et al. 2011). To determine the effect of *CEP72* overexpression on the maintenance of chromosomal stability, the karyotype of the single cell clones was analysed by means of metaphase chromosome spreads (Figure 3.16 a). Since HCT116 cells exhibit a near diploid and chromosomally stable karyotype, they are well suitable for the detection of chromosome mis-segregations. To be able to detect changes in the karyotype, single cell clones were established and cultivated for 30 generations prior to karyotyping (as already described in 3.2.2). The subsequent analysis of cells stably expressing *CEP72* revealed a much broader distribution of individual chromosome numbers compared to control cells, whereas the modal number of 45 chromosomes remained unchanged (Figure 3.16 b). While control cells showed chromosome numbers deviating from the modal of 12% and 16%, the amount of aneuploid cells in single cell clones with a stable *CEP72* overexpression was increased to 40%, 49%, 30% and 40% (Figure 3.16 c).

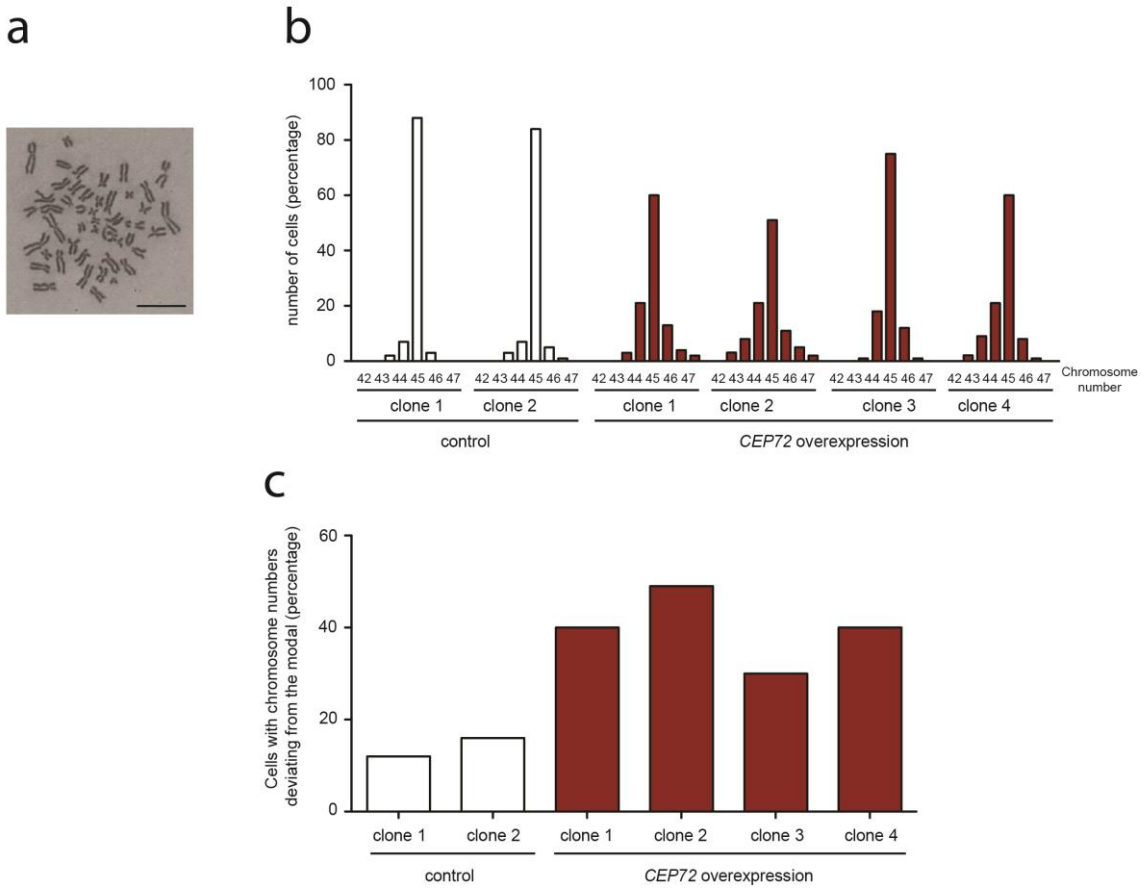

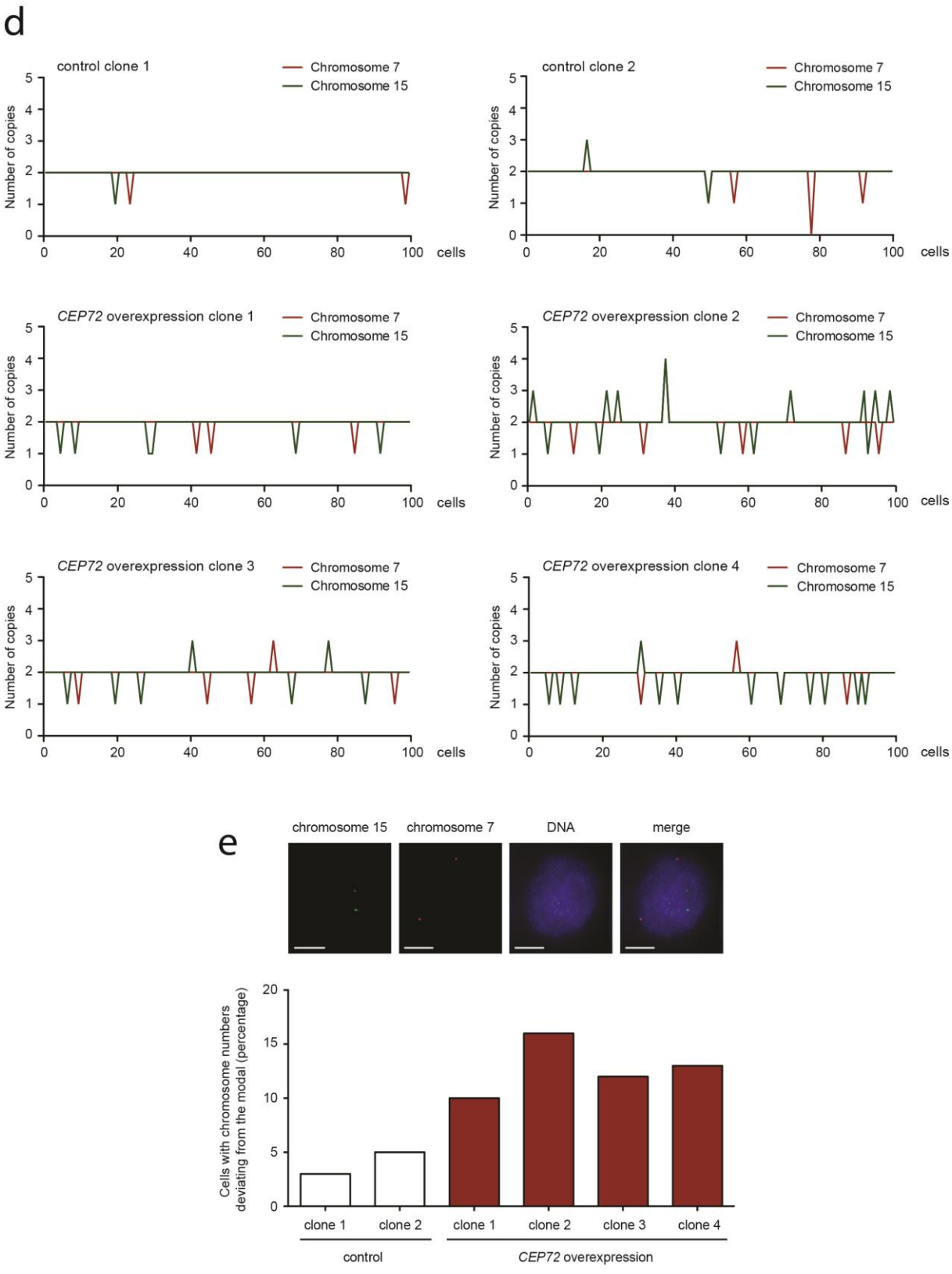

Figure 3.16 The overexpression of *CEP72* leads to chromosomal instability. (a) Representative example image of a metaphase chromosome spread acquired by transmitted light microscopy. Scale bar 10 µm. **(b)** The karyotype analysis of four independent cell clones with a stable overexpression of *CEP72* as well as two control clones was performed after 30 generations. The amount of chromosomes was determined for 100 cells *via* metaphase spread analysis and

visualized as a bar plot showing the amount of cells with indicated chromosome numbers (n=100 cells). The modal chromosome number of HCT116 cells was determined to be 45. **(c)** On the basis of the chromosome numbers shown in (a), the percentage of cells deviating from the modal was calculated and visualized in a bar plot (n=100 cells). **(d)** CEP-FISH analysis for chromosome 7 and 15 of four independent cell clones with a stable overexpression of *CEP72* as well as two control clones was performed after 30 generations. The graphs show the numbers of copies for chromosome 7 and 15 for 100 cells analysed. The modal chromosome number of HCT116 cells for chromosome 7 and 15 was determined to be 2. **(e)** The proportion of cells that deviate from the modal chromosome number of chromosome 7 and chromosome 15 was calculated on the basis of CEP-FISH data shown in (d) (n=100 cells). A representative CEP-FISH image for chromosome 7 and chromosome 15 is given above. Scale bar: 10 µm

This indicates a perpetual gain and loss of whole chromosomes after *CEP72* overexpression. To further investigate chromosome mis-segregation events, the number of individual chromosomes was determined. For this, single cell clones were subjected to fluorescence in situ hybridisation (FISH) using chromosome enumeration probes (CEP). The application of fluorescence labelled probes, which specifically hybridize with centromeric regions of defined chromosomes, allows the detection of single chromosomes in mitotic cells and interphase nuclei.

The CEP-FISH analysis of the single cell clones stably overexpressing *CEP72* was performed in interphase nuclei with probes targeting chromosome 7 and 15 (Figure 3.16 e, top). The quantification revealed for both chromosomes a modal number of 2. In total, both, chromosome gains and losses were observed, whereupon the appearance of chromosome loss prevailed (Figure 3.16 d). For the calculation of chromosome numbers deviating from the modal, chromosome 7 and 15 were included. Whereas control cell clones showed with 3% and 5% a low amount of chromosome number alterations, the number of cells with chromosome numbers deviating from 2 was increased to 10%, 16%, 12% and 13% in single cell clones stably overexpressing *CEP72* (Figure 3.16 e, bottom).

Moreover, it was investigated, whether the perpetual chromosome mis-segregation in cells overexpressing *CEP72* can be reversed by restoration of normal spindle microtubule plus-end assembly rates.

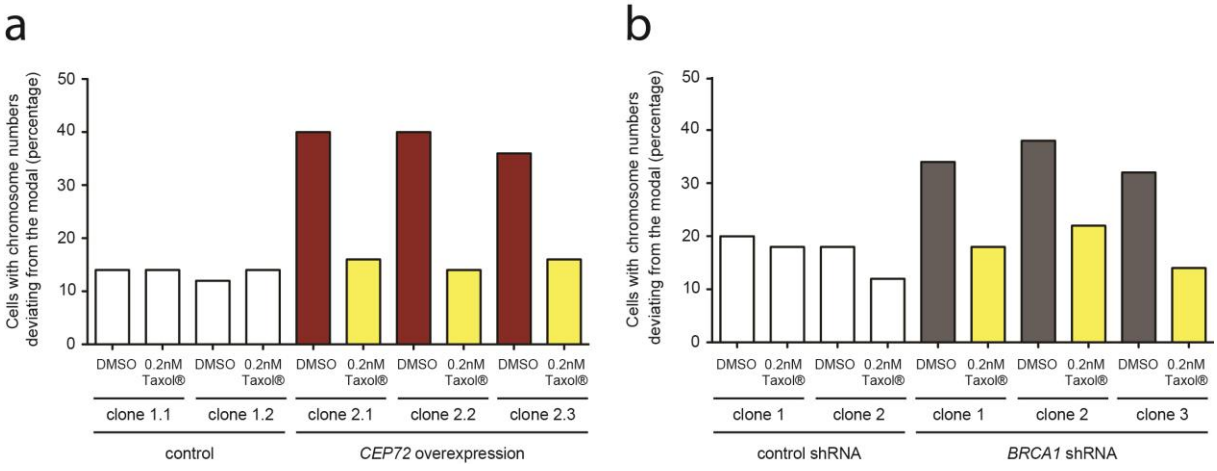

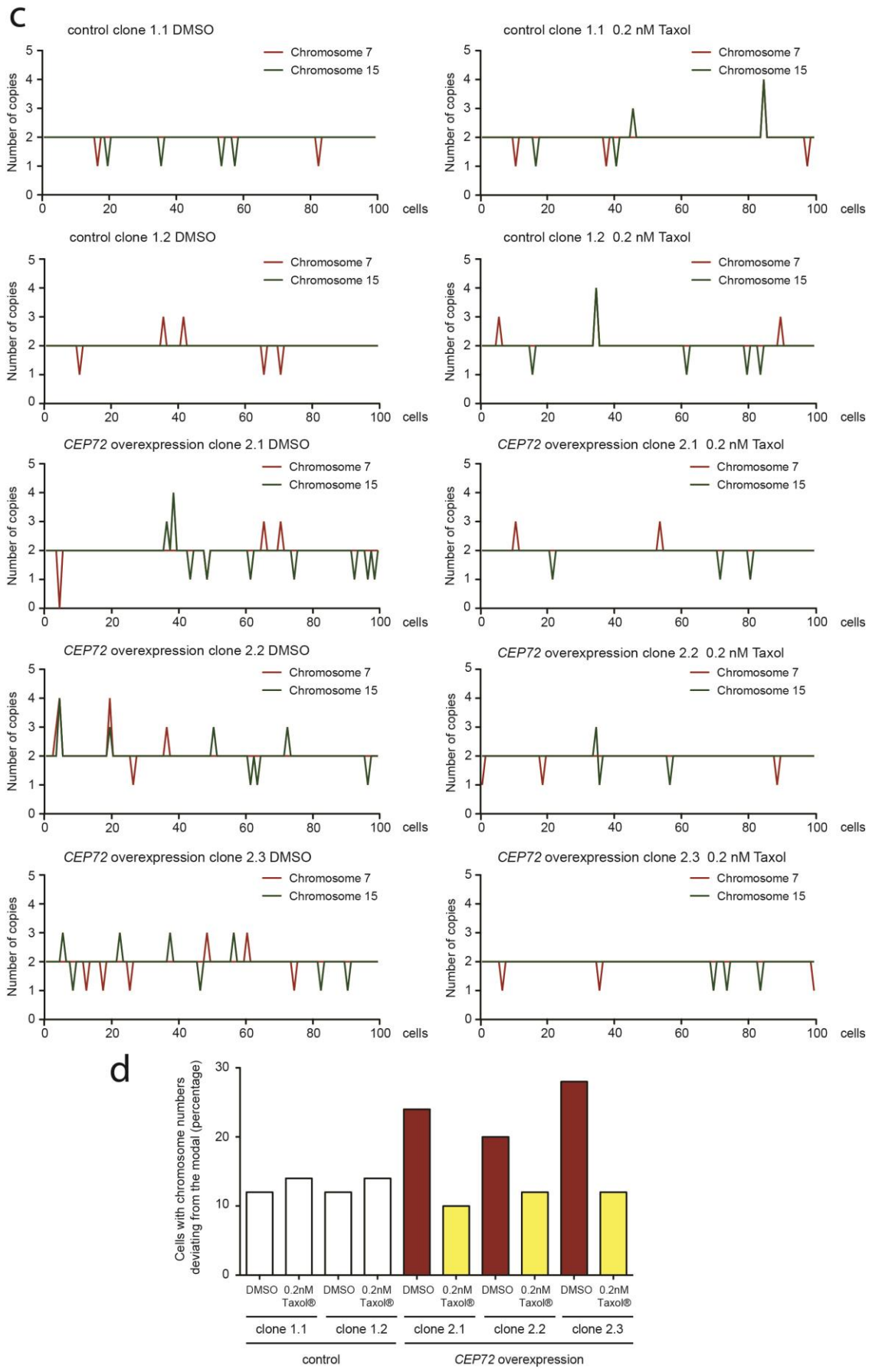
c
control clone 1.1 DMSO
control clone 1.1 0.2 nM Taxol
control clone 1.2 DMSO
control clone 1.2 0.2 nM Taxol
CEP72 overexpression clone 2.1 DMSO
CEP72 overexpression clone 2.1 0.2 nM Taxol
CEP72 overexpression clone 2.2 DMSO
CEP72 overexpression clone 2.2 0.2 nM Taxol
CEP72 overexpression clone 2.3 DMSO
CEP72 overexpression clone 2.3 0.2 nM Taxol
Chromosome 7
Chromosome 15
Number of copies
cells
d
Cells with chromosome numbers deviating from the modal (percentage)
DMSO
0.2nM Taxol®
clone 1.1
clone 1.2
clone 2.1
clone 2.2
clone 2.3
control
CEP72 overexpression

Figure 3.17 Chromosomal instability caused by *CEP72* overexpression and *BRCA1* repression is dependent on increased spindle microtubule assembly rates. (a) Determination of the karyotype of six independent cell clones with a stable overexpression of *CEP72* generated in the presence of either DMSO or 0.2 nM Taxol®. The chromosome quantification was performed after 30 generations by means of metaphase spreads (n=50 cells evaluated). **(b)** Karyotype analyses of six independent cell clones with a stable repression of *BRCA1* generated in the presence of DMSO or 0.2 nM Taxol® were performed after 30 generations using metaphase spreads. (n=50 cells evaluated). **(c)** CEP-FISH analysis for chromosome 7 and 15 of six independent cell clones with a stable overexpression of CEP72 generated in the presence of DMSO or 0.2 nM Taxol®. The karyotype was determined after 30 generations. The graphs show the copy numbers for chromosome 7 and 15 for 100 cells analysed. The modal chromosome number of HCT116 cells for chromosome 7 and 15 was determined to be 2. **(d)** For the further determination of the chromosome number variability the proportion of cells that deviate from the modal chromosome number of chromosome 7 and chromosome 15 was calculated on the basis of the data shown in (a) (n=100 cells).

For this, the karyotype of the single cell subclones with a *CEP72* overexpression generated in the presence of either DMSO or low dose Taxol® (3.2.2) was determined after 30 generations. Cell clones with a *CEP72* overexpression and grown in the presence of DMSO showed with 40%, 40% and 36% significantly increased amounts of aneuploid cells, whereas the number of chromosomes deviating from the modal in *CEP72* overexpressing cell clones grown in the presence of 0.2 nM Taxol® (16%, 14% and 16%) did not differ from control cells (DMSO 14% and 12%, 0.2nM Taxol® 14% and 14%) (Figure 3.17 a). A comparison with cell clones stably repressing *BRCA1* (3.2.2) revealed the same phenotype as observed in *CEP72* overexpressing cell clones. The stable repression of *BRCA1* induced 34%, 38% and 32% aneuploid cells (Figure 3.17 b). In contrast, the amount of cells with chromosome numbers deviating from the modal grown in the presence of 0.2 nM Taxol® resembled with 18%, 22% and 12% the ones quantified in control cells (DMSO 20% and 18%, 0.2 nM Taxol® 18% and 12%). To further validate the results, the *CEP72* overexpressing subclones were additionally analysed by CEP-FISH. The analysis revealed that cells with a *CEP72* overexpression exhibited in the presence of DMSO with 12%, 10% and 14% significantly increased numbers of cells with chromosome numbers deviating from the modal, whereas only 5%, 6% and 6% of cells overexpressing *CEP72*, which were grown in the presence of low dose Taxol® showed abnormal copy numbers of chromosome 7 and 15 (Figure 3.17 c and d).

To ensure that the induction of chromosomal instability upon *CEP72* overexpression is not due to centrosome amplification, centrosome numbers in interphase cells overexpressing *CEP72* were determined. As a positive control for the induction of centrosome amplification cells with a *PLK4* overexpression were analysed. In control transfected cells 4.8% exhibited more than two centrosomes and importantly, the percentage was not significantly increased in cells overexpressing *CEP72* (Figure 3.18). In contrast cells with an overexpression of *PLK4* exhibited centrosome amplification in 21.5% of the cells analysed.

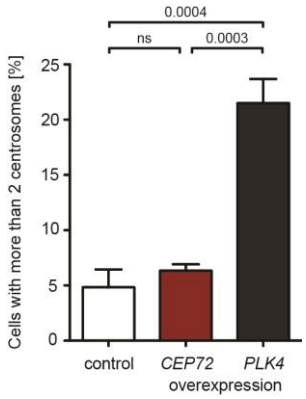

Figure 3.18 The chromosomal instability caused by *CEP72* overexpression is not dependent on centrosome amplification. Determination of centrosome numbers in cells overexpressing *CEP72* or *PLK4*. The analysis was performed on interphase cells by immunofluorescence analysis of centrosomes visualized by γ-tubulin staining. The bar plot shows the percentage of cells with more than 2 centrosomes (mean values ± s.e.m n=600 cells analysed in three independent experiments).

Thus, karyotype analysis by two independent methods showed that *CEP72* overexpression leads to chromosomal instability, which is dependent on increased spindle microtubule plus-end assembly during mitosis and not due to centrosome amplification. Moreover the data show that a stable *BRCA1* repression mirrors the phenotype observed in *CEP72* overexpressing cells.

3.3 Cep72 counteracts Chk2 and regulates Brca1 in an inhibitory fashion

The previous results showed that both, overexpression of *CEP72* and *BRCA1* repression causes enhanced spindle microtubule polymerization, which results in spindle morphology alterations, chromosome mis-segregation and the induction of chromosomal instability (3.2.2 - 3.2.5). In addition, partial loss of the positive Brca1 regulator Chk2 alters microtubule dynamics (Figure 3.5 a) and influences the interaction between Cep72 and Brca1 (Figure 3.1 c). Thus, Cep72 overexpression mirrors the consequences of Brca1 repression or reduced Chk2 mediated Brca1 stimulation leading to the hypothesis that Cep72 might negatively regulate Brca1's function during mitosis thereby antagonizing the positive Brca1 regulator Chk2 (Figure 3.19).

If this model is true, simultaneous overexpression of *CHK2* is expected to restore normal microtubule plus-end assembly when *CEP72* is overexpressed. *Vice versa*, a concurrent knock down of *CEP72* might reverse spindle microtubule polymerization defects caused by *CHK2* repression.

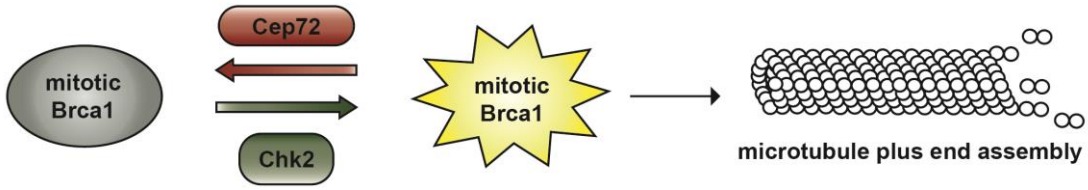

Figure 3.19 Model: The balanced regulation of Brca1 mediated by Chk2 and Cep72 ensures proper spindle microtubule plus-end assembly during mitosis.

on western blots (Figure 3.20 a). For the determination of spindle microtubule plus-end assembly rates during mitosis, the EB3-GFP fusion protein was co-expressed. Additionally the cells were treated with 2 µM DME for 2h prior to live cell microscopy. The analysis revealed significantly increased spindle microtubule polymerization for cells overexpressing *CEP72* (19.4 µm/min) when compared to control transfected cells (17.0 µm/min) (Figure 3.20 b). Interestingly, the simultaneous overexpression of *CHK2* restored normal spindle microtubule growth rates. In contrast downregulation of *CHK2* in *CEP72* overexpressing cells did not further increase spindle microtubule polymerization (18.7 µm/min). Moreover it was examined, whether a concomitant overexpression also prevents the induction of spindle morphology alterations and erroneous kinetochore-microtubule attachments. Thus, curved spindles and lagging chromosomes were quantified as already described in 3.2.3 and 3.2.4. Whereas, overexpression of *CEP72* results in an increase of the amount of cells with curved spindles from 5.3 % to 19.7 %, this effect was suppressed by concomitant overexpression of *CHK2* (Figure 3.20 c). In contrast, a concurrent downregulation of *CHK2* (18.7 %) did not influence the induction of altered spindle formation in cells overexpressing *CEP72*. The quantification of lagging chromosomes also revealed that only 1.7% of the cells with a simultaneous overexpression of *CEP72* and *CHK2* showed chromosome mal-attachments, whereas the sole overexpression of *CEP72* enhanced the amount of lagging chromosomes to 4.7% (Figure 3.20 d). In contrast, the concomitant downregulation of *CHK2* (5%) did not prevent the induction of lagging chromosomes in cells with a *CEP72* overexpression.

Moreover, *CEP72* was either repressed or overexpressed in the presence of a *CHK2* downregulation. The knock down and overexpression efficiency was verified by western blot analysis (Figure 3.20 e). The determination of spindle microtubule assembly rates revealed an increase to 18.7 µm/min by *CHK2* knock down, which was not influenced by simultaneous *CEP72* overexpression (18.7 µm/min) (Figure 3.20 f). In contrast, cells with a concurrent repression of *CHK2* and *CEP72* exhibited with 16.8 µm/min spindle

microtubule polymerization rates resembling control levels (16.1 µm/min). The analysis of the spindle morphology and the quantification of lagging chromosomes showed that the simultaneous repression of *CHK2* and *CEP72* re-established proper values. Whereas both, the sole *CHK2* knock down (20.3%) and the simultaneous overexpression of *CEP72* (18.7%) led to enhanced amounts of cells showing spindle morphology alterations, cells with a concurrent downregulation of *CHK2* and *CEP72* exhibited only 5.3% of curved spindles resembling the value measured in control cells (5.0%) (Figure 3.20 g). The quantification of lagging chromosomes revealed an increase from 1.7% to 5.3% induced by *CHK2* knock down, whereupon normal levels could be restored by simultaneous repression of *CHK2* and *CEP72* (1.7%) (Figure 3.20 h).

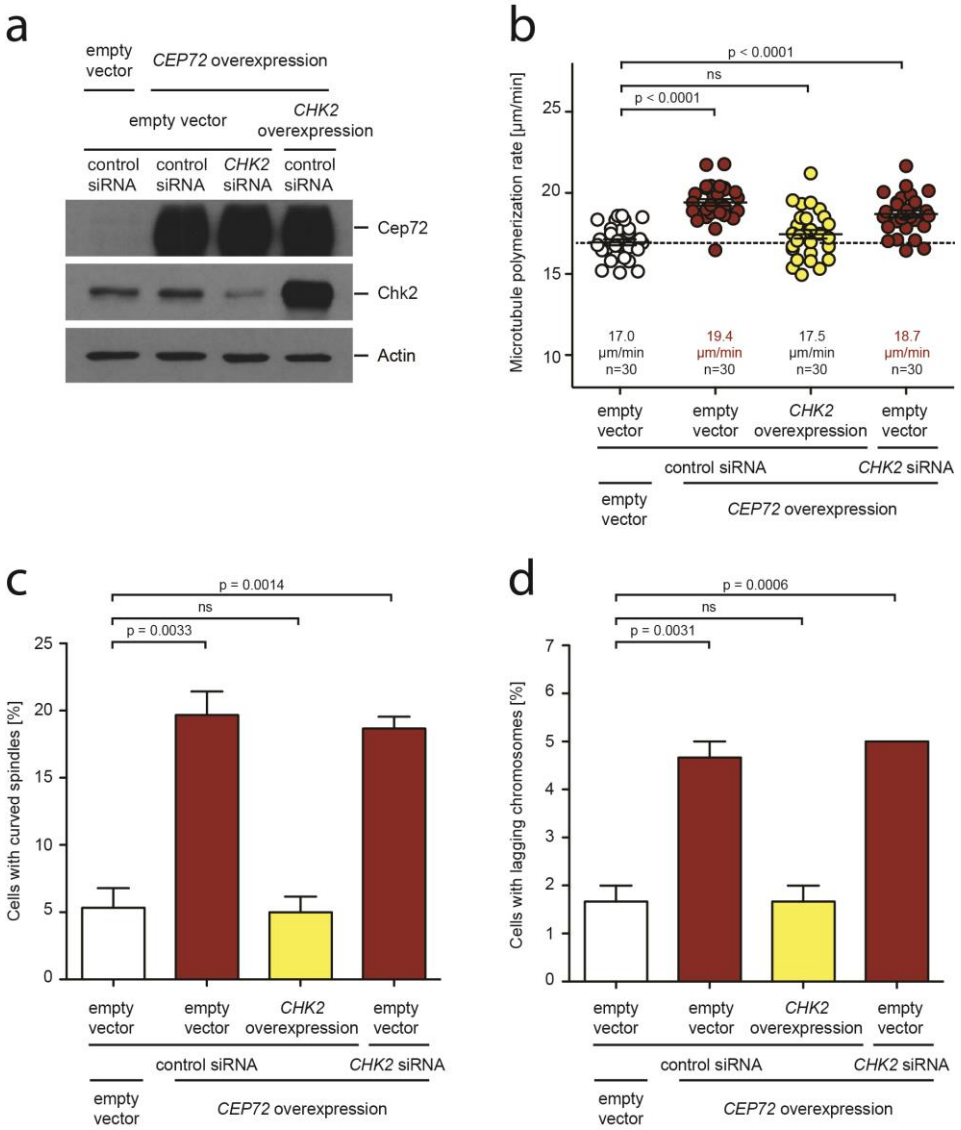

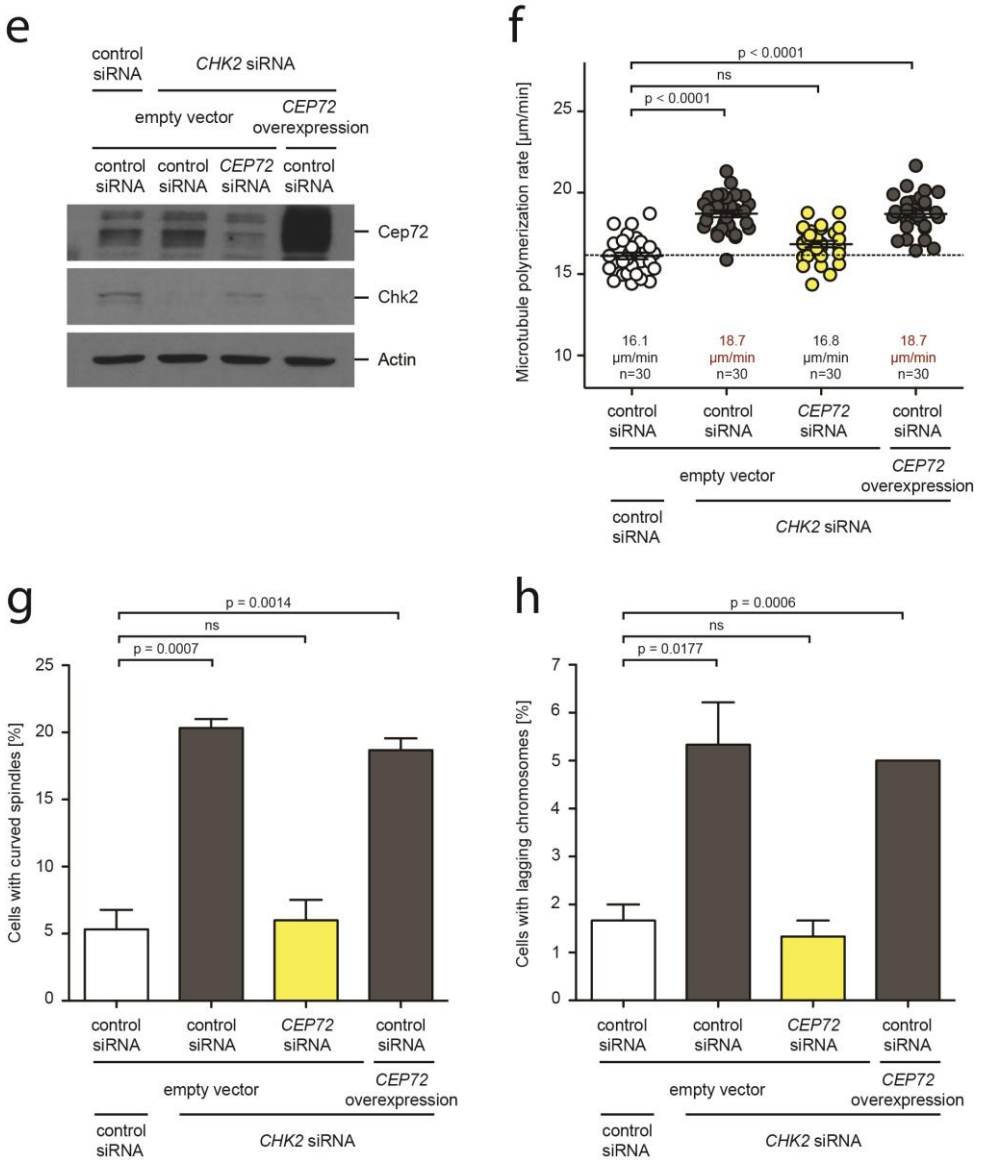

Figure 3.20 Cep72 and Chk2 act antagonistically for the regulation of mitotic microtubule plus end assembly, spindle formation and chromosomal stability (a) HCT116 cells were transfected with 40 pmol siRNA 4 h prior to PEI mediated transfection of 2 µg plasmid. 48 h later the cells were analysed and the protein levels were checked by western blot. The given western blots are representative examples using ß-actin as a loading control. **(b)** Measurements of mitotic spindle microtubule plus-end assembly rates after either *CHK2* repression or overexpression in cells transiently overexpressing *CEP72*. The EB3 measurements were performed on monoastral spindles with cells synchronized in mitosis by treatment with 2 µM DME for 2 h. Scatter dot plots show average plus-end assembly rates based on measurement of 20 microtubules per cell (mean ± s.e.m., t-test, n=30 cells from three independent experiments). **(c)** Quantification of curved spindles in cells with a transient overexpression of *CEP72* and in combination with a *CHK2* knock down and overexpression. Cells were synchronized in G1/S phase *via* double thymidine block, released into medium for 6.5 h and arrested in mitosis by treatment with 20 µM MG132 for further 3 h. Subsequently the spindle morphology was detected and quantified by immunofluorescence analysis (mean ± s.d.; t-test, n=300 bipolar spindles of three independent experiments). **(d)** Quantification of lagging chromosomes in cells transiently overexpressing *CEP72* after repression or downregulation of *CHK2*. The cells were synchronized in G1/S phase *via* double thymidine block, released into medium for 9.5 h and analysed by immunofluorescence microscopy. The graph shows mean values ± s.e.m (t-test, n=3 independent experiments with 300 cells evaluated in total). **(e)** Representative western blots showing the protein levels of cells which were transfected as described in (a). **(f)** Measurement of mitotic spindle microtubule plus-end assembly rates after

transient *CHK2* knock down and concomitant *CEP72* downregulation or overexpression, respectively. The EB3 measurements were performed as described in (b) and average plus-end assembly rates based on measurement of 20 microtubules per cell were plotted (mean ± s.e.m., t-test, n=30 cells from three independent experiments). **(g)** Quantification of curved spindles in cells repressing *CHK2* after concurrent *CEP72* downregulation or overexpression. Cells were treated as described in (c) (mean ± s.d.; t-test, n=300 bipolar spindles of three independent experiments. **(h)** Detection and quantification of lagging chromosomes in cells with a transient knock down of *CHK2* and in combination with a knock down and overexpression of *CEP72*. The cell treatment was carried out as described in (d) (mean values ± s.e.m, t-test, n=3 independent experiments with 300 cells evaluated in total).

Assuming that Chk2 *per se* is essential for the function of Brca1 to ensure proper spindle microtubule assembly, reducing the inhibitory effect of Cep72 should not be sufficient anymore to restore normal spindle microtubule growth after total loss of *CHK2*. In order to verify this hypothesis, *CHK2* deficient (HCT116-*CHK2*$^{-/-}$) cells were transfected with either control or *CEP72* siRNA and the protein levels were checked by western blot (Figure 3.21 a). The subsequent determination of spindle microtubule plus-end assembly rates revealed that simultaneous *CEP72* repression did not restore normal spindle microtubule growth when *CHK2* was completely lost. In the presence and in the absence of a simultaneous *CEP72* repression, HCT116-*CHK2*$^{-/-}$ cells showed enhanced spindle microtubule polymerization rates (19.8 µm/min and 19.5 µm/min) (Figure 3.21 b).

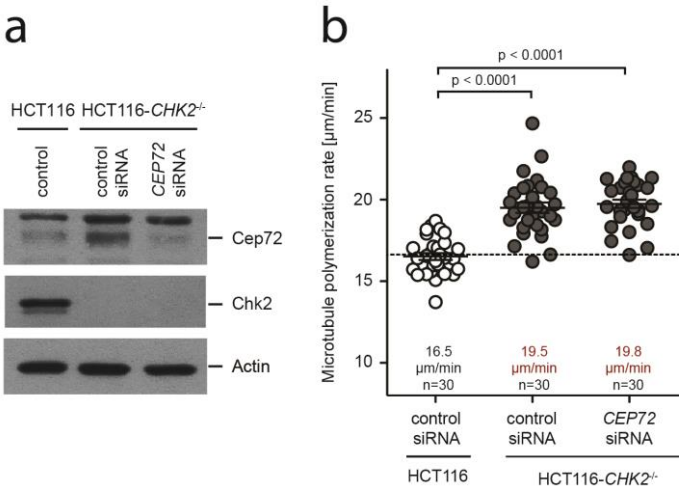

Figure 3.21 The presence of residual Chk2 is essential for the proper regulation of microtubule plus-end assembly during mitosis. (a) HCT116 and HCT116-*CHK2*$^{-/-}$ cells were transfected with 40 pmol *CEP72* siRNA 48 h prior to analysis. In order to verify the knock down efficiency, the protein levels were checked by western blot. The given western blots are representative examples using ß-actin as a loading control. **(b)** Measurement of mitotic spindle microtubule plus-end assembly rates in HCT116 and isogenic *CHK2* deficient cells (HCT116-*CHK2*$^{-/-}$) after transfection with control and *CEP72* siRNA. Scatter dot plots show average plus-end assembly rates of monoastral spindles based on measurement of 20 microtubules per cell (mean ± s.e.m., t-test, n=30 cells from three independent experiments).

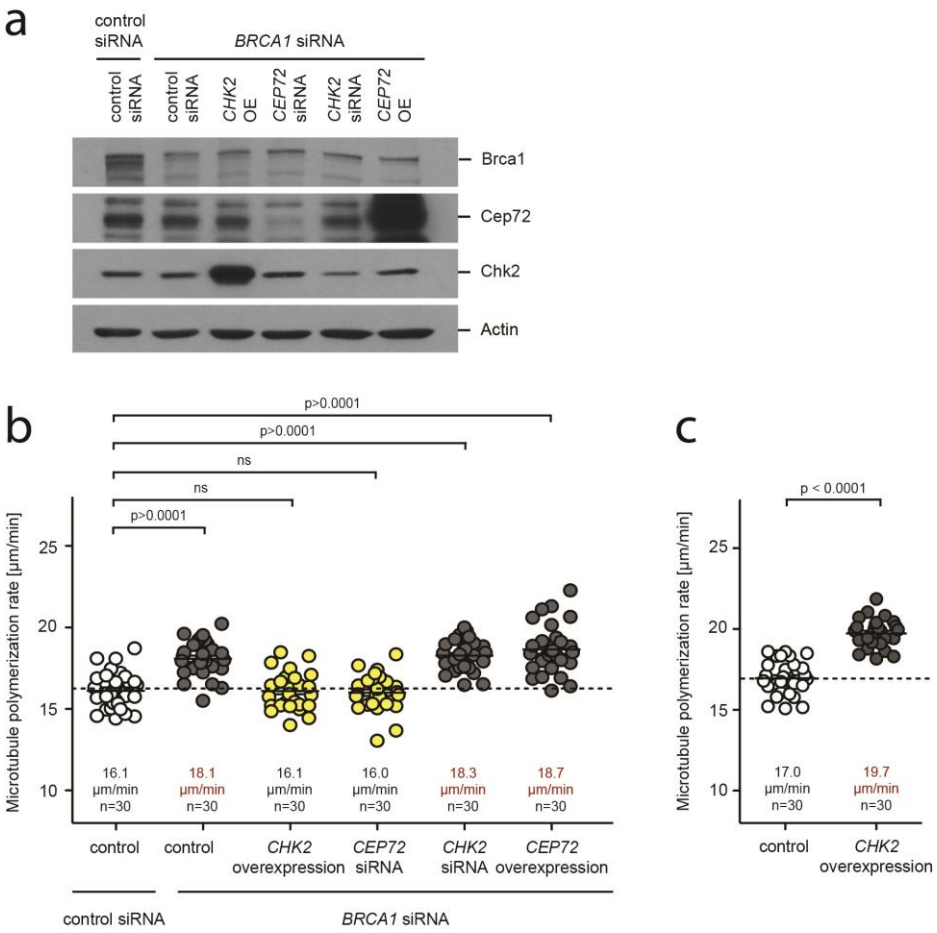

Figure 3.22 The fine tuning of Brca1 activation is essential for proper spindle microtubule plus-end assembly. (a) HCT116 cells were transfected with 40 pmol siRNA 4 h prior to PEI mediated transfection of 2 µg plasmid. After 48 h the protein levels were determined by western blot analysis. A representative example is given using ß-actin as a loading control. **(b)** Measurements of mitotic spindle microtubule plus-end assembly rates after transient *BRCA1* knock down and in combination with a *CEP72* or *CHK2* knock down and overexpression, respectively. The EB3 measurements were performed on monoastral spindles with cells, which were synchronized in mitosis by treatment with 2 µM DME for 2 h. Scatter dot plots show average plus-end assembly rates based on measurement of 20 microtubules per cell (mean ± s.e.m., *t*-test, *n*=30 cells from three independent experiments). **(c)** Measurements of mitotic spindle microtubule plus-end assembly rates upon *CHK2* overexpression. The cells were treated as described in (b). Scatter dot plots show average plus-end assembly rates based on measurement of 20 microtubules per cell (mean ± s.e.m., *t*-test, *n*=30 cells from three independent experiments).

Moreover, the question was addressed whether the increase in microtubule growth upon *BRCA1* repression can be prevented by entirely stimulating the remaining Brca1 protein. Thus, spindle microtubule plus-end assembly was determined in cells with a transient *BRCA1* knock down, in which simultaneously either the positive regulator *CHK2* was overexpressed or the potential Brca1 inhibitor *CEP72* was repressed. Cells with repression of *BRCA1* in combination with concomitant *CHK2* overexpression and *CEP72* knock down, respectively, were used as control. Compared to control transfected cells (16.1 µm/min), an siRNA mediated knock down of *BRCA1* resulted in increased spindle microtubule polymerization rates of 18.1 µm/min (Figure 3.22 a). Interestingly, a

simultaneous *CHK2* overexpression and *CEP72* repression, respectively, restored normal microtubule growth rates in cells with reduced *BRCA1* expression. In contrast, the concurrent repression of *CHK2* or *CEP72* overexpression did not further influence the enhanced spindle microtubule assembly rates caused by *BRCA1* down regulation.

To further investigate the consequences of a Brca1 hyperstimulation, *CHK2* was overexpressed in HCT116 cells. Here, the subsequent EB3 measurement revealed an increase in spindle microtubule plus-end assembly of 15.6% upon *CHK2* overexpression when compared to control transfected cells (Figure 3.22 c)

These results support the theory, that the Chk2 mediated positive regulation of Brca1 is counteracted by Cep72 (Figure 3.19). Moreover, balancing the stimulation of Brca1 during mitosis seems to be crucial for the maintenance of proper microtubule dynamics and accurate spindle assembly.

3.4 Repression of *CEP72* in human colorectal HCT116 cells

While it was shown by (Stolz et al. 2010) that Brca1's function during mitosis is positively regulated by Chk2 mediated phosphorylation at Ser988, the previous studies indicate an inhibitory function for Cep72. The overexpression of the Brca1 stimulating kinase *CHK2* resulted in increased spindle microtubule growth, suggesting that a tight regulation of the Brca1 stimulation is needed to ensure a proper assembly of the mitotic spindle. In order to estimate how important the presence of Cep72 is, the causes of a *CEP72* repression were investigated in the following sections.

3.4.1 The repression of *CEP72* causes enhanced spindle microtubule plus-end assembly

Initially, spindle microtubule plus end assembly rates were analysed. For that purpose the EB3-GFP was expressed in cells with a transient repression of *CEP72* and control transfected cells and the protein levels were verified by western blot analysis (Figure 3.23 a). The spindle microtubule plus-end assembly rates were measured in monoastral, mitotic spindles. Whereas control transfected cells showed an average microtubule polymerization of 18.1 µm/min, the microtubule assembly rates in cells repressing *CEP72* were significantly increased to 20.2 µm/min (Figure 3.23 b). Furthermore the microtubule dynamics were investigated in interphase. Cells with a repression of *CEP72* showed with 18.1 µm/min a microtubule polymerization, which was not significantly

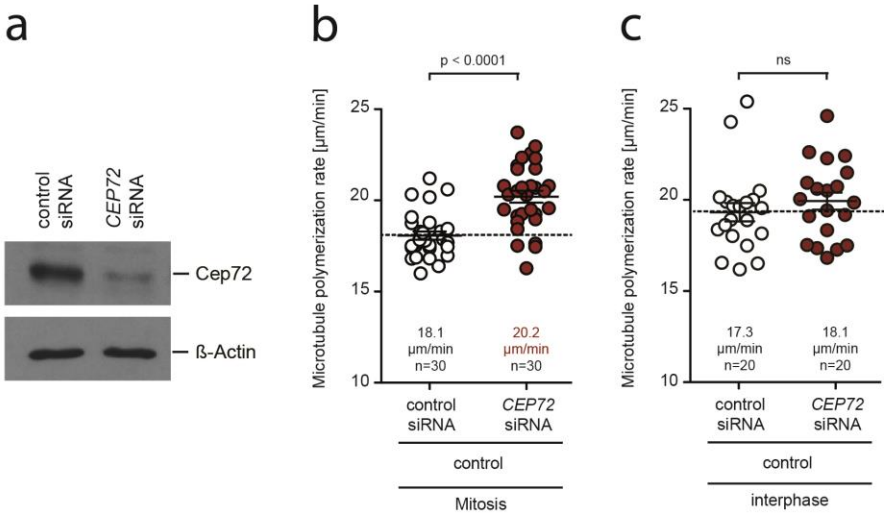

Figure 3.23 The transient repression of *CEP72* leads to enhanced spindle microtubule plus-end assembly rates during mitosis. (a) HCT116 cells were transfected with 40 pmol siRNA 48h prior to analysis. The protein repression was verified by western blot analysis, whereupon ß-actin was used as a loading control. A representative example is shown. **(b)** For the investigation of the spindle microtubule plus-end assembly rates in mitosis after knock down of *CEP72*, cells were synchronized in mitosis by treatment with 2 µM DME for 2h. The EB3 measurement was performed on monoastral spindles. The scatter dot plots show average plus-end assembly rates based on measurement of 20 microtubules per cell (mean ± s.e.m., *t*-test, *n*=30 cells from three independent experiments). **(c)** To investigate spindle microtubule plus-end assembly rates in interphase upon knock down of *CEP72*, the EB3 measurement was performed on interphase cells. The scatter dot plots show average plus-end assembly rates based on measurement of 20 microtubules per cell (mean ± s.e.m., *t*-test, *n*=20 cells from two independent experiments).

enhanced in comparison to microtubule assembly rates measured in control cells (17.3 µm/min) (Figure 3.23 c).

These results show, that the repression of *CEP72* leads to an increase of the microtubule plus-end assembly in mitotic spindles, but not in interphase cells.

In order to determine, whether increased spindle microtubule polymerization induced by *CEP72* knock down can be restored by interfering with microtubule dynamics, mitotic cells repressed for *CEP72* and control cells were treated with DMSO or 0.2 nM Taxol®. The protein levels were analysed by western blot and an influence of Taxol® on protein levels was excluded (Figure 3.24 a). Additionally, the low dose Taxol® did not affect the microtubule polymerization in control cells exhibiting a rate of 18.2 µm/min after treatment with DMSO and 0.2 nM Taxol®, respectively. In cells with a transient knock down for *CEP72*, the treatment with 0.2 nM Taxol® reduced the enhanced spindle microtubule plus-end assembly from 20.1 µm/min to 18.0 µm/min (Figure 3.24 b).

To further investigate the repression of *CEP72* in a stable cell system, HCT116 cells were stably transfected with plasmids expressing either control shRNA or *CEP72* shRNA.

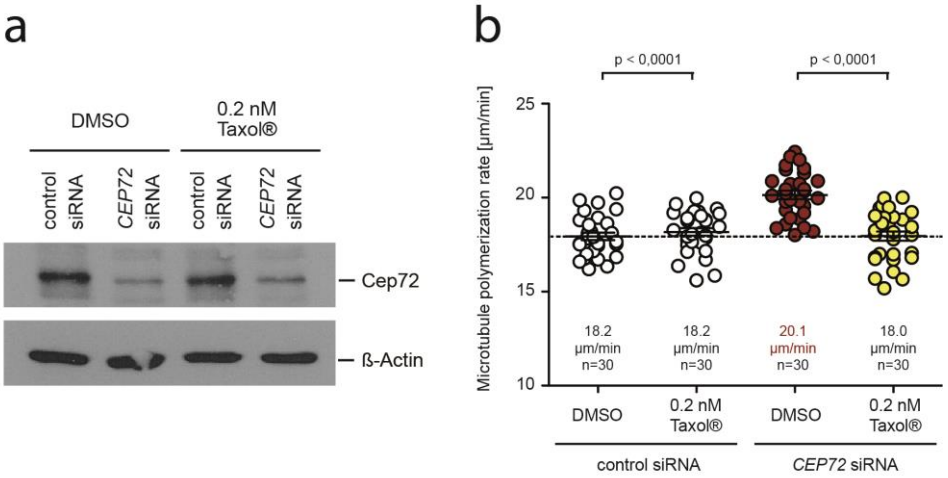

Figure 3.24 The enhanced spindle microtubule plus-end assembly rates during mitosis caused by *CEP72* repression can be suppressed by treatment with low dose Taxol®. (a) A transient knock down of *CEP72* was achieved by siRNA transfection using 40 pmol siRNA. Simultaneously, the cells were treated with either DMSO or 2.0 nM Taxol® prior to EB3 measurement. The protein repression was verified by western blot analysis (a representative example is given). ß-actin was used as a loading control. **(b)** To determine the influence of low dose Taxol® on spindle microtubule plus-end assembly rates after *CEP72* knock down, cells were treated with either DMSO or 2.0 nM Taxol® for 24h prior to live cell analysis. The EB3 measurement was performed on mitotic monoastral spindles and the results are represented in form of scatter dot plots showing the average plus-end assembly rates based on measurement of 20 microtubules per cell (mean ± s.e.m., t-test, n=30 cells from three independent experiments).

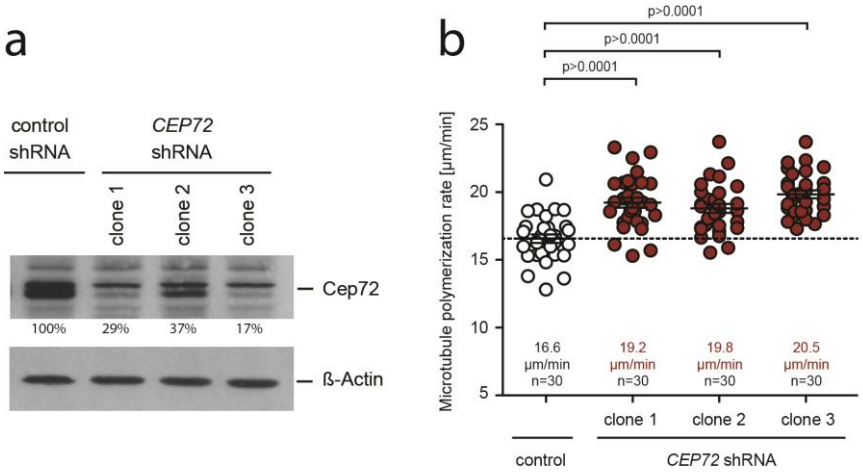

Figure 3.25 Stable repression of *CEP72* leads to increased spindle microtubule plus-end assembly rates during mitosis. (a) HCT116 cells were transfected with a control or *CEP72* shRNA expressing plasmid and single cell clones were generated *via* puromycin selection. The protein repression was checked by western blot analysis, whereupon ß-actin was used as a loading control. A representative example is shown. **(b)** For the investigation of the spindle microtubule plus-end assembly rates in mitosis after stable knock down of *CEP72*, three independent single cell clones were analysed. The EB3 measurement was performed on monoastral spindles and the results are represented in form of scatter dot plots showing the average plus-end assembly rates based on measurement of 20 microtubules per cell (mean ± s.e.m., t-test, n=30 cells from three independent experiments).

By puromycin selection single cell clones with a stable repression of *CEP72* were generated and identified by western blot (Figure 3.25 a). Compared to control cells, the Cep72 protein levels of the single cell clones stably repressing *CEP72* were reduced to 29%, 37% and 17%. The EB3-measurement of the three independent single cell clones in mitosis revealed a significant increase of the microtubule polymerization of 15.6%, 19.3% and 23.5% compared to stable control cells (Figure 3.25 b).

Hence, both, the transient and the stable repression of *CEP72*, lead to increased spindle microtubule plus-end assembly during mitosis, which can be reversed by treatment with low dose Taxol®.

3.4.2 The repression of *CEP72* leads to alterations in the spindle morphology

In 3.2.3 it was shown, that increased spindle microtubule plus-end assembly can lead to spindle morphology alterations during mitosis. In order to investigate the spindle morphology upon *CEP72* repression, cells with a stable knock down of *CEP72* were synchronized in metaphase by double thymidine block and subsequent treatment with the proteasome inhibitor MG132. By immunofluorescence analysis it could be observed

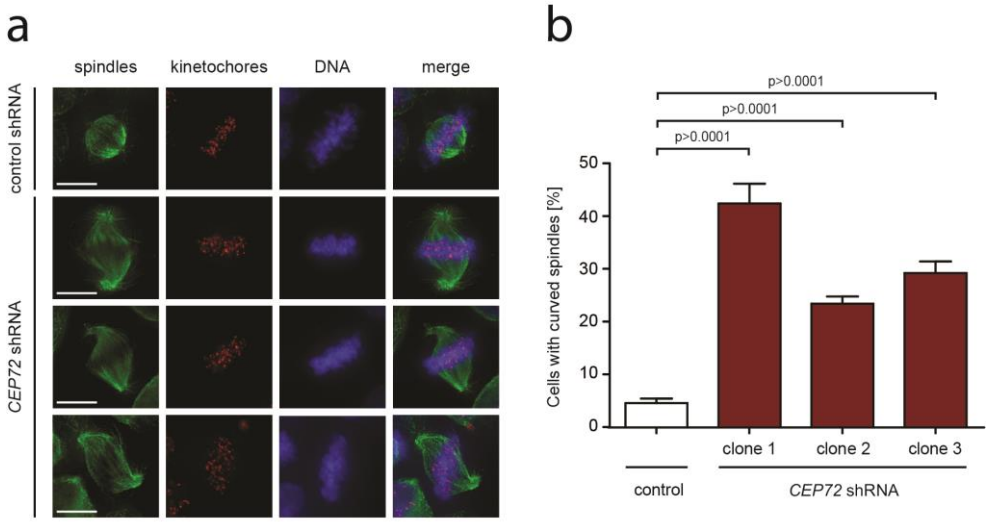

Figure 3.26 The stable repression of *CEP72* leads to spindle morphology alterations during mitosis. (a) Representative example of immunofluorescence images showing the mitotic spindle morphology of HCT116 cells stably expressing control and *CEP72* shRNA, respectively. The cells were synchronized in G1/S phase *via* double thymidine block, released into medium for 6.5 h and arrested in mitosis by treatment with 20 µM MG132 for further 3 h. By immunofluorescence staining the spindles (α-tubulin, green), kinetochores (Crest, red) and the DNA (Hoechst33342, blue) were visualized. Scale bar: 10 µm. **(b)** For the quantification of curved spindles in cells with a stable repression of *CEP72*, three independent single cell clones were analysed and compared to control transfected cells. The cells were treated as described in (a) and subsequently the spindle morphology was detected and quantified by immunofluorescence analysis (mean ± s.d.; t-test, n=550 metaphase spindles of three independent experiments).

that cells with a stable repression of *CEP72* exhibited an aberrant spindle morphology (Figure 3.26 a), which resembled the phenotype seen upon *CEP72* overexpression (Figure 3.12 a). While control cells exhibited almost round mitotic spindles with a uniform shape, cells with a *CEP72* repression showed curved spindles, which were partially S-shaped. The quantification revealed 4.6% curved spindles in control cells, which was increased to 42.4 %, 23.7% and 29.3% in cells with a stable *CEP72* knock down (Figure 3.26 b).

These results show that the presence of Cep72 is important for the proper spindle formation during mitosis.

3.4.3 The repression of *CEP72* causes lagging chromosomes and chromosomal instability

In order to investigate whether the alterations in mitotic spindle formation caused by repression of *CEP72* lead to merotelic attachments and subsequent chromosome mis-segregation, cells were analysed with respect to the induction of lagging chromosomes. For this, independent single cell clones stably expressing either control or *CEP72* shRNA were synchronized in G1/S phase *via* double thymidine block and released into medium for 9.5 h. Subsequently anaphase cells were analysed by immunofluorescence

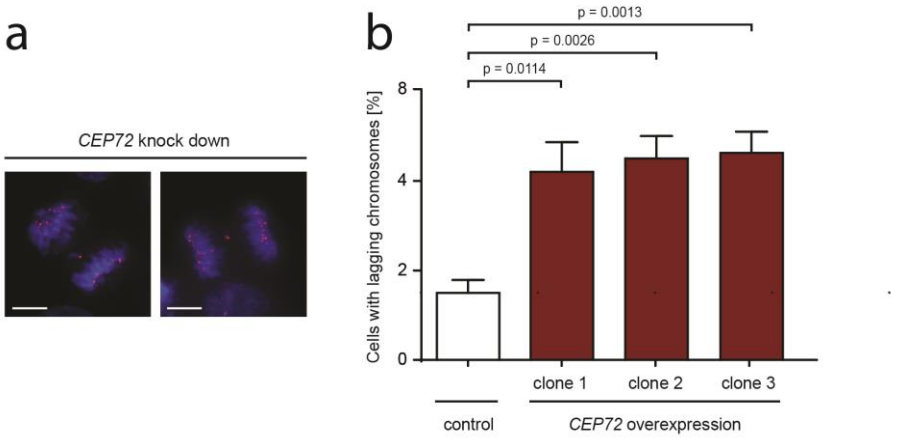

Figure 3.27 Stable repression of *CEP72* leads to the generation of lagging chromosomes. **(a)** Representative example of immunofluorescence images showing lagging chromosomes in anaphase cells stably expressing *CEP72* shRNA. Cells were released from a double thymidine block for 9.5 h and cells in anaphase were evaluated by immunofluorescence staining (kinetochores (Crest, red), DNA (Hoechst33342, blue)). Scale bar: 10 µm. **(b)** For the quantification of lagging chromosomes in cells with a stable repression of *CEP72*, three independent single cell clones were analysed and compared to control transfected cells. The cells were treated as decribed in (a) and subsequently lagging chromosomes were quantified by immunofluorescence analysis (mean ± s.d.; t-test, n=500 cells of three independent experiments).

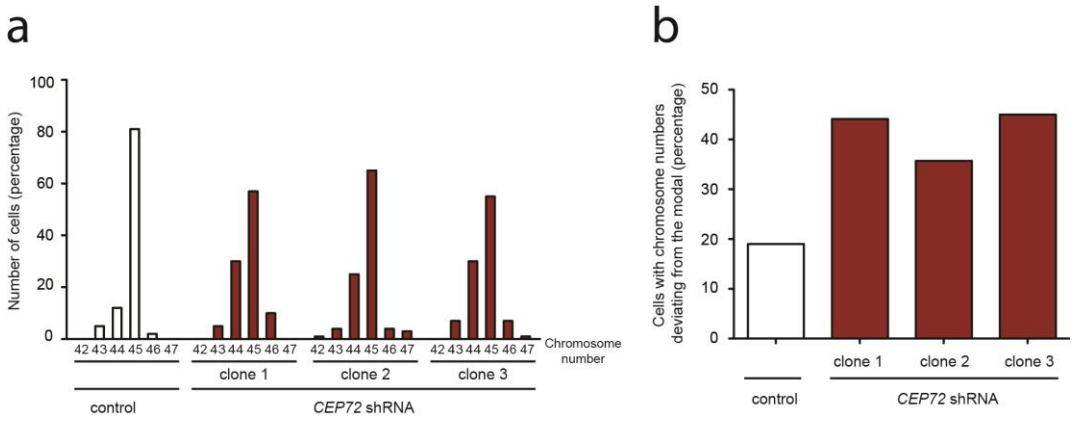

Figure 3.28 The stable repression of *CEP72* leads to chromosomal instability. (a) Karyotype analyses of the three independent cell clones with a stable repression of *CEP72* and cultivated for 30 generations. The amount of chromosomes was determined for 100 cells and visualized as a bar plot showing the amount of cells exhibiting the indicated chromosome numbers (n=100 cells). The modal chromosome number of HCT116 cells was determined to be 45. **(b)** On the basis of the chromosome numbers shown in (a), the percentage of cells deviating from the modal was calculated and visualized in a bar plot (n=100 cells).

microscopy. Whereas only 1.5% of control transfected cells exhibited lagging chromosomes, the percentage was increased to 4.2%, 4.5% and 4.6% in the single cell clones with a stable *CEP72* knock down (Figure 3.27 a and b).

To determine the effect of *CEP72* repression on the maintenance of chromosomal stability, the karyotype of the single cell clones was analysed after 30 generations by means of metaphase chromosome counting. The analyses revealed that cells with a stable knock down of *CEP72* showed a much broader distribution on different chromosome numbers compared to control cells, whereupon the modal number of 45 chromosomes remained unchanged (Figure 3.28 a). While 19% of the control cells showed an aneuploid phenotype, the amount of cells exhibiting a chromosome number deviating from the modal increased to 42%, 44% and 45% in in cells stably repressing *CEP72* (Figure 3.28 b).

Summarized it can be noted that the presence of Cep72 is important for proper chromosome segregation and the maintenance of chromosomal stability.

3.4.4 Chromosomal instability induced by *CEP72* repression is caused by increased spindle microtubule plus-end assembly

To further examine, whether the increase in spindle microtubule plus-end assembly is responsible for the induction of chromosomal instability after partial loss of *CEP72*, HCT116-*CEP72*-shRNA clone 1 and control cells were cultivated in the presence of either

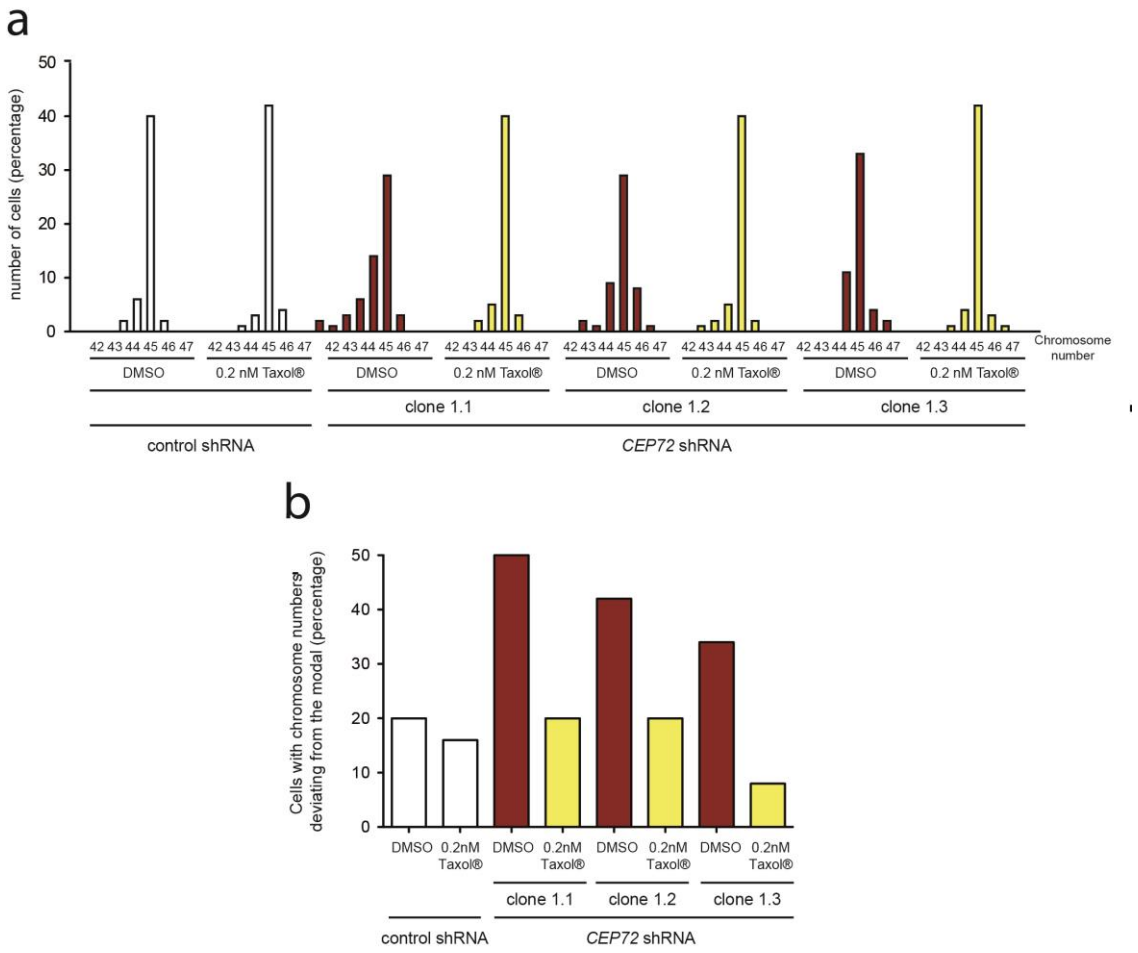

Figure 3.29 Chromosomal instability caused by stable *CEP72* repression can be suppressed by restoration of normal spindle microtubule plus-end assembly rates. (a) The karyotype analysis of the three independent cell clones with a stable repression of *CEP72* and grown in in the presence of DMSO or 0.2 nM Taxol®, was performed after 30 generations. The number of whole chromosomes was determined for 100 cells and visualized as a bar plot showing the distribution of cells on different chromosome numbers (n=100 cells). The modal chromosome number of HCT116 cells was determined to be 45. **(b)** On the basis of the chromosome numbers shown in (b), the percentage of cells deviating from the modal was calculated and visualized in a bar plot (n=100 cells).

DMSO or 0.2 nM Taxol for 30 generations. Subsequently, the karyotype of the subclones was re-examined. The analysis revealed that treatment with low dose Taxol® largely prevented the mis-segregation of chromosomes caused by *CEP72* knock down (Figure 3.29 a and b). In contrast to *CEP72* repressing subclones generated in the presence of DMSO exhibiting 50%, 42% and 34% of aneuploid cells, the treatment with low dose Taxol® maintained aneuploidy of 8% - 20%. Control clones showed in the presence and in the absence of 0.2 nM Taxol® 20% and 16% aneuploid cells, respectively.

These results show that the chromosomal instability induced by *CEP72* repression is dependent on enhanced spindle microtubule polymerization during mitosis.

3.4.5 Increased spindle microtubule assembly rates seen after *CEP72* repression are dependent on elevated Aurora A kinase activity

Previous studies from our lab revealed that in colorectal cancer cells enhanced Aurora A kinase activity is a common cause for increased spindle microtubule plus-end assembly and the formation of chromosomal instability. Additionally, it was shown that Chk2 restrains Aurora A kinase activity through the phosphorylation of Brca1 during mitosis. A loss of *CHK2* or *BRCA1* caused elevated levels of phosphorylated and thus, active Aurora A at centrosomes, which in turn results in increased spindle microtubule polymerization (Ertych et al. 2014). Since a repression of *CEP72* also leads to enhanced spindle microtubule plus-end assembly and the occurrence of chromosomal instability in the colorectal cancer cell line HCT116, the question arises, whether this is dependent on increased Aurora A kinase activity. In order to investigate this, it was taken advantage of a monopolar spindle assay, which was previously introduced by Stolz et al. 2015. This assay allows the detection of cells with enhanced spindle microtubule plus-end assembly rates by analyzing the morphology of monopolar spindles. In fact, by inhibition of the Eg5/Kif11 kinesin using DME, the centrosome separation is inhibited and monopolar spindles are formed. Importantly, cells with increased spindle microtubule plus-end assembly rates show highly asymmetric monopolar spindles, while cells with normal growth rates exhibit ball-like monoasters (Stolz et al. 2015).

To test whether the increase in microtubule plus end assembly after repression of *CEP72* can be detected by this assay, the cell clones with a stable *CEP72* knock down were analysed regarding increased spindle microtubule plus-end assembly during mitosis. For this purpose, the cells were treated with 2 µM DME for 4 h and subsequently analysed by immunofluorescence microscopy. Here, asymmetric monopolar spindles were observed in cells with a stable repression of *CEP72* (Figure 3.30 a). The quantification revealed an amount of 6.8% asymmetric spindles in control cells, which increased to 20.0%, 16.6% and 19.4% in cells with a stable *CEP72* knock down (Figure 3.30 b). Additionally, cells with asymmetric spindles were quantified upon transient knock down of either *CEP72* or *CHK2*, treated with DMSO and Taxol®, respectively. However, in contrast to all previous studies performed using 0.2 nM Taxol®, the concentration for the monopolar spindle assay was elevated to 2 nM according to Stolz et al. 2015. Whereas the repression of *CEP72* and *CHK2* caused 29.5% and 22.2% of cells with asymmetric spindles, this numbers were reduced to 1.9% and 1.4% by treatment with 2 nM Taxol® (Figure 3.30 c). Control transfected cells exhibited 10.7% of asymmetric spindles in the presence of DMSO, whereupon the percentage was reduced to 0.5% upon treatment with 2 nM Taxol®. This significant decrease might be explained by the proportionally high Taxol® concentration used. In general, the results match the data obtained by EB3 measurement in 3.2.2 and 3.4.1.

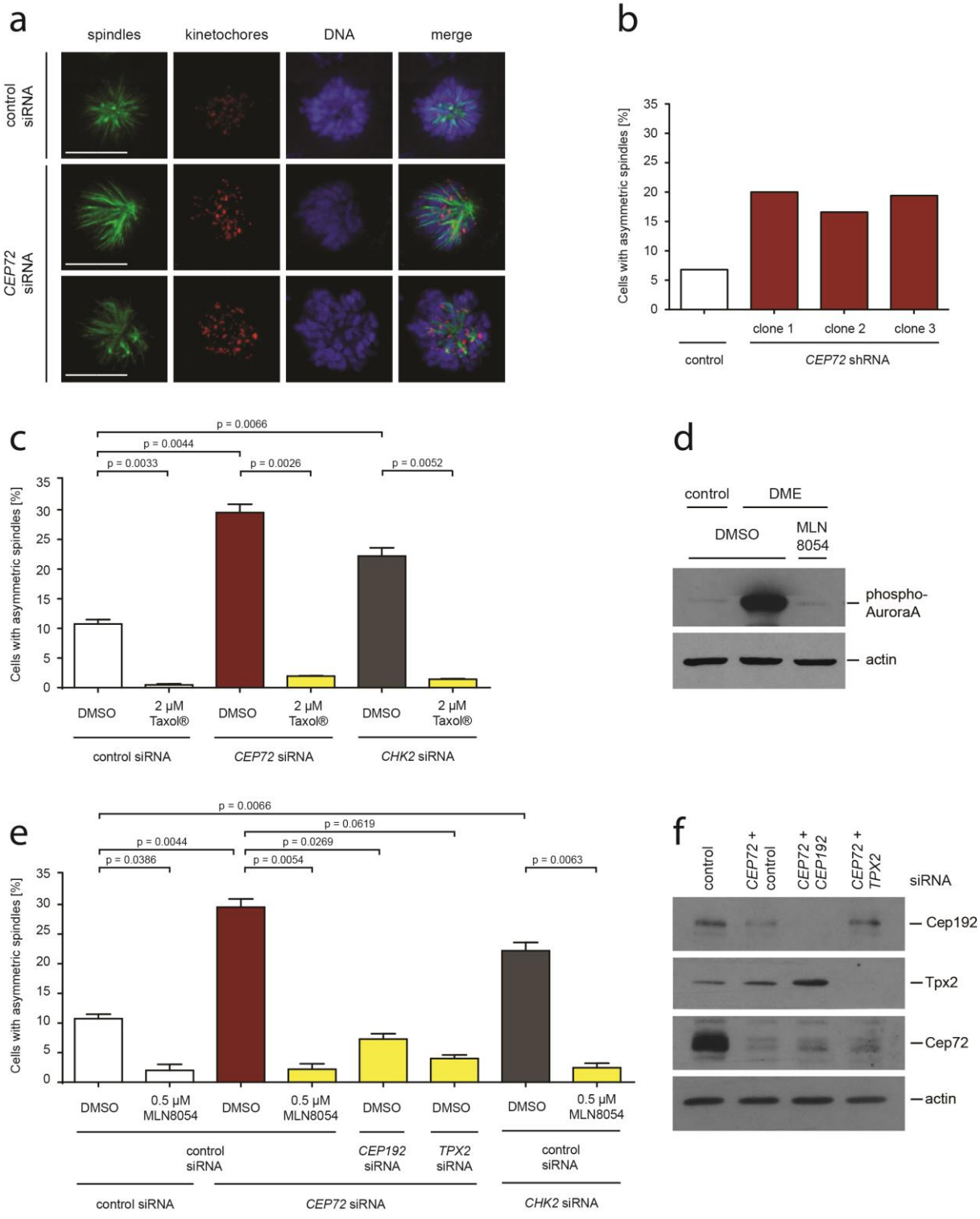

Figure 3.30 The knock down of *CEP72* leads to the formation of asymmetric monopolar spindles, which can be reversed by low dose Taxol® and inhibition of Aurora A kinase activity. (a) Representative example of immunofluorescence images upon Eg5/Kif11 inhibition showing the monopolar spindle morphology of HCT116 cells stably expressing control or *CEP72* shRNA. The cells were synchronized in mitosis by treatment with 2 µM DME for 4 h. By immunofluorescence staining spindles (α-tubulin, green), kinetochores (Crest, red) and DNA (Hoechst33342, blue) were visualized. Scale bar: 10 µm. **(b)** For the quantification of asymmetric, monopolar spindles in cells with a stable repression of *CEP72*, three independent single cell clones were analysed and compared to control transfected cells. The cells were treated as described in (a)

and subsequently, the spindle morphology was detected and quantified by immunofluorescence analysis (mean ± s.d.; t-test, n=500 monopolar spindles). **(c)** For the quantification of asymmetric, monopolar spindles in cells with a transient knock down of *CEP72* and *CHK2* cells were arrested in mitosis by treatment with 2 µm DME for 4 h. To further determine the influence of Taxol® on the formation of asymmetric monopolar spindles after *CEP72* and *CHK2* knock down, cells were treated with either DMSO or 2 nM Taxol® for 24h prior to immunofluorescence analysis (mean ± s.d.; t-test, n=1500 monopolar spindles of three independent experiments). **(d)** In order to investigate whether active Aurora A can be efficiently inhibited by MLN8054, cells were initially arrested in mitosis by treatment with 2µM DME for 15 h. This process ensures the phosphorylation, meaning activation of Aurora A. Subsequently, the cells were treated with DMSO or 0.5 µM of the Aurora A inhibitor MLN8054 for 1 h. The phosphorylation status of Aurora A, serving as a marker for the activation, was checked by western blot in mitotic cells. Untreated cells were taken as a control. **(e)** Cells were treated with either DMSO or 0.5 µM MLN8054 for 1 h. Additionally *TPX2* or *CEP192* were simultaneously repressed by siRNA. The cells were synchronized in mitosis by 2µM DME treatment for 4 h. Subsequently the spindle morphology was detected and quantified by immunofluorescence analysis (mean ± s.d.; t-test, n=1500 monopolar spindles of three independent experiments). **(f)** HCT116 cells were transfected with control, *CEP72*, *CEP192* and *TPX2* siRNA (30 pmol each). The protein repression was checked by western blot analysis, whereupon ß-actin was used as a loading control. A representative example is shown.

In order to see, whether the increased spindle microtubule polymerization caused by *CEP72* repression is dependent on elevated Aurora A kinase activity, cells with a transient knock down of *CEP72* and *CHK2* were treated with 0.5 µM of the Aurora A kinase small molecule inhibitor MLN8054 (Stolz et al. 2015; Ertych et al. 2014; Manfredi et al. 2007). A significant reduction of the Aurora A phosphorylation upon treatment with 0.5 µM MLN8054 was verified by western blot (Figure 3.30 d). The subsequent immunofluorescence analysis revealed that cells with a transient repression of *CEP72* only show 2.2% asymmetric spindles by simultaneous inhibition of Aurora A (Figure 3.30 e). This mirrors the result obtained upon *CHK2* knock down (2.4%), where, as already described by Stolz *et al.* 2015, the inhibition of the Aurora A activity restores normal spindle microtubule polymerization rates.

The activation of Aurora A is mediated by auto-phosphorylation at Thr288. The proteins Cep192 (Joukov et al. 2010) and Tpx2 (Eyers & Maller 2004) has been shown to stimulate this auto-phosphorylation during mitosis. In order to exclude unspecific effects of the small molecule inhibitor, the Aurora A activity was reduced in *CEP72* repressing cells by simultaneous knock down of either *CEP192* or *TPX2*. The knock down efficiency was ensured by western blot analysis (Figure 3.30 f) and the cells were analysed by the monopolar spindle assay. While the simultaneous knock down of *CEP192* in cells transiently repressing *CEP72* reduced the amount of asymmetric cells from 29.5% to 7.3%, the downregulation of *TPX2* lead to a decrease to 4% (Figure 3.30 e).

These results indicate that the increased spindle microtubule plus-end assembly, which can be observed after downregulation of *CEP72*, is dependent on enhanced Aurora A kinase activity.

4 DISCUSSION

Brca1 is a major tumour suppressor gene, which is particularly associated with breast and ovarian cancer (Miki, Y.et al. 1994). However, the way Brca1 exerts its tumour suppressive function is still unclear and controversially discussed. During mitosis, Brca1 ensures proper spindle assembly and chromosome segregation, thereby maintaining whole chromosomal stability (Stolz et al. 2010). It is positively regulated by Chk2 mediated phosphorylation at S988 and restrains the accumulation of active Aurora A at mitotic centrosomes. Thus, Brca1 prevents increased microtubule polymerization that is responsible for abnormal spindle formation, chromosome mis-segregation and chromosomal instability (Stolz et al. 2010; Ertych et al. 2014). Nevertheless, other regulators of the Chk2-Brca1 tumour suppressor pathway remain elusive and the mechanism how Brca1 regulates spindle microtubule dynamics is so far unknown.

In this thesis, the centrosomal protein Cep72 was identified as a new protein interacting with Brca1 during interphase and mitosis (3.1). Cep72 is a poorly studied protein, which was shown to be essential for maintaining microtubule nucleation and the structural integrity of the centrosome (Oshimori et al. 2009). Moreover, Cep72 localizes to centriolar satellites and participates in the formation of the primary cilium (Stowe et al. 2012). However, functions beyond remain undetected. Importantly, we demonstrated that *CEP72* is highly overexpressed in human colorectal cancer (3.2.1) suggesting that it represents a hitherto unknown, putative oncogene. The overexpression of *CEP72* leads to increased spindle microtubule polymerization, which causes spindle assembly defects and results in lagging chromosomes and CIN (3.2.2 - 3.2.5). Since chromosomal instability is a hallmark of human cancer, which contributes to tumourigenesis, therapy resistance and a poor patient prognosis (Orr & Compton 2013), the identification of *CEP72* as a new *bona fide* CIN gene is of great importance. Furthermore, *CEP72* overexpression mirrors the consequences of a Brca1 repression leading to the hypothesis that Cep72 negatively regulates Brca1's function during mitosis, thereby antagonizing the positive Brca1 regulator Chk2 (Figure 4.1). In fact, *CHK2* repression and overexpression of *CEP72* cause the same mitotic defects, which are reversible by adjusting the protein levels of the respective antagonist (Figure 3.20). More precisely, elevating the levels of the positive regulator Chk2, when negative regulation by Cep72 is enhanced and, *vice versa*, reducing the levels of the inhibitor when the activator is repressed, restores proper spindle assembly rates and prevents chromosome mis-segregation. Moreover, either overexpression of *CHK2* or repression of *CEP72* can restore normal microtubule polymerization rates upon partial repression of *BRCA1* (Figure 3.22) supporting the

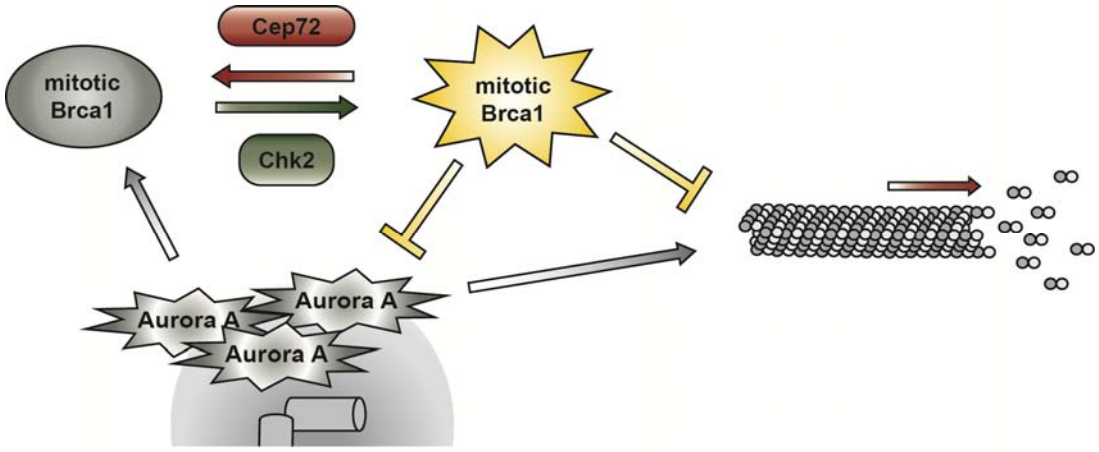

Figure 4.1 Model: Regulation of Brca1 during mitosis. The balanced regulation of Brca1 mediated by Chk2 and Cep72 ensures proper spindle microtubule plus-end assembly during mitosis. While Cep72 negatively regulates Brca1's function during mitosis, it is positively stimulated by Chk2 and restrains mitotic spindle microtubule plus end assembly. Moreover, phosphorylated Brca1 confines the accumulation of active Aurora A at mitotic centrosomes, which in turn promotes microtubule polymerization and inhibits Brca1 by phosphorylation at S308.

notion that Chk2 and Cep72 act in an opposing manner on Brca1 during mitosis. Beyond that, also the overexpression of *CHK2* or the repression of *CEP72* causes increased spindle microtubule polymerization (Figure 3.22 and 3.4) indicating that not only a reduced stimulation, but also a hyperstimulation of Brca1 is detrimental for spindle assembly. Thus, in addition to the Chk2 mediated phosphorylation, the inhibitory effect of Cep72 balancing the stimulation of Brca1 seems to be essential for accurate mitotic progression and the maintenance of chromosomal stability (Figure 4.2).

During mitosis Chk2 supports the binding between Cep72 and Brca1 (Figure 3.1). Since Cep72 acts antagonistically to Chk2 (3.3), this finding appears to be quite surprising. However, as the balanced regulation of Brca1 by Chk2 and Cep72 seems to be crucial for proper regulation of spindle assembly, Chk2 might facilitate the binding between Brca1 and Cep72 in order to equilibrate positive and negative stimuli.

Although, I showed that the regulation of spindle microtubule plus end assembly by Cep72 and Brca1 is specific for mitosis (Figure 3.11), the interaction between Brca1 and Cep72 is more prominent in interphase (Figure 3.1). This indicates that Cep72 might also play a role in regulating Brca1 with regard to other functions during interphase. Since in interphase Cep72 localizes to centrosomes and centriolar satellites, a Cep72-dependent regulation of Brca1 with respect to its function in the cellular stress response upon DNA damage which takes place in the nucleus seems to be unlikely.

However, at interphase centrosomes Brca1 was shown to restrain microtubule nucleation activity by promoting the disassembly of γ-tubulin and other γ-TuRC subunits (Sankaran et al. 2005; Sankaran et al. 2007).

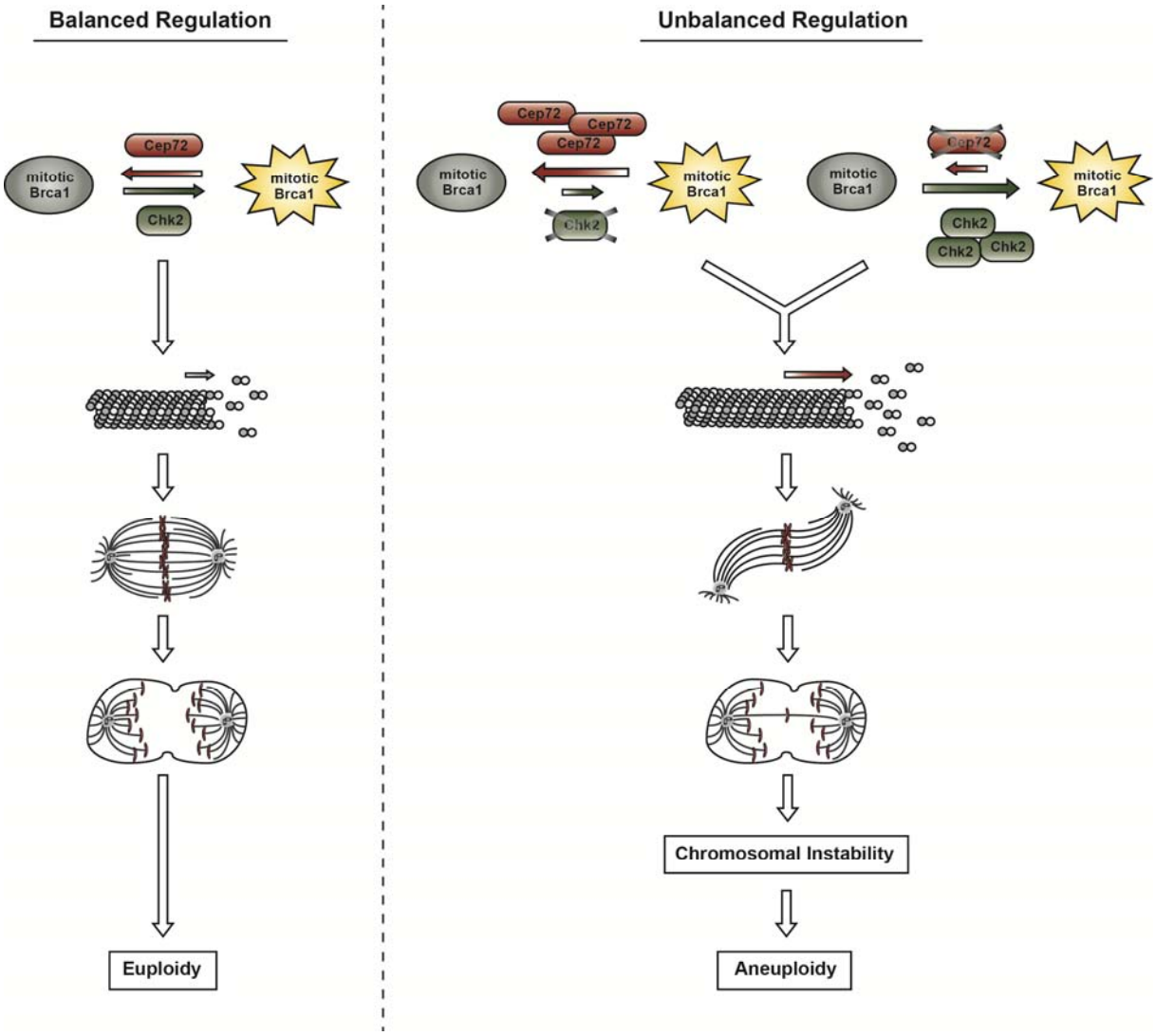

Figure 4.2 The balanced regulation of Brca1 mediated by Chk2 and Cep72 ensures proper mitotic spindle assembly and the maintenance of euploidy. In contrast, insufficient stimulation of Brca1 caused by overexpression of *CEP72* or repression of *CHK2* as well as Brca1 hyperstimulation by *CHK2* overexpression or *CEP72* repression leads to enhanced spindle microtubule plus-end assembly which in turn results in aberrant spindle formation, lagging chromosomes and chromosomal instability.

Conversely, Cep72 is involved in recruiting γ-TuRCs to the centrosome and maintains their microtubule nucleation potential by simultaneous recruitment of CG-NAP/AKAP450 (Oshimori et al. 2009). Thus, it might be possible that Cep72 promotes microtubule nucleation in interphase not only by recruiting the respective proteins to the centrosome, but also by negatively modulating Brca1's function to limit microtubule formation.

Nevertheless, the way Cep72 exerts its inhibitory function on Brca1 remains speculative. It was shown that the Chk2 mediated phosphorylation of Brca1 at S988 is essential to stimulate Brca1's function during mitosis (Figure 3.21) (Stolz et al. 2010). Thus, in order to antagonize this positive modification, Cep72 might be involved in removal of the

phosphate group, conceivably by recruitment of a protein phosphatase. Interestingly, matching this theory, Cep72 has been identified to interact with several regulatory and catalytical subunits of the serine / threonine protein phosphatase 1 (PP1) (The BioGRID[3.2] Interaction Database, www.thebiogrid.org; Hutchins et al., 2010). The holoenzyme PP1 forms a complex with one of three catalytical subunits (α, γ, and δ). Their activity is modulated by regulatory subunits, which activate or inhibit the phosphatase or, alternatively, mediate its subcellular localization (Yu et al. 2008; Liu et al. 2002; Hsu 2007; Figueiredo et al. 2014). Together, PP1 complexes have been shown to be involved in the regulation of diverse cellular processes including cell cycle progression, DNA damage response, chromosome segregation and cytokinesis (Ceulemans & Bollen 2004; Yu et al. 2008). Importantly, Brca1 contains a binding site for PP1 (Hsu 2007) and the catalytical subunit PP1α was shown to specifically dephosphorylate multiple serine residues that are phosphorylated by ATM (S1423), ATR (S1524) and Chk2 (S988) indicating that PP1 may serve as general regulator for Brca1 phosphorylation (Yu et al. 2008; Liu et al. 2002; Hsu 2007; Figueiredo et al. 2014). Moreover, during mitosis, both, PP1α and Brca1 localize to centrosomes (Liu et al. 2002; Starita & Parvin 2006) supporting the idea that Cep72 might regulate the removal of the Chk2 mediated phosphorylation of Brca1 at S988 by serving as a recruitment factor for PP1α. In addition, it is possible that Cep72 serves as linker between Brca1 and PP1α, hence, facilitating Brca1 dephosphorylation. Nevertheless, this function of Cep72 remains unclear and due to the lack of specific S988 antibodies further investigations on this have not been possible, yet.

Moreover, the partial localization of Cep72 in non-centrosomal structures could shed light on its mode of action. Pericentriolar satellites gradually disappear when cells enter mitosis. However, they are visibly present until metaphase, almost disappear in anaphase and re-assemble in telophase (Kubo & Tsukita 2003). They were shown to act as storage sites for proteins, which are delivered to the centrosome by dynein mediated transport in times when the centrosome is subject to rapid changes of its composition. In this context, centriolar satellites are likely to be of major importance for centrosome maturation prior to mitosis, centriole duplication and ciliogenesis (Bärenz et al. 2011; Villumsen et al. 2013). Furthermore, it was proposed that pericentriolar satellites also play a role in the temporal sequestration of different proteins in order to prevent their localization to centrosomes and other cell compartments (Stowe et al. 2012; Lopes et al. 2011; Tollenaere et al. 2014). Thus, also the temporary sequestration of activating and inhibitory proteins, which needs to be duly delivered to the centrosome by pericentriolar satellites could contribute to Brca1 regulation during mitosis. In such a scenario the Chk2-mediated phosphorylation of Brca1 during mitosis might trigger the centrosome-

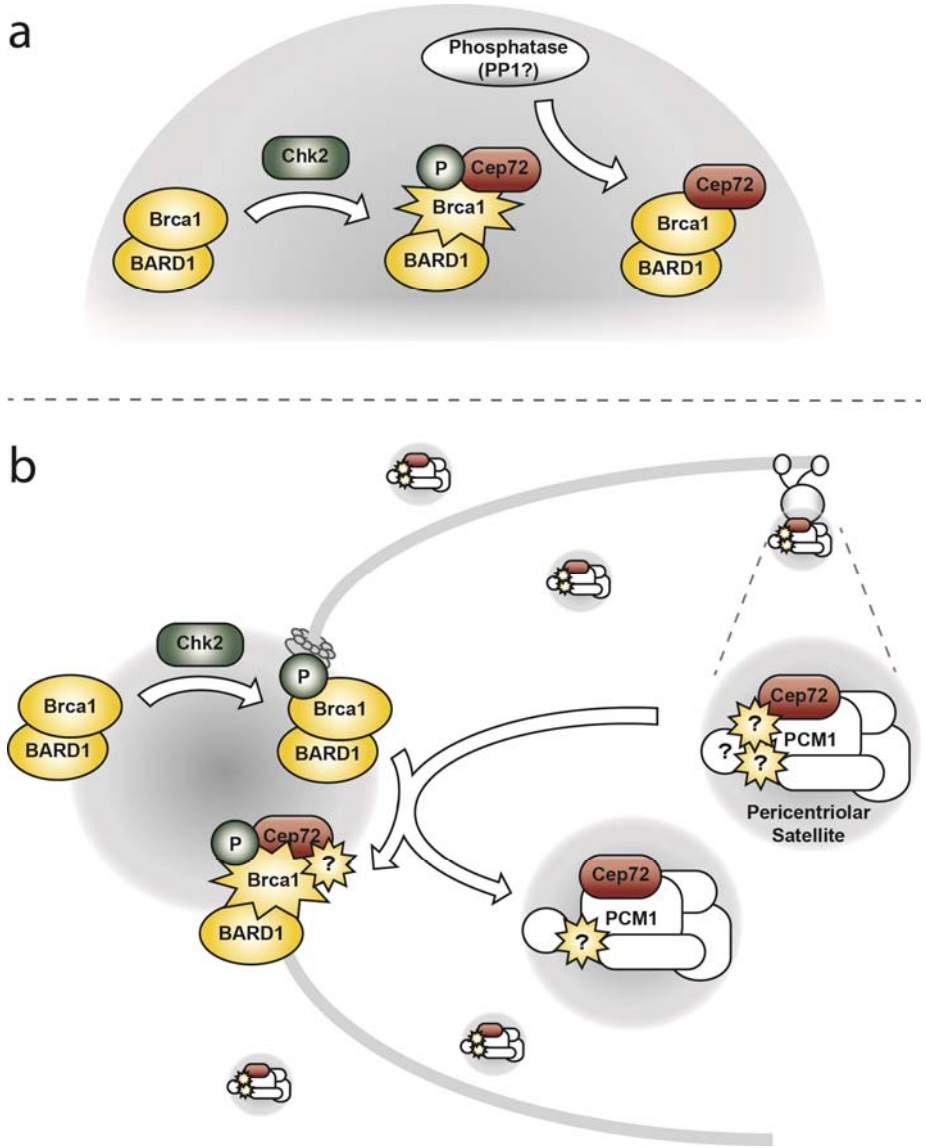

Figure 4.3 Possible mechanisms for the Cep72 mediated regulation of Brca1. a) Whereas the Chk2 mediated phosphorylation of Brca1 at S988 positively regulates Brca1's function during mitosis, Cep72 might counteract Chk2 by serving as a recruitment factor or linker protein for a protein phosphatase like PP1, which removes the Brca1 phosphorylation at S988. **b)** Pericentriolar satellites are thought to sequester proteins in order to temporally prevent their centrosomal localization. To regulate Brca1's mitotic function with respect to the particular cell cycle phase, Chk2-mediated phosphorylation of Brca1 might trigger Cep72-dependent delivery of potential Brca1 stimulating proteins to the centrosome.

directed transport of pericentriolar satellite associated proteins (Figure 4.3. b). Consequently, it is conceivable that Cep72 is responsible for the conveyance of proteins that stimulate Brca1's mitotic function. Interestingly, the finding that partial loss of *CHK2* impairs Brca1-Cep72 binding (Figure 3.1 c) might support this theory. Hence, Chk2 would temporally regulate Brca1's function by triggering Cep72-mediated delivery of Brca1 stimulating proteins to the centrosome.

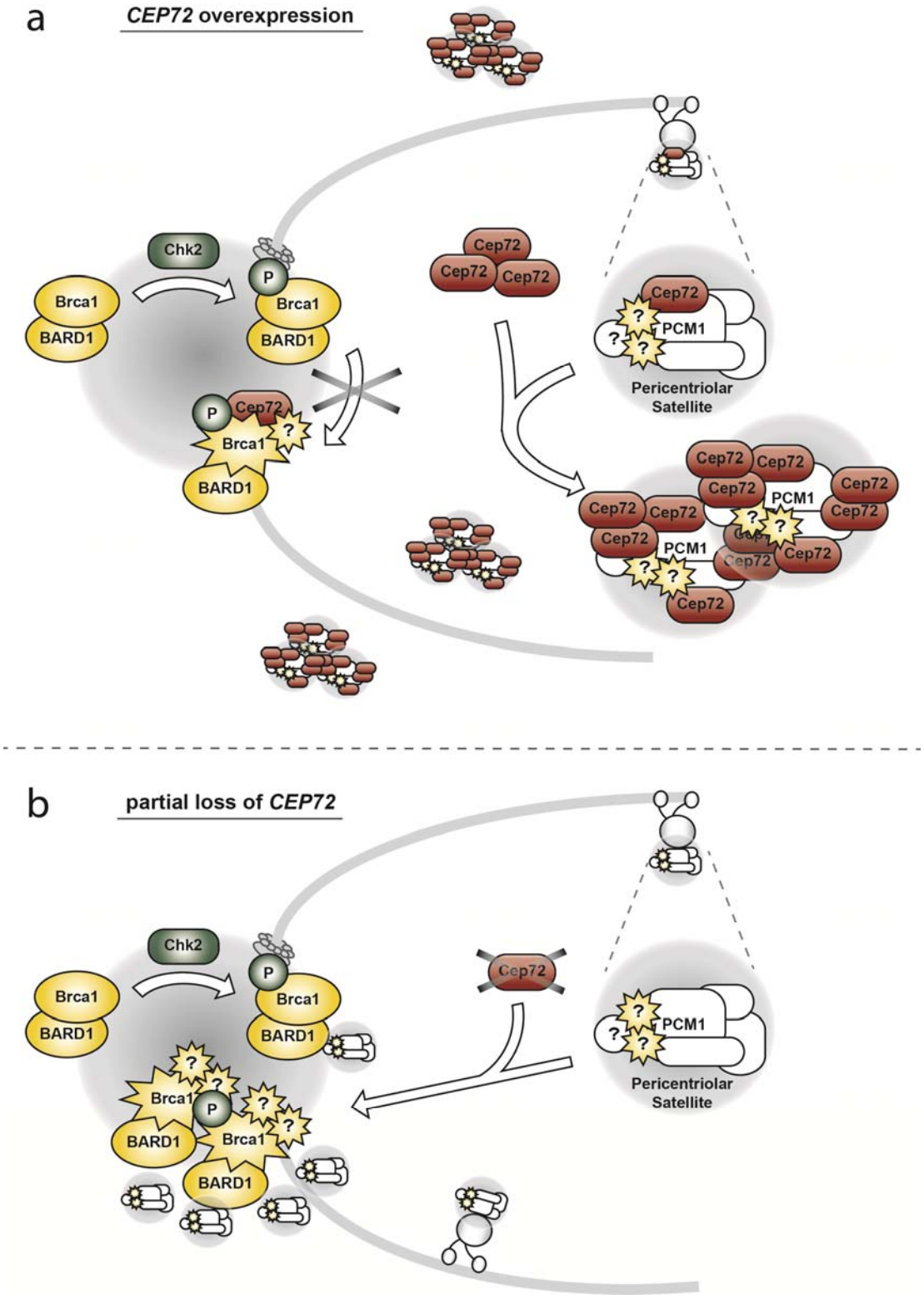

Figure 4.4 Overexpression as well as repression of *CEP72* cause the disruption of pericentriolar satellites, which might interfere with proper and timely stimulation of Brca1 during mitosis. a) Overexpression of *CEP72* leads to disruption of pericentriolar satellites and forms cytoplasmic aggregates that sequester particular satellite proteins like PCM1 or Cep290. The sequestration might include potential positive regulators of Brca1, thus, impairing Brca1 stimulation during mitosis. **b)** Partial loss of *CEP72* causes pericentriolar satellite fragmentation and

the accumulation of associated proteins at centrosomes. Agglomeration of potential Brca1 stimulating proteins might cause Brca1 hyperstimulation and thereby altered spindle microtubule polymerization.

Importantly, both, the downregulation and the overexpression of *CEP72* results in the disruption of pericentriolar satellites (Stowe et al. 2012). Whereas *CEP72* repression causes satellites fragmentation and the accumulation of associated proteins at centrosomes, the overexpression of *CEP72* leads to the formation of cytoplasmic aggregates that sequester particular satellite proteins like PCM1 or Cep290 (Stowe et al. 2012). Consequently, partial loss of *CEP72* would cause a centrosomal agglomeration of activating proteins, which might result in aberrant hyperstimulation of Brca1 (Figure 4.4). In contrast, lasting sequestration of a Brca1 activating protein within Cep72 aggregates would impair the stimulation of Brca1's function to regulate mitotic spindle assembly. Thus, also the timely regulation of Brca1 by Cep72 localization in pericentriolar satellites might represent a possible mechanism. Another protein being crucial for the integrity of centriolar satellites is their scaffolding component PCM1. As in the case of *CEP72*, downregulation of *PCM1* also results in the disruption of centriolar satellites and associated proteins are transported to the centrosome where they accumulate (Lopes et al. 2011; Stowe et al. 2012; Tollenaere et al. 2014; Bärenz et al. 2011). Interestingly, both, repression of *PCM1* and the partial loss of dynein mediating the retrograde transport of pericentriolar satellites and thus, the delivery of associated proteins to the centrosome (Tollenaere et al. 2014; Dammermann & Merdes 2002), causes enhanced spindle microtubule growth rates as well (my unpublished data, Stolz et al. 2015). This might support the hypothesis that centriolar satellites are possibly involved in the regulation of mitotic spindle assembly probably by sequestration of activating or inhibitory proteins.

Although the identification of Cep72 gives new insights into the regulation of Brca1 during mitosis, the way Brca1 exerts its function to regulate spindle microtubule assembly remains elusive. However, evidence that Brca1 restrains the hyper-activation of Aurora A at mitotic centrosomes was already given by Ertych et al., 2014. Aurora A in turn might promote microtubule polymerization by phosphorylating TACC3, thus, triggering the recruitment of the microtubule polymerase ch-TOG to mitotic centrosomes and the mitotic spindle (Barr & Gergely 2008; LeRoy et al. 2007; Thakur et al. 2013; Brouhard et al. 2008; Widlund et al. 2011). A loss or deregulation of Brca1 would consequently result in an increased level of active Aurora A at mitotic centrosomes (Ertych et al. 2014), which than stimulates microtubule plus end assembly by the TACC3-ch-TOG axis. Furthermore Aurora A was shown to regulate the microtubule depolymerase Kif2a during mitosis. The Aurora A mediated phosphorylation of Kif2a confines its localization to spindle microtubules as well as mitotic centrosomes and inhibits its

depolymerase activity (Jang et al. 2009). Interestingly, the repression of Kif2a causes enhanced spindle microtubule polymerization rates (my unpublished data) and is associated with elongated spindles (Ganem & Compton 2004) as seen upon *CEP72* overexpression or repression of *BRCA1* (3.2.3). Thus, elevated Aurora A activity might also stimulate microtubule assembly by inhibiting the microtubule depolymerase Kif2A.

Moreover, it is conceivable that Brca1 directly regulates spindle microtubule dynamics. Brca1 contains a RING domain as well as two BRCT domains and the question, which domain mediates the tumour suppressive function of Brca1 is controversially discussed. While the BRCT domains represent phospho-protein specific binding motifs (Henderson 2012; Yu 2003), which are crucial for the formation of Brca1 complexes mainly involved in DNA damage repair (Savage & Harkin 2014), the RING domain enables the interaction with its obligatory binding partner BARD1. Together, both proteins form a heterodimer and complement an E3-ubiquitin ligase being responsible for the ubiquitination of various substrates (Hashizume et al., 2001; Wu etal. 2008; Savage & Harkin, 2014). Also during mitosis the domain mediating Brca1's function to ensure proper spindle assembly is unknown. Interestingly, the disruption of the E3-ubiquitin ligase function of Brca1 by repression of *BARD1* or by using a Brca1 mutant lacking E3 ubiquitin-ligase activity leads to increased spindle microtubule plus end assembly as induced upon repression of *BRCA1* (Figure 3.5). These findings indicate that the ubiquitination activity of Brca1 might be crucial for its mitotic function to counteract microtubule polymerization. Consequently, Brca1 seems to promote the destabilization of spindle microtubules, which is possible in three different ways: 1) by impairing polymerization, 2) by promoting depolymerization or 3) by triggering catastrophe events (van der Vaart et al. 2009). Thus, Brca1 might trigger the activity of microtubule depolymerizing enzymes at mitotic centrosomes such as Kif2a and Kif2b (Manning et al. 2007). However, direct interactions or evidence for such a regulation have not been given, yet. Another interesting candidate is the microtubule associated protein 4 (MAP4), which, together with Cep72, was identified as new protein interacting with Brca1 during mitosis (Lüddecke et al. 2015). Associated with microtubules throughout the cell cycle MAP4 counteracts catastrophe induction and promotes rescue events (Ookata et al. 1995), hence triggering microtubule assembly in interphase and mitosis (Illenberger et al. 1996; Ebneth et al. 1999; Chang et al. 2001; Xiao et al. 2012; Zahnleiter et al. 2015). In order to prevent enhanced microtubule polymerization Brca1 might ubiquitinate and therefore restrain the function of MAP4 during mitosis. Furthermore, Brca1 was shown to regulate microtubule nucleation activity by ubiquitination of γ-tubulin and subunits of the γ-TuRC complex, which results in disassembly from the centrosomes and a low microtubule nucleation potential during interphase (Sankaran et al., 2007, 2005). In mitosis the Aurora A mediated phosphorylation of Brca1 inhibits this post-translational modification and γ-TuRCs re-

assemble into the PCM leading to an increased microtubule nucleation activity in order to form the mitotic spindle (Sankaran et al., 2007). Interestingly, several mutations in γ-TuRC subunits were shown to severely influence microtubule dynamicity *per se*. In fission yeast, mutations in homologues of GCP2 were shown to cause continuously growing microtubule plus-ends in interphase and mitosis (Zimmerman & Chang 2005). Moreover, mutations in the GCP2 homologue alp4 or the overexpression of its C-terminal fragment reduced catastrophe rates (Zimmerman & Chang 2005; Masuda et al. 2006; Raynaud-Messina & Merdes 2007). Also in Drosophila γ-TuRCs localize along microtubules at least in interphase and promote their stabilization by reducing catastrophe events. During mitosis γ-TuRCs are further important for stabilization of astral microtubules in order to achieve a proper spindle anchorage. Depletion of the γ-TuRC component Dgrip75 results in spindle misorientation and elongated spindles due to enhanced microtubule dynamicity, which can be reversed by treatment with microtubule stabilizing drugs and downregulation of proteins that promote microtubule dynamics such as EB1 (Bouissou et al. 2014). In fact, also the depletion of human GCP4 leads to spindle orientation defects and the mislocalization of EB1. Upon GCP4 repression, EB1 localizes along whole microtubules rather than only at plus tips resulting in increased GTP-bound tubulin along the lattice and microtubules, which spent longer time in the growing state (Bouissou et al. 2014). Similarly, the deregulation of the Chk2-Cep72-Brca1 axis causes, beside elongated microtubules (Figure 3.13), spindles with orientation defects during prometaphase (Ertych et al. 2014), resembling the phenotype observed after depletion of different γ-TuRC components. Likewise, the defects are reversible by lowering spindle microtubule polymerization rates using low dose Taxol® (Figure 3.12)(Ertych et al. 2014) as observed by Bouissou et al., 2014. Thus, it might be possible that Brca1/BARD1 mediated ubiquitination of γ-tubulin or other GCPs might be crucial for proper γ-TuRC function to regulate microtubule dynamics along spindle microtubules during mitosis. Moreover, other E3 ubiquitin ligases were shown to directly ubiquitinate subunits of the α/ß-tubulin heterodimer. While Parkin was shown to ubiquitinate α- and ß-tubulin in order to degrade misfolded tubulin subunits (Ren et al. 2003; Srivastava & Chakrabarti 2014), the E3 ubiquitin-ligase Mohugonin ring-finger 1 (MGRN1) polyubiquitinates α-tubulin and positively modulates microtubule polymerization. Accordingly, an inhibition of MGRN1 activity results in reduced spindle aster length and spindle orientation defects (Srivastava & Chakrabarti 2014). Interestingly, MGRN1 influences α-tubulin properties by Lys6-linked polyubiquitination (Srivastava & Chakrabarti 2014), an uncommon ubiquitin linkage, which is also mediated by Brca1/BARD1 (Morris & Solomon, 2004; Nishikawa et al., 2004; Wu-Baer et al. 2003). Moreover, Lotti et al. detected a co-localization of Brca1 and α- as well as ß-tubulin to spindle microtubules and mitotic centrosomes. The interactions were further confirmed by coimmunoprecipitations (Lotti et al. 2002) and are also present in our own analyses of Brca1 interacting proteins during mitosis (Lüddecke

et al. 2015). Therefore, it might be possible that the Brca1/BARD1 heterodimer, similar to MGRN1, directly modulates α- or ß-tubulin properties, thus promoting microtubule disassembly or catastrophe events.

Enhanced spindle microtubule polymerization, which is caused by deregulation of the Chk2-Cep72-Brca1 pathway, or in particular, as induced upon downregulation of *BRCA1* or *CEP72* overexpression, results in abnormal spindle formation (3.2.3). In contrast to ball-like spindle structures, cells with increased spindle microtubule growth exhibit curved or distorted spindles. The closer investigation of those spindles revealed significantly longer microtubules, which were accompanied by increased inter-centrosomal distance (Figure 3.13). This phenotype is presumably due to perpetual increased microtubule plus end assembly, while the depolymerization at the minus end remains constant or is even impaired. When the polymerization speed at the plus tip exceeds the depolymerization rate at the minus end, net growth is induced, providing an explanation for the elongation of microtubules upon enhanced microtubule polymerization. Since microtubules emanating from both spindle poles are antiparallel linked by Eg5 (Kapitein et al. 2005) or connected by particular binding to chromosomes at the equatorial plane of the spindle, enhanced microtubule growth generates forces, which pushes centrosomes apart. Additionally, the cell membrane limits the space for centrosome separation. When microtubules keep growing and thus, continue elongation, it is likely that they take a curved and distorted spindle structure. Furthermore, the deregulation of other mechanisms involved in balancing spindle length might contribute to increased inter-centrosomal distance. Kinesins, which are attached to chromosome arms can exert an outward pushing force (Dumont & Mitchison 2009; Kwon et al. 2004), whereas dynein at the cell cortex was reported to provide a pulling force on astral microtubules (Tanenbaum & Medema 2010).

Nevertheless, a balanced regulation of inward and outward forces and thus, the maintenance of a proper spindle length is required for accurate microtubule-kinetochore attachment and chromosome segregation (van Heesbeen et al. 2014; Syrovatkina et al. 2013). Consequently, cells with longer or shorter spindles show chromosome segregation defects, which is in line with the findings in this study (3.2.3). The enhanced microtubule plus end assembly caused by overexpression of *CEP72* and a deregulation of the Chk2-Brca1 axis during mitosis leads to the formation of elongated spindles with a curved and distorted morphology. This, in turn, is associated with spindle geometry defects that facilitate merotelic attachments, lagging chromosomes and CIN (Nam et al. 2014; Silkworth & Cimini 2012; Stolz et al. 2014). Since increased spindle microtubule polymerization does not affect the error correction machinery *per se* (Ertych et al. 2014; Stolz et al. 2014), it is likely that elevated formation of erroneous microtubule-kinetochore attachments overwhelms the error-correction machinery.

In summary, we identified Cep72 as a hitherto unknown interaction partner and inhibitor of the tumour suppressor Brca1. Like a loss of *BRCA1*, the overexpression of *CEP72* is linked to aberrant mitotic cell division and the induction of chromosomal instability. Hence, *CEP72* represents a putative onco- and *bona fide* CIN gene. While *BRCA1* is famous for being mutated or lost in human breast cancer (Savage & Harkin 2014), *CEP72* expression is rarely affected in this tumour entity (3.2.1). However, in human colorectal cancer, which is highly associated with chromosomal instability, *CEP72* is strikingly overexpressed (3.2.1). In addition, *CEP72* localizes to the lung cancer susceptibility gene locus 5p15.33, and was shown to be frequently amplified in non-small cell lung cancer comprising lung adenocarcinoma and squamous cell carcinoma (Kang et al., 2008; cBioPortal for Cancer Genomics www.cbioportal.org). Remarkably, beside breast and colorectal cancer, non-small cell lung cancer represents another tumour entity, which is frequently linked to CIN and a poor patient outcome (McGranahan et al. 2012; Masuda & Takahashi 2002). Thus, *CEP72* gene amplification, which comes along with overexpression of *CEP72* (cBioPortal for Cancer Genomics www.cbioportal.org) might also contribute to chromosomal instability in tumour types other than colorectal cancer. Substantial similarities can be found to alterations in the *CHK2* expression, which is frequently lost or repressed in colorectal (Stolz et al. 2010; Ertych et al. 2014) and lung cancer (P. Zhang et al. 2004; Stolz et al. 2010). Furthermore, *CHK2* is often mutated in breast cancer entities, which are not affected by *BRCA1* mutations (Meijers-Heijboer et al. 2002). Consequently, in addition to *BRCA1* mutations, alterations of the Brca1 stimulating proteins Cep72 and Chk2 might represent alternative genetic lesions which contribute to chromosomal instability and poor patient prognosis.

5 REFERENCES

Akhshi, T.K et al., 2014. Microtubules and actin crosstalk in cell migration and division. *Cytoskeleton*, 71(January), pp.1–23.

Alberts, B. et al., 2007. *Molecular Biology of the Cell*, Taylor & Francis publishing company, 5th Revised edition

Andersen, J.S. et al., 2003. Proteomic characterization of the human centrosome by protein correlation profiling. *Nature*, 426(6966), pp.570–574.

Bakhoum, S. et al., 2014. DNA-damage responde during mitosis induces whole-chromosome missegregation. *Cancer Discov.*, 4(11), pp.1281–1289.

Bakhoum, S.F. & Compton, D. A., 2012. Chromosomal instability and cancer : a complex relationship with therapeutic potential. *The Journal of Clinical Investigation*, 122(4), pp.1138–1143.

Barber, T.D. et al., 2008. Chromatid cohesion defects may underlie chromosome instability in human colorectal cancers. *Proceedings of the National Academy of Sciences of the United States of America*, 105(9), pp.3443–3448.

Bärenz, F. et al., 2013. The centriolar satellite protein SSX2IP promotes centrosome maturation. *Journal of Cell Biology*, 202(1), pp.81–95.

Bärenz, F., Mayilo, D. & Gruss, O.J., 2011. Centriolar satellites: Busy orbits around the centrosome. *European Journal of Cell Biology*, 90, pp.983–989.

Barr, A.R. & Gergely, F., 2008. MCAK-independent functions of ch-Tog/XMAP215 in microtubule plus-end dynamics. *Molecular and cellular biology*, 28(23), pp.7199–7211.

Bettencourt-Dias, M. & Glover, D.M., 2007. Centrosome biogenesis and function: centrosomics brings new understanding. *Nature reviews. Molecular cell biology*, 8(June), pp.451–463.

Booth, D.G. et al., 2011. A TACC3/ch-TOG/clathrin complex stabilises kinetochore fibres by inter-microtubule bridging. *The EMBO journal*, 30(5), pp.906–919.

Bornens, M., 2012. The Centrosome in Cells and Organisms. *Science*, 335, pp.422–426.

Bornstein, G. et al., 2003. Role of the SCFSkp2 ubiquitin ligase in the degradation of p21Cip1 in S phase. *Journal of Biological Chemistry*, 278(28), pp.25752–25757.

Bouissou, A. et al., 2014. γ-Tubulin ring complexes and EB1 play antagonistic roles in microtubule dynamics and spindle positioning. *EMBO Journal*, 33(2), pp.114–128.

Boveri, T., 1914. *Zur Frage der Entstehung maligner Tumore*, Würzburg: Verlag von Gustav Fischer.

Brattain, M.G., Fine, W.D. & Khaled, F.M., 1981. Heterogeneity of Malignant Cells from a Human Colonic Carcinoma of Malignant Cells from a Human Colonie Carcinoma1. , (May), pp.1751–1756.

Brinkley, B., 2001. Managing the centrosome number game: from chaos to stability in cancer cell division. *Trends in Cell Biology*, 11(1), pp.18–21.

Brouhard, G.J. et al., 2008. XMAP215 is a processive microtubule polymerase. *Cell*, 132(1), pp.79–88.

Brouhard, G.J. & Rice, L.M., 2014. The contribution of -tubulin curvature to microtubule dynamics. *The Journal of Cell Biology*, 207(3), pp.323–334.

Brzovic, P.S. et al., 2003. Binding and recognition in the assembly of an active BRCA1/BARD1 ubiquitin-ligase complex. *Proceedings of the National Academy of Sciences of the United States of America*, 100(Track II), pp.5646–5651.

Burke, B. & Ellenberg, J., 2002. Remodelling the walls of the nucleus. *Nat Rev Mol Cell Biol*, 3(7), pp.487–497.

Burrell, R. a et al., 2013. Replication stress links structural and numerical cancer chromosomal instability. *Nature*, 494(7438), pp.492–6.

Cahill, D.P. et al., 1998. Mutations of mitotic checkpoint genes in human cancers. *Nature*, 392(6673), pp.300 – 303.

Cai, S. et al., 2009. Chromosome Congression in the Absence of K-Fibres. *Nat Cell Biol*, 11(7), pp.832–838.

De Cárcer, G. et al., 2011. From Plk1 to Plk5: Functional evolution of Polo-like kinases. *Cell Cycle*, 10 (March 2015), pp.2255–2262.

Carrano, A. et al., 1999. SKP2 is required for ubiquitin-mediated degradation of the CDK inhibitor p27. *Nat Cell Biol*, 1(4), pp.193–199.

Ceulemans, H. & Bollen, M., 2004. Functional Diversity of Protein Phosphatase 1, a Cellular Economizer and Reset Button. *Physiological reviews*, 84(1), pp.1–39.

Chang, W. et al., 2001. Phosphorylation of MAP4 affects microtubule properties and cell cycle progression. *Journal of cell science*, 114, pp.2879–2887.

Cheeseman, I.M. et al., 2006. The Conserved KMN Network Constitutes the Core Microtubule-Binding Site of the Kinetochore. *Cell*, 127, pp.983–997.

Cheeseman, I.M., 2014. The Kinetochore: *Cold Spring Harb Perspect Biol*, 6(7).

Cheeseman, I.M. & Desai, A., 2008. Molecular architecture of the kinetochore-microtubule interface. *Nature reviews. Molecular cell biology*, 9(january), pp.33–46.

Cheeseman, L.P. et al., 2013. Specific removal of TACC3-ch-TOG-clathrin at metaphase deregulates kinetochore fiber tension. *Journal of cell science*, 126, pp.2102–13.

Crasta, K. et al., 2012. DNA breaks and chromosome pulverization from errors in mitosis. *Nature*, 482, pp.53–58.

Cruz-Garcia, A., Lopez-Saavedra, A. & Huertas, P., 2014. BRCA1 accelerates CtIP-mediated DNA-end resection. *Cell Reports*, 9(2), pp.451–459.

Dammermann, A. & Merdes, A., 2002. Assembly of centrosomal proteins and microtubule organization depends on PCM-1. *Journal of Cell Biology*, 159, pp.255–266.

Delgehyr, N., Sillibourne, J. & Bornens, M., 2005. Microtubule nucleation and anchoring at the centrosome are independent processes linked by ninein function. *Journal of cell science*, 118, pp.1565–1575.

Drost, R. et al., 2011. BRCA1 RING function is essential for tumor suppression but dispensable for therapy resistance. *Cancer Cell*, 20(6), pp.797–809.

Dumont, S. & Mitchison, T.J., 2009. Force and Length in the Mitotic Spindle. *Current Biology*, 19(17), pp.R749–R761.

Ebneth, A. et al., 1999. Phosphorylation of MAP2c and MAP4 by MARK kinases leads to the destabilization of microtubules in cells. *Cell Motil Cytoskeleton*, 44(3), pp.209–224.

Elbashir, S.M. et al., 2001. Duplexes of 21-nucleotide RNAs meditae RNA interference in cultured mammalian cells. *Nature*, 411(May), pp.1–5.

Ertych, N. et al., 2014. Increased microtubule assembly rates influence chromosomal instability in colorectal cancer cells. *Nature cell biology*, 16(7), pp 779-91.

Escribano-Díaz, C. et al., 2013. A Cell Cycle-Dependent Regulatory Circuit Composed of 53BP1-RIF1 and BRCA1-CtIP Controls DNA Repair Pathway Choice. *Molecular Cell*, 49, pp.872–883.

Eyers, P. a. & Maller, J.L., 2004. Regulation of Xenopus Aurora A Activation by TPX2. *Journal of Biological Chemistry*, 279(10), pp.9008–9015.

Eyers, P.A. & Maller, J.L., 2003. Regulating the Regulators - Aurora A Activation and Mitosis. *Cell Cycle*, 295(August), pp.287–289.

Fant, X., Merdes, A. & Haren, L., 2004. Cell and Molecular Biology of Spindle Poles and NuMA. In B. T.-I. R. of Cytology, ed. Academic Press, pp. 1–57.

Figueiredo, J. et al. 2014. Protein phosphatase 1 and its complexes in carcinogenesis. *Current cancer drug targets*, 14, pp.2–29.

Foley, E.A. & Kapoor, T.M., 2013. Microtubule attachment and spindle assembly checkpoint signaling at the kinetochore. *Nat Rev Mol*, 14(1), pp.25–37.

Fong, K.-W. et al., 2008. CDK5RAP2 Is a Pericentriolar Protein Taht Functions in Centrosomal Attachment of the y-Tubulin Ring Complex. *Molecular biology of the cell*, 19(January), pp.115–125.

Fu, J. & Glover, D.M., 2012. Structured illumination of the interface between centriole and peri-centriolar material. *Open Biology*, 2, pp.120104.

Fu, W. et al., 2010. Clathrin recruits phosphorylated TACC3 to spindle poles for bipolar spindle assembly and chromosome alignment. *Journal of cell science*, 123, pp.3645–3651.

Ganem, N.J. & Compton, D. A., 2004. The KinI kinesin Kif2a is required for bipolar spindle assembly through a functional relationship with MCAK. *Journal of Cell Biology*, 166, pp.473–478.

Ganem, N.J et al., 2009. A Mechanism Linking Extra Centrosomes to Chromosomal Instability. *Nature*, 460(7252), pp.278–282.

Gomez-Ferreria, M.A. et al., 2007. Human Cep192 Is Required for Mitotic Centrosome and Spindle Assembly. *Current Biology*, 17, pp.1960–1966.

Goshima, G. et al., 2008. Augmin: A protein complex required for centrosome-independent microtubule generation within the spindle. *Journal of Cell Biology*, 181(3), pp.421–429.

Goshima, G. & Kimura, A., 2010. New look inside the spindle: microtubule-dependent microtubule generation within the spindle. *Current Opinion in Cell Biology*, 22(1), pp.44–49.

Gregan, J. et al., 2011. Merotelic kinetochore attachments: causes and effects. *Trends in Cell Biology*, 21, pp.374–381.

Groth, a C. et al., 2000. A phage integrase directs efficient site-specific integration in human cells. *Proceedings of the National Academy of Sciences of the United States of America*, 97(11), pp.5995–6000.

Gruss, O.J. et al., 2002. Chromosome-induced microtubule assembly mediated by TPX2 is required for spindle formation in HeLa cells. *Nature cell biology*, 4, pp.871–879.

Gruss, O.J. et al., 2001. Ran induces spindle assembly by reversing the inhibitory effect of importin α on TPX2 activity. *Cell*, 104, pp.83–93.

Von Hansemann, D., 1890. Über asymmetrische Zellteilung in Epithelkrebsen und deren biologische Bedeutung. *Virchows Arch Pathol Anat*, 119, pp.299–326.

Haren, L. et al., 2006. NEDD1-dependent recruitment of the γ-tubulin ring complex to the centrosome is necessary for centriole duplication and spindle assembly. *Journal of Cell Biology*, 172(4), pp.505–515.

Hashizume, R. et al., 2001. The RING Heterodimer BRCA1-BARD1 Is a Ubiquitin Ligase Inactivated by a Breast Cancer-derived Mutation. *Journal of Biological Chemistry*, 276, pp.14537–14540.

Van Heesbeen, R.G.H.P et al., 2014. Balanced Activity of Three Mitotic Motors Is Required for Bipolar Spindle Assembly and Chromosome Segregation. *Cell Reports*, 8, pp.948–956.

Helmke et al., 2013. *Interplay between spindle architecture and function* 1st ed., Elsevier Inc.

Henderson, B.R., 2012. The BRCA1 Breast Cancer Suppressor: Regulation of Transport, Dynamics, and Function at Multiple Subcellular Locations. *Scientifica*, 2012, p.796808.

Hershko, a & Ciechanover, a, 1998. The ubiquitin system. *Annual review of biochemistry*, 67, pp.425–479.

Hochegger et al., 2013. Aurora at the pole and equator: overlapping functions of Aurora kinases in the mitotic spindle. *Open Biology*, 3, p.120185.

Holland, A.J. & Cleveland, D.W., 2012. Losing balance: the origin and impact of aneuploidy in cancer. *EMBO reports*, 13(6), pp.501–514.

Holland, A.J et al., 2010. Centriole duplication: A lesson in self-control. *Cell Cycle*, 9(January 2015), pp.2731–2736.

Hoyer-Fender, S., 2010. Centriole maturation and transformation to basal body. *Seminars in Cell & Developmental Biology*, 21(2), pp.142–147.

Hsu, L.-C., 2007. Identification and functional characterization of a PP1-binding site in BRCA1. *Biochem Biophys Res Commun*, 360(2), pp.507–512.

Hsu, L.C. & White, R.L., 1998. BRCA1 is associated with the centrosome during mitosis. *Proceedings of the National Academy of Sciences of the United States of America*, 95(October), pp.12983–12988.

Hutchins, J.R. a et al., 2010. Systematic Characterization of Human Protein Complexes Identifies Chromosome Segregation Proteins. *Science*, 328(5978), pp.593–599.

Illenberger, S. et al., 1996. Phosphorylation of Microtubule-associated Proteins MAP2 and MAP4 by the Protein Kinase p110[IMAGE]. *Journal of Biological Chemistry*, 271(18), pp.10834–10843.

Jallepalli, P. V. et al., 2003. The Chk2 tumor suppressor is not required for p53 responses in human cancer cells. *Journal of Biological Chemistry*, 278(23), pp.20475–20479.

Jang, C.Y. et al., 2008. DDA3 recruits microtubule depolymerase Kif2a to spindle poles and controls spindle dynamics and mitotic chromosome movement. *Journal of Cell Biology*, 181(2), pp.255–267.

Jang, C.-Y. et al., 2009. Plk1 and Aurora A regulate the depolymerase activity and the cellular localization of Kif2a. *Journal of cell science*, 122, pp.1334–1341.

Jordan, M.A. & Wilson, L., 2004. Microtubules as a target for anticancer drugs. *Nat Rev Cancer*, 4(4), pp.253–265.

Joukov, V. et al., 2010. Centrosomal protein of 192 kDa (Cep192) promotes centrosome-driven spindle assembly by engaging in organelle-specific Aurora A activation. *Proceedings of the National Academy of Sciences of the United States of America*, 107(49), pp.21022–21027.

Joukov, V. et al., 2006. The BRCA1/BARD1 Heterodimer Modulates Ran-Dependent Mitotic Spindle Assembly. *Cell*, 127, pp.539–552.

Kang, J.U. et al., 2008. Gain at chromosomal region 5p15.33, containing TERT, is the most frequent genetic event in early stages of non-small cell lung cancer. *Cancer Genetics and Cytogenetics*, 182(1), pp.1–11. Available at: http://www.cancergeneticsjournal.org/article/S0165-4608(07)00809-6/abstract.

Kapitein, L.C. et al., 2005. The bipolar mitotic kinesin Eg5 moves on both microtubules that it crosslinks. *Nature*, 435(7038), pp.114–118.

Kapoor, T.M. et al., 2000. Probing spindle assembly mechanisms with monastrol, a small molecule inhibitor of the mitotic kinesin, Eg5. *Journal of Cell Biology*, 150(5), pp.975–988.

Karsenti, E. & Vernos, I., 2001. The Mitotic Spindle : A Self-Made Machine. , 294(October), pp.543–548.

Khodjakov, A. & Rieder, C.L., 1999. The sudden recruitment of y-tubulin to the centrosome at the onset of mitosis and its dynamic exchange throughout the cell cycle, do not require microtubules. *Journal of Cell Biology*, 146(3), pp.585–596.

Kim, K et al., 2012. CEP90 Is Required for the Assembly and Centrosomal Accumulation of Centriolar Satellites, Which Is Essential for Primary Cilia Formation. *PLoS ONE*, 7(10), pp.1–9.

Kiyomitsu, T. & Cheeseman, I.M., 2012. Chromosome- and spindle-pole-derived signals generate an intrinsic code for spindle position and orientation. *Nature Cell Biology*, 14(3), pp.311–317.

Kiyomitsu, T. & Cheeseman, I.M., 2013. Cortical dynein and asymmetric membrane elongation coordinately position the spindle in anaphase. *Cell*, 154(2), p.1401.

Kleiman, F.E. et al., 2005. BRCA1/BARD1 inhibition of mRNA 3' processing involves targeted degradation of RNA polymerase II. *Genes and Development*, 19, pp.1227–1237.

Komander, D., 2009. The emerging complexity of protein ubiquitination. *Biochemical Society transactions*, 37, pp.937–953.

Komander, D et al., 2009. Breaking the chains: structure and function of the deubiquitinases. *Nat Rev Mol Cell Biol*, 10(8), pp.550–563.

Kops, G.J.P.L et al., 2004. Lethality to human cancer cells through massive chromosome loss by inhibition of the mitotic checkpoint. *Proceedings of the National Academy of Sciences of the United States of America*, 101(23), pp.8699–8704.

Kubo, A. & Tsukita, S., 2003. Non-membranous granular organelle consisting of PCM-1: subcellular distribution and cell-cycle-dependent assembly/disassembly. *Journal of cell science*, 116, pp.919–928.

Kwon, M. et al., 2004. The Chromokinesin, KLP3A, Drives Mitotic Spindle Pole Separation during Prometaphase and Anaphase and Facilitates Chromatid Motility. *Molecular biology of the cell*, 15(January), pp.219–233.

Lara-Gonzalez, P. et al., 2012. The spindle assembly checkpoint. *Current Biology*, 22(22), pp.R966–R980.

Lawo, S. et al., 2009. HAUS, the 8-Subunit Human Augmin Complex, Regulates Centrosome and Spindle Integrity. *Current Biology*, 19, pp.816–826.

Lawo, S. et al., 2012. Subdiffraction imaging of centrosomes reveals higher-order organizational features of pericentriolar material. *Nat Cell Biol*, 14(11), pp.1148–1158.

Lecland, N. & Lüders, J., 2014. The dynamics of microtubule minus ends in the human mitotic spindle. *Nature cell biology*, 16(8).

Lee, E.K. & Diehl, J. a, 2014. SCFs in the new millennium. *Oncogene*, 33(16), pp.2011–8.

Lee, K. & Rhee, K., 2011. PLK1 phosphorylation of pericentrin initiates centrosome maturation at the onset of mitosis. *Journal of Cell Biology*, 195(7), pp.1093–1101.

Lee, S. & Rhee, K., 2010. CEP215 is involved in the dynein-dependent accumulation of pericentriolar matrix proteins for spindle pole formation. *Cell Cycle*, 9(February 2015), pp.775–784.

Lengauer, C., Kinzler, K.W. & Vogelstein, B., 1997. Genetic instabilities in human cancers. *Nature*, 396(6625), pp.623–627.

LeRoy, P.J. et al., 2007. Localization of human TACC3 to mitotic spindles is mediated by phosphorylation on Ser558 by Aurora A: A novel pharmacodynamic method for measuring Aurora A activity. *Cancer Research*, 67(11), pp.5362–5370.

Li, H.Y.et al., 2003. A mechanism of coupling RCC1 mobility to RanGTP production on the chromatin in vivo. *Journal of Cell Biology*, 160, pp.635–644.

Lin, C.H. et al., 2010. Clathrin heavy chain mediates TACC3 targeting to mitotic spindles to ensure spindle stability. *Journal of Cell Biology*, 189(7), pp.1097–1105.

Liu, C. et al., 2014. A fine-scale dissection of the DNA double-strand break repair machinery and its implications for breast cancer therapy. *Nucleic Acids Research*, 42(10), pp.6106–6127.

Liu, Y. et al., 2002. Regulation of BRCA1 Phosphorylation by Interaction with Protein Phosphatase 1 α. *Cancer R*, 62, pp.6357–6361.

Lopes, C. A. M. et al., 2011. Centriolar satellites are assembly points for proteins implicated in human ciliopathies, including oral-facial-digital syndrome 1. *Journal of cell science*, 124, pp.600–612.

Lotti, L.V. et al., 2002. Subcellular localization of the BRCA1 gene product in mitotic cells. *Genes, Chromosomes and Cancer*, 35(3), pp.193–203.

Lou, Z. et al., 2003. Mediator of DNA damage checkpoint protein 1 regulates BRCA1 localization and phosphorylation in DNA damage checkpoint control. *The Journal of biological chemistry*, 278, pp.13599–13602.

Lüddecke, S. et al., 2015. The putative oncogene CEP72 inhibits the mitotic function of BRCA1 and induces chromosomal instability. *Oncogene*. (in press, doi: 10.1038/ONC.2015.290)

Lüders, J et al., 2006. GCP-WD is a gamma-tubulin targeting factor required for centrosomal and chromatin-mediated microtubule nucleation. *Nature cell biology*, 8(2), pp.137–147.

Lüders, J. & Stearns, T., 2007. Microtubule-organizing centres: a re-evaluation. , 8(February), pp.161–167.

Macůrek, L. et al., 2008. Polo-like kinase-1 is activated by aurora A to promote checkpoint recovery. *Nature*, 455(September), pp.119–123.

Magidson, V. et al., 2011. The spatial arrangemant of chromosomes during prometaphase facilitates spindle assembly. *Cell*, 146(4), pp.555–567.

Manchado, E. et al., 2012. Killing cells by targeting mitosis. *Cell Death and Differentiation*, 19, pp.369–377.

Manfredi, M.G. et al., 2007. Antitumor activity of MLN8054, an orally active small-molecule inhibitor of Aurora A kinase. *Proceedings of the National Academy of Sciences of the United States of America*, 104(10), pp.4106–4111.

Manning, A.L. et al., 2007. The Kinesin-13 Proteins Kif2a, Kif2b, and Kif2c/MCAK Have Distinct Roles during Mitosis in Human Cells. *Molecular biology of the cell*, 18, pp.2970–2979.

Mardin, B.R. & Schiebel, E., 2012. Breaking the ties that bind: New advances in centrosome biology. *Journal of Cell Biology*, 197(1), pp.11–18.

Masuda, A. & Takahashi, T., 2002. Chromosome instability in human lung cancers: possible underlying mechanisms and potential consequences in the pathogenesis. *Oncogene*, 21, pp.6884–6897.

Masuda, H. et al., 2006. The carboxyterminus of Alp4 alters microtubule dynamics to induce oscillatory nuclear movement led by the spindle pole body in Schizosaccharomyces pombe. *Genes Cells*, 11(4), pp.337–352.

Matsuzawa, A. et al., 2014. The BRCA1/BARD1-Interacting Protein OLA1 Functions in Centrosome Regulation. *Molecular Cell*, 53(1), pp.101–114.

Maxwell, C.A. et al., 2003. RHAMM Is a Centrosomal Protein That Interacts with Dynein and Maintains Spindle Pole Integrity. *Molecular biology of the cell*, 14(June), pp.2262–2276.

McEwen, B.F. et al., 1997. Kinetochore fiber maturation in PtK1 cells and its implications for the mechanisms of chromosome congression and anaphase onset. *Journal of Cell Biology*, 137(7), pp.1567–1580.

McGranahan, N. et al., 2012. Cancer chromosomal instability: therapeutic and diagnostic challenges. *EMBO reports*, 13(6), pp.528–538.

Mehta, G.D. et al., 2013. Cohesin: Functions beyond sister chromatid cohesion. *FEBS Letters*, 587(15), pp.2299–2312.

Meijers-Heijboer, H. et al., 2002. Low-penetrance susceptibility to breast cancer due to CHEK2(*)1100delC in noncarriers of BRCA1 or BRCA2 mutations. *Nature genetics*, 31(may), pp.55–59.

Menella, V. et al., 2014. Amorphous no more- subdiffraction view of the pericentriolar material architecture. *2014*, 24(3), pp.188 – 197.

Menella, V. et al., 2012. Sub-diffraction- resolution fluorescence microscopy reveals a domain of the centrosome critical for pericentriolar material organization. *Nat Cell Biol*, 14(11), pp.1159–1168.

Metzger, M.B. et al., 2012. HECT and RING finger families of E3 ubiquitin ligases at a glance. *Journal of Cell Science*, 125(3), pp.531–537.

Meunier, S. & Vernos, I., 2012. Microtubule assembly during mitosis - from distinct origins to distinct functions? *Journal of Cell Science*, 125, pp.2805–2814.

Miki, Y., Swensen, J., Shattuck-Eidens, D., Futreal, A., P., Harshman, K., 1994. A strong candidate for the breast and ovarian cancer susceptibility gene BRCA1. *Science*, 266, pp.66–71.

Mimori-Kiyosue, Y. et al., 2005. CLASP1 and CLASP2 bind to EB1 and regulate microtubule plus-end dynamics at the cell cortex. *Journal of Cell Biology*, 168(32), pp.141–153.

Morgan, D.O., 2007. *The Cell Cycle - Principles of Control*,

Morris, J.R. & Solomon, E., 2004. BRCA1: BARD1 induces the formation of conjugated ubiquitin structures, dependent on K6 of ubiquitin, in cells during DNA replication and repair. *Human Molecular Genetics*, 13(8), pp.807–817.

Mountain, V. et al., 1999. HSET Cross-links Microtubules in the Mammalian Mitotic Spindle. *Jcb*, 147(2), pp.351–365.

Mukhopadhyay, D. & Riezman, H., 2009. Proteasome-independent functions of ubiquitin in endocytosis and signaling. *Science*, 315(5809), pp.201–205.

Müller, C. et al., 2007. Inhibitors of kinesin Eg5: antiproliferative activity of monastrol analogues against human glioblastoma cells. *Cancer Chemotherapy and Pharmacology*, 59(2), pp.157–164.

Musacchio, A. & Salmon, E.D., 2007. The spindle-assembly checkpoint in space and time. *Nature reviews. Molecular cell biology*, 8(May), pp.379–393.

Nam, H. et al., 2014. Centrosome dynamics as a source of chromosomal instability. *Trends in Cell Biology*, pp.1–9.

Neumayer, G. et al., 2014. TPX2: of spindle assembly, DNA damage response, and cancer. *Cellular and molecular life sciences : CMLS*, pp.3027–3047.

Ng, T.M. et al., 2010. Pericentromeric Sister Chromatid Cohesion Promotes Kinetochore Biorientation. *Molecular biology of the cell*, 20, pp.3818–3827.

Nigg, E.A., 2002. Centrosome aberrations: Cause or consequence of cancer progression? *Nature Reviews Genetics*, 3(November), pp.815–815.

Nigg, E.A. & Raff, J.W., 2009. Centrioles, Centrosomes, and Cilia in Health and Disease. *Cell*, 139(C), pp.663–678.

Nishikawa, H. et al., 2004. Mass Spectrometric and Mutational Analyses Reveal Lys-6-linked Polyubiquitin Chains Catalyzed by BRCA1-BARD1 Ubiquitin Ligase. *Journal of Biological Chemistry*, 279(6), pp.3916–3924.

Ookata, K. et al., 1995. Cyclin B Interaction with Microtubule-associated Protein 4 (MAP4) Targets p34 eda Kinase to Microtubules and Is a Potential Regulator of M-phase Microtubule Dynamics. *Cell*, 128(5), pp.849–862.

Orr, B. & Compton, D. A, 2013. A double-edged sword: how oncogenes and tumor suppressor genes can contribute to chromosomal instability. *Frontiers in oncology*, 3(June), p.164.

Oshimori, N. et al., 2009. Cep72 regulates the localization of key centrosomal proteins and proper bipolar spindle formation. *The EMBO journal*, 28(14), pp.2066–2076.

Oshimori, N. et al., 2006. The Plk1 target Kizuna stabilizes mitotic centrosomes to ensure spindle bipolarity. *Nat Cell Biol*, 8(10), pp.1095–1101.

Ouchi, M. et al., 2004. BRCA1 Phosphorylation by Aurora-A in the Regulation of G2 to M Transition. *Journal of Biological Chemistry*, 279(19), pp.19643–19648.

Ouchi, T., 2006. BRCA1 phosphorylation: Biological consequences. *Cancer Biology and Therapy*, 5(January 2015), pp.470–475.

Petronczki, M. et al., 2008. Polo on the Rise-from Mitotic Entry to Cytokinesis with Plk1. *Developmental Cell*, 14, pp.646–659.

Piehl, M. et al., 2004. Centrosome maturation: measurement of microtubule nucleation throughout the cell cycle by using GFP-tagged EB1. *Proceedings of the National Academy of Sciences of the United States of America*, 101(6), pp.1584–1588.

Pihan, G.A., 2013. Centrosome dysfunction contributes to chromosome instability, chromoanagenesis, and genome reprograming in cancer. *Frontiers in oncology*, 3(November), p.277.

Pinyol, R. et al., 2013. The role of NEDD1 phosphorylation by Aurora A in chromosomal microtubule nucleation and spindle function. *Current Biology*, 23(2), pp.143–149.

Primorac, I. & Musacchio, A., 2013. Panta rhei: The APC/C at steady state. *Journal of Cell Biology*, 201(2), pp.177–189.

Purohit, A. et al., 1999. Direct interaction of pericentrin with cytoplasmic dynein light intermediate chain contributes to mitotic spindle organization. *Journal of Cell Biology*, 147(3), pp.481–491.

Raynaud-Messina, B. & Merdes, A., 2007. Gamma-Tubulin Complexes and Microtubule Organization. *Current Opinion in Cell Biology*, 19, pp.24–30.

Reinhardt, C.H. & Yaffe, M.B., 2009. Kinases that Control the Cell Cycle in Response to DNA Damage: Chk1, Chk2, and MK2. *Curr Opin Cell Biol*, 21(2), pp.245–255.

Reinhardt, H.C. et al., 2007. p53-Deficient Cells Rely on ATM- and ATR-Mediated Checkpoint Signaling through the p38MAPK/MK2 Pathway for Survival after DNA Damage. *Cancer Cell*, 11(February), pp.175–189.

Ren, Y., Zhao, J. & Feng, J., 2003. Parkin binds to alpha/beta tubulin and increases their ubiquitination and degradation. *The Journal of neuroscience : the official journal of the Society for Neuroscience*, 23(8), pp.3316–3324.

Reyes Turcu, F.E. et al., 2009. Regulation and Cellular Roles of Ubiquitin-specific Deubiquitinating Enzymes. *Annu Rev Biochem*, 78, pp.363–397.

Ricke, R.M. & van Deursen, J.M., 2013. Aneuploidy in health, disease, and aging. *The Journal of Cell Biology*, 201(1), pp.11–21.

Royle, S.J., 2012. The role of clathrin in mitotic spindle organisation. *Journal of Cell Science*, 125, pp.19–28.

Ryser, S. et al., 2009. Distinct roles of BARD1 isoforms in mitosis: Full-length BARD1 mediates Aurora B degradation, cancer-associated BARD1β scaffolds Aurora B and BRCA2. *Cancer Research*, 69(3), pp.1125–1134.

Sankaran, S. et al., 2007. Aurora-A kinase regulates breast cancer-associated gene 1 inhibition of centrosome-dependent microtubule nucleation. *Cancer Research*, 67(5), pp.11186–11194.

Sankaran, S. et al., 2007. BRCA1 Regulates y-Tubulin Binding to Centrosomes. *Cancer Biol Ther*, 6(12), pp.1853–1857.

Sankaran, S. et al., 2005. Centrosomal microtubule nucleation activity is inhibited by BRCA1-dependent ubiquitination. *Molecular and cellular biology*, 25, pp.8656–8668.

Sankaran, S. et al., 2006. Identification of domains of BRCA1 critical for the ubiquitin-dependent inhibition of centrosome function. *Cancer Research*, 66(8), pp.4100–4107.

Sankaran, S. & Parvin, J.D., 2006. Centrosome function in normal and tumor cells. *Journal of Cellular Biochemistry*, 99, pp.1240–1250.

Savage, K.I. & Harkin, D.P., 2014. BRCA1 , a " complex " protein involved in the maintenance of genomic stability. *FEBS J*. 282(4),pp.630-46

Schlegel, B.P. et al., 2003. Overexpression of a protein fragment of RNA helicase A causes inhibition of endogenous BRCA1 function and defects in ploidy and cytokinesis in mammary epithelial cells. *Oncogene*, 22, pp.983–991.

Schneider, L. et al., 2007. The transforming acidic coiled coil 3 protein is essential for spindle-dependent chromosome alignment and mitotic survival. *Journal of Biological Chemistry*, 282, pp.29273–29283.

Schnell, J.D. & Hicke, L., 2003. Non-traditional functions of ubiquitin and ubiquitin-binding proteins. *Journal of Biological Chemistry*, 278, pp.35857–35860.

Scrofani, J. et al., 2015. Microtubule Nucleation in Mitosis by a RanGTP-Dependent Protein Complex. *Current Biology*, 25(2), pp.131–140.

Scully, R. et al., 1997. Dynamic changes of BRCA1 subnuclear location and phosphorylation state are initiated by DNA damage. *Cell*, 90(3), pp.425–435.

Scully, R. et al., 2004. Molecular functions of BRCA1 in the DNA damage response. *Cancer Biology and Therapy*, 3(January 2015), pp.521–527.

Seki, A. et al., 2008. Bora and Aurora A Cooperatively Activate Plk1 and Control the Entry into Mitosis. *Science (New York,*, 320(5883), pp.1655–1658.

Shakya, R. et al., 2011. BRCA1 Tumor Suppression Depends on BRCT Phosphoprotein Binding, But Not Its E3 Ligase Activity. *Science*, 334(2011), pp.525–528.

Shaltiel, I. a. et al., 2015. The same, only different - DNA damage checkpoints and their reversal throughout the cell cycle. *Journal of Cell Science*, 2, pp.607–620.

Sheltzer, J.M. & Amon, A., 2011. The Aneuploidy Paradox: Costs and Benefits of an Incorrect Karyotype. *Trends Genet.*, 27(11), pp.446–453.

Silkworth, W.T. et al., 2012. Timing of centrosome separation is important for accurate chromosome segregation. *Molecular Biology of the Cell*, 23(3), pp.401–411.

Silkworth, W.T. & Cimini, D., 2012. Transient defects of mitotic spindle geometry and chromosome segregation errors. *Cell Division*, 7(1), p.19.

Smith, J. et al., 2010. *The ATM-Chk2 and ATR-Chk1 pathways in DNA damage signaling and cancer* 1st ed., Elsevier Inc.

Solomon, D. a et al., 2011. Mutational Inactivation of STAG2 Causes Aneuploidy in Human Cancer. *Science*, 333(6045), pp.1039–1043.

Sonnen, K.F. et al., 2012. 3D-structured illumination microscopy provides novel insight into architecture of human centrosomes. *Biology Open*, 1, pp.965–976.

Srivastava, D. & Chakrabarti, O., 2014. Mahogunin-mediated α-tubulin ubiquitination via noncanonical K6 linkage regulates microtubule stability and mitotic spindle orientation. *Cell death & disease*, 5(2), p.e1064.

Staples, C.J. et al., 2014. Ccdc13; a novel human centriolar satellite protein required for ciliogenesis and genome stability. *Journal of cell science*, pp.2910–2919.

Staples, C.J. et al., 2012. The centriolar satellite protein Cep131 is important for genome stability. *Journal of Cell Science*, pp.4770–4779.

Starita, L.M. et al., 2004. BRCA1-Dependent Ubiquitination of γ -Tubulin Regulates Centrosome Number, *Molecular and cellular biology* 24(19), pp.8457–8466.

Starita, L.M. & Parvin, J.D., 2006. Substrates of the BRCA1-Dependent Ubiquitin Ligase. *Therapy*, (February), pp.137–141.

Stearns, T. & Kirschner, M., 1994. In vitro reconstitution of centrosome assembly and function: The central role of γ-tubulin. *Cell*, 76(4), pp.623–637.

Stepanova, T. et al., 2003. Visualization of microtubule growth in cultured neurons via the use of EB3-GFP (end-binding protein 3-green fluorescent protein). *The Journal of neuroscience : the official journal of the Society for Neuroscience*, 23(7), pp.2655–2664.

Stolz, A. et al., 2010. The CHK2-BRCA1 tumour suppressor pathway ensures chromosomal stability in human somatic cells. *Nature cell biology*, 12(5), pp.492–499.

Stolz, A. et al., 2015. A phenotypic screen identifies microtubule plus end assembly regulators that can function in mitotic spindle orientation. *Cell Cycle*, 14(6), pp. 827-837.

Stolz, A. et al., 2014. Microtubule plus tips: A dynamic route to chromosomal instability. *Molecular & Cellular Oncology*, 2(2), p.e960768.

Stowe, T.R. et al., 2012. The centriolar satellite proteins Cep72 and Cep290 interact and are required for recruitment of BBS proteins to the cilium. *Molecular Biology of the Cell*, 23, pp.3322–3335.

Stumpff, J. et al., 2012. Kif18A and chromokinesins confine centromere movements via microtubule growth suppression and spatial control of kinetochore tension. *Dev Cell*, 22(5), pp.1017–1029.

Sy, S.M.H. et al., 2009. PALB2 is an integral component of the BRCA complex required for homologous recombination repair. *Proceedings of the National Academy of Sciences of the United States of America*, 106(17), pp.7155–7160.

Syrovatkina, V. et al., 2013. Antagonistic spindle motors and MAPs regulate metaphase spindle length and chromosome segregation. *Current Biology*, 23(23), pp.2423–2429.

Takahashi, Y. et al., 2002. Centrosomal Proteins CG-NAP and Kendrin Provide Microtubule Nucleation Sites by Anchoring γ-Tubulin Ring Complex. *Molecular biology of the cell*, 13(September), pp.3235–3245.

Tanenbaum, M.E. & Medema, R.H., 2010. Mechanisms of Centrosome Separation and Bipolar Spindle Assembly. *Developmental Cell*, 19, pp.797–806.

Tanenbaum, M.E. et al., 2009. Kif15 cooperates with eg5 to promote bipolar spindle assembly. *Current Biology*, 19, pp.1703–1711.

Taylor, S. & Peters, J.-M., 2008. Polo and Aurora kinases - lessons derived from chemical biology. *Current Opinion in Cell Biology*, 20(1), pp.77–84.

Thakur, H.C. et al., 2013. Role of centrosomal adaptor proteins of the TACC family in the regulation of microtubule dynamics during mitotic cell division. *Biological Chemistry*, 394(11), pp.1411–1423.

Thompson, S.L., Bakhoum, S.F. & Compton, D. a, 2010. Mechanisms of Chromosomal Instability. *Curr Opin Cell Biol*, 20(6), pp.285–295.

Tollenaere, M. A. X. et al., 2014. Centriolar satellites: key mediators of centrosome functions. *Cellular and Molecular Life Sciences*, 72, pp.11–23.

Tsai, M.-Y. et al., 2003. A Ran signalling pathway mediated by the mitotic kinase Aurora A in spindle assembly. *Nat Cell Biol*, 5(3), pp.242–248.

Van der Vaart, B. et al., 2011. SLAIN2 links microtubule plus end-tracking proteins and controls microtubule growth in interphase. *Journal of Cell Biology*, 193(6), pp.1083–1099.

Van der Vaart, B. et al., 2009. Regulation of microtubule dynamic instability. *Biochemical Society Transactions*, 37, pp.1007–1013.

Vakifahmetoglu, H. et al., 2008. Death through a tragedy: mitotic catastrophe. *Cell death and differentiation*, 15, pp.1153–1162.

Vicente, J.J. & Wordeman, L., 2015. Mitosis, microtubule dynamics and the evolution of kinesins. *Experimental Cell Research*, pp.1–9.

Villumsen, B.H. et al., 2013. A new cellular stress response that triggers centriolar satellite reorganization and ciliogenesis. *The EMBO journal*, 32(23), pp.3029–40.

Vitre, B.D. & Cleveland, D.W., 2012. Centrosomes, chromosomal instability (CIN) and aneuploidie. *Curr Opin Cell Biol*, 24(6), pp.809–815.

Vodermaier, H.C., 2004. APC/C and SCF: Controlling each other and the cell cycle. *Current Biology*, 14, pp.787–796.

Weaver, B. a a et al., 2007. Aneuploidy Acts Both Oncogenically and as a Tumor Suppressor. *Cancer Cell*, 11(January), pp.25–36.

Wei, L. et al., 2008. Rapid recruitment of BRCA1 to DNA double-strand breaks is dependent on its association with Ku80. *Molecular and cellular biology*, 28(24), pp.7380–7393.

Weichert, W. et al., 2008. Association of patterns of class I histone deacetylase expression with patient prognosis in gastric cancer: a retrospective analysis. *The Lancet Oncology*, 9(2), pp.139–148.

Widlund, P.O. et al., 2011. XMAP215 polymerase activity is built by combining multiple tubulin-binding TOG domains and a basic lattice-binding region. *Proceedings of the National Academy of Sciences of the United States of America*, 108(14), pp.2741–2746.

Wiese, C. & Zheng, Y., 2006. Microtubule nucleation: gamma-tubulin and beyond. *Journal of cell science*, 119, pp.4143–4153.

Williams, B. et al., 2008. Aneuploidy affects proliferation and spontaneous immortalization in mammalian cells. *Science*, 322(5902), pp.703–709.

Wong, J. et al., 2008. Aurora A Regulates the Activity of HURP by Controlling the Accessibility of Its Microtubule-binding Domain. *Molecular biology of the cell*, 19(May), pp.2083–2091.

Wong, J. & Fang, G., 2006. HURP controls spindle dynamics to promote proper interkinetochore tension and efficient kinetochore capture. *Journal of Cell Biology*, 173(6), pp.879–891.

Wu, W. et al., 2008. The ubiquitin E3 ligase activity of BRCA1 and its biological functions. *Cell division*, 3, pp.1-10.

Wu-Baer, F. et al., 2003. The BRCA1/BARD1 heterodimer assembles polyubiquitin chains through an unconventional linkage involving lysine residue K6 of ubiquitin. *Journal of Biological Chemistry*, 278, pp.34743–34746.

Xiao, H. et al., 2012. Structural evidence for cooperative microtubule stabilization by Taxol and the endogenous dynamics regulator MAP4. *ACS Chem. Biol.*, 7(4), pp.774–752.

Yu, X., 2003. The BRCT Domain Is a Phospho-Protein Binding Domain. *Science*, 302(5645), pp.639–642.

Yu, Y.M. et al., 2008. A PP1-binding motif present in BRCA1 plays a role in its DNA repair function. *International Journal of Biological Sciences*, 4(6), pp.352–361.

Zahnleiter, D. et al., 2015. MAP4-Dependent Regulation of Microtubule Formation Affects Centrosome, Cilia, and Golgi Architecture as a Central Mechanism in Growth Regulation. *Human Mutation*, 36, pp.87–97.

Zhang, J. et al., 2004. Chk2 Phosphorylation of BRCA1 Regulates DNA Double-Strand Break Repair Chk2 Phosphorylation of BRCA1 Regulates DNA Double-Strand Break Repair. *Molecular and cellular biology*, 24(2), pp.708–718.

Zhang, P. et al., 2004. CHK2 kinase expression is down-regulated due to promoter methylation in non-small cell lung cancer. *Molecular cancer*, 3, p.14.

Zheng, Y. et al., 1995. Nucleation of microtubule assembly by a gamma-tubulin-containing ring complex. *Nature*, 378(6557), pp.578–583.

Zhong, Q. et al., 2002. Deficient nonhomologous end-joining activity in cell-free extracts from BRCA1-null fibroblasts. *Cancer Research*, 62, pp.3966–3970.

Zhu, Q. et al., 2011. BRCA1 tumour suppression occurs via heterochromatin-mediated silencing. *Nature*, 477(7363), pp.179–184.

Zimmerman, S. & Chang, F., 2005. Effects of γ-Tubulin Complex Proteins on Microtubule Nucleation and Catastrophe in Fission Yeast. *Molecular Biology of the Cell*, 16(June), pp.2719–2733.

Zimmerman, W.C. et al., 2004. Mitosis-specific Anchoring of γ Tubulin Complexes by Pericentrin Controls Spindle Organization and Mitotic Entry. *Molecular biology of the cell*, 15(August), pp.3642–3657.

ACKNOLEDGEMENTS – DANKSAGUNG

An dieser Stelle möchte ich allen danken die zum Gelingen dieser Arbeit beigetragen und mich während der letzten dreieinhalb begleitet und tatkräftigt unterstützt haben.

Mein besonderer Dank gilt meinem Doktorvater Professor Dr. Holger Bastians der es mir ermöglicht hat an diesem spannenden Thema zu arbeiten. Danke für die exzellente Betreuung und Unterstützung, sowie die ständige Bereitschaft zur Beantwortung und Diskussion von Fragen, Problemen und Theorien.

Des Weiteren möchte ich den Mitgliedern meines Thesis Committees Professor Dr. Sigrid Hoyer-Fender und Professor Dr. Peter Burfeind danken, dass sie meine Doktorarbeit begleitet und mit wertvollen Anmerkungen unterstützt haben. Ebenfalls möchte ich mich bei Professor Dr. Heike Krebber für die Bereitstellung von Arbeitsmöglichkeiten bedanken.

Vielen Dank an Dr. Norman Ertych und Dr. Oliver Valerius für die Entdeckung der Brca1-Cep72 Interaktion und somit der Grundsteinlegung für mein Projekt. Darüber hinaus danke ich Professor Dr. Wilko Weichert, Dr. Albrecht Stenziger und Dr. Jerzy Dyczkowski für die Analyse der *CEP72* Expression in humanen Tumoren.

Den aktuellen und ehemaligen Mitgliedern der AG Bastians danke ich aus vollstem Herzen für die tolle Arbeitsatmosphäre und die tatkräftige Unterstützung bei kleinen und großen Problemen. Danke für all die schönen Stunden und die fröhlichen, lustigen Momente. Vielen Dank insbesondere an Ailine Stolz, Norman Ertych und Katharina Berger, dass ihr trotz meiner teils wirren Gedankengänge meine Fragen verstanden, beantwortet und mit mir diskutiert habt. Danke Norman für die Geduld die du für mich und meine Computerprobleme aufgebracht hast.

Für das Lesen und die Korrektur des Manuskripts, sowie für ihre Unterstützung und Freundschaft danke ich ganz herzlich Katharina Berger.

Zu guter Letzt gilt mein größter Dank meiner Familie und meinem Freund Dennis. Danke, dass ihr immer für mich da seid und mich grenzenlos unterstützt. Danke für euer Verständnis, eure Akzeptanz und Liebe. Ohne euch wäre diese Arbeit nicht möglich gewesen.